

Experimental Studies of Wind Turbine Wakes

—

Power Optimisation and Meandering

by

Davide Medici

December 2005
Technical Reports from
KTH Mechanics
Royal Institute of Technology
S-100 44 Stockholm, Sweden

Akademisk avhandling som med tillstånd av Kungliga Tekniska Högskolan i Stockholm framlägges till offentlig granskning för avläggande av teknologie doktorsexamen fredagen den 10:e februari 2006 kl 10.15 i Sal D3, Lindstedtsv. 5 Entreplan, KTH, Stockholm.

©Davide Medici 2005

Universitetsservice US AB, Stockholm 2005

D. Medici 2005, **Experimental Studies of Wind Turbine Wakes - Power Optimisation and Meandering**

KTH Mechanics, Royal Institute of Technology
S-100 44 Stockholm, Sweden

Abstract

Wind tunnel studies of the wake behind model wind turbines with one, two and three blades have been made in order to get a better understanding of wake development as well as the possibility to predict the power output from downstream turbines working in the wake of an upstream one. Both two-component hot-wire anemometry and particle image velocimetry (PIV) have been used to map the flow field downstream as well as upstream the turbine. All three velocity components were measured both for the turbine rotor normal to the oncoming flow as well as with the turbine inclined to the free stream direction (the yaw angle was varied from 0 to 30 degrees). The measurements showed, as expected, a wake rotation in the opposite direction to that of the turbine. A yawed turbine is found to clearly deflect the wake flow to the side showing the potential of controlling the wake position by yawing the turbine. The power output of a yawed turbine was found to depend strongly on the rotor. The possibility to use active wake control by yawing an upstream turbine was evaluated and was shown to have a potential to increase the power output significantly for certain configurations.

An unexpected feature of the flow was that spectra from the time signals showed the appearance of a low frequency fluctuation both in the wake and in the flow outside. This fluctuation was found both with and without free stream turbulence and also with a yawed turbine. The non-dimensional frequency (Strouhal number) was independent of the freestream velocity and turbulence level but increases with the yaw angle. However the low frequency fluctuations were only observed when the tip speed ratio was high. Porous discs have been used to compare the meandering frequencies and the cause in wind turbines seems to be related to the blade rotational frequency. It is hypothesized that the observed meandering of wakes in field measurements is due to this shedding.

Descriptors: Wind Energy, Power Optimisation, Active Control, Yaw, Vortex Shedding, Wake Meandering

Preface

The first part of this thesis consists of an introduction to utilising wind energy for electricity power production, its principles and a description of wake stability, a review of relevant work, a description of the techniques and equipment used in the experiments and a short summary of the results. The second part consists of seven research papers that describe the results in detail. The contents of the papers have not been changed as compared to the published versions, except for some typographical errors, but they have been adapted to the present thesis format. The papers still to be submitted for journal publication present the most recent results.

*” Venimmo al pie’ d’un nobile castello,
sette volte cerchiato d’alte mura,
difeso intorno d’un bel fiumicello.*

Dante, *Inf.*, IV, 106-108.

(At foot of a magnificent castle we arrived,
seven times with lofty walls begirt,
and around defended by a pleasant stream.)”

Contents

Abstract	iii
Preface	iv
Chapter 1. Introduction	1
1.1. World energy resources	2
1.2. Up-to-date wind energy facts	3
1.3. A view for the future	5
1.4. Objectives of the thesis	6
Chapter 2. Wind turbines design	8
2.1. Historical development	8
2.2. Background	10
2.3. Torque at the shaft	13
Chapter 3. Wake principles	16
3.1. Bluff body wakes	16
3.2. Wind turbine wakes	17
3.3. Wind turbine wake meandering	25
Chapter 4. Experimental Methods	27
4.1. Wind tunnels	27
4.2. Measurement techniques	29
4.3. Turbine models	32
Chapter 5. Summary of papers and authors contributions	41
5.1. Summary of papers	42
Acknowledgements	44
Bibliography	45

Paper 1	51
Paper 2	65
Paper 3	87
Paper 4	103
Paper 5	119
Paper 6	145
Paper 7	165

CHAPTER 1

Introduction

The footnote in my *Divina Commedia* explained Dante's words, quote: *The castle is the human philosophy, i.e. the Knowledge, and its seven walls are metaphysics, physics, mathematics, ethics, economy, dialectic and politics.* It is interesting that except the first one, all are needed to build a wind farm and I hope that Dante is not too upset about my comparison. Convincing the public is today's real challenge, since the technical problems are easier to solve and sometimes they can be just a matter of convenience and investment. R&D can provide many answers and luckily even more questions, since every single component must be of the top quality to have a good wind turbine. This thesis deals with only some of the technical aspects, but the first chapter is meant as an introduction for the reader who is unfamiliar with the wide world of wind energy.

In principle, it is easy to install a wind farm: ask where the wind blows, check for some signs like trees bending predominantly in one direction, install a tower with 3-4 anemometers at different heights and a vane to measure the wind direction and measure for at least one year to be sure of capturing the seasonal winds. With these data it is possible to calculate if the wind is strong and constant enough, and if so buy a wind turbine and install it. An on-shore wind turbine costs about 900 euros/kW rated power, but since it can be a good investment the issue is nowadays mainly political. Which are the mostly mentioned problems of wind turbines? A wind turbine is seen as a bird-killer and a source of stress for the animals and people leaving nearby. Anyone who has visited the wind farms on Gotland must have seen ducks flying happily few meters from the 80 m diameter wind turbines, not a slaughter of birds under the rotor. It will be shown in **paper 4** how the flow is affected far upstream of a wind turbine, and the above mentioned ducks can definitely sense this. Of course some areas should be off-limits (e.g. the migration routes and national parks), but this would leave enough resources to develop wind energy to a considerably higher level than today. Noise can be a serious issue and for some old wind turbines it was a problem, but the technology has remarkably improved and new solutions are under development.

The visual impact is usually the main approach to oppose wind farms. Wind turbine manufacturers have during the years developed more slender

machines and they have paid more attention to the design, but more can be done. Of course at the end it all comes down to convenience and the world situation in the last years has contributed to increase the attention towards other energy sources, since oil prices are constantly rising and pollution too. Europe imports 50% of its energy needs and the oil is located primary in politically unstable regions, while nuclear power is hardly an option not only for the public opinion aversion, but also for the limited uranium reserves. The energy demands coming from China will surely affect the West, and it looks like green policy is not their primary worry (see Hassan (2005)). Acceptance comes after knowledge and it is possible to notice an increased attention about renewable energy (Lemonick *et al.* (2005), Parfit (2005)). The use of renewable energy sources goes together with energy saving policies, and of course with the traditional sources. Renewable energy resources can compete with the traditional and wind energy, although it is not the only answer, can have a leading role.

1.1. World energy resources

When it comes to the statistics of the actual use of energy supplies, there exist small discrepancies between different studies due to differences in the definitions and methods used to evaluate the resources. Here the general definitions used by the International Energy Agency (IEA, www.iea.org) will be adopted. It states that *renewable energy sources* include hydro, geothermal, solar photovoltaics, solar thermal, tide, wave, ocean, wind, solid biomass, gases from biomass, liquid biofuels, and renewable municipal solid waste. In general energy independence is probably a dream for most countries, but energy production is not. A look at the 2003 fuel shares of the world energy production in figure 1.1(a) as from IEA (2005a), shows the strong dependency from few energy sources. Crude oil supplies more than one third of the total $1.23 \cdot 10^5$ TWh¹. Five countries in Europe are among the first ten importers of oil in the world. If the picture is restricted to the electricity production (figure 1.1(b)), coal is the most commonly used source. Italy has the first position among the importers of electricity (not such a privileged leadership) with 51 TWh in 2003. Accordingly to the *Statistiska Centralbyrån* SCB (statistics Sweden), Sweden has produced 155.6 TWh of electricity from October 2004 to September 2005, with approximately 91% equally divided between nuclear and water power.

The use and production of energy is strictly connected, after the industrial revolution, to the emissions of CO₂. Only in 2003 the total emission of carbon dioxide was 24983 Mt (million tonnes), equal to the amount emitted in 1000 years by Mount Etna in Sicily. The fuel shares for 2003 is shown in figure 1.2.

¹This value is usually given in toe= tonne of oil equivalent and corresponds to 10579 Mtoe, 1 Mtoe = 11.63 TWh.

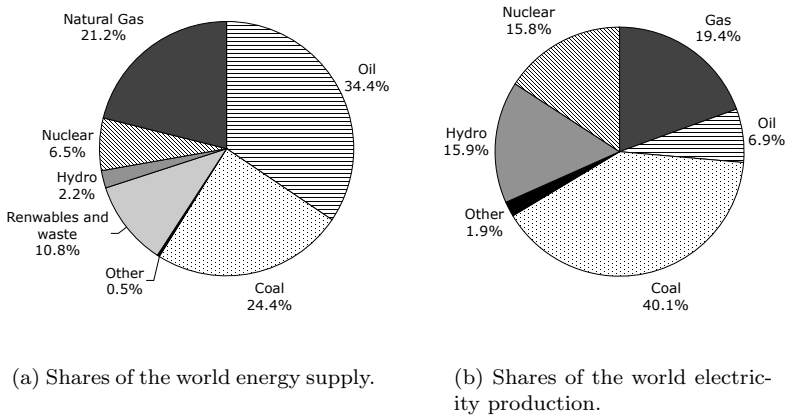


FIGURE 1.1. Source: IEA (2005a), data from 2003.

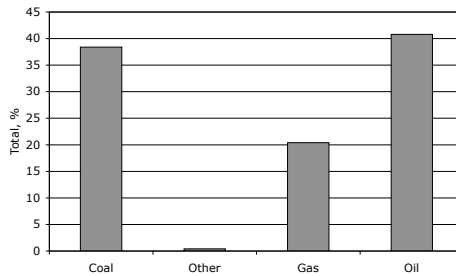


FIGURE 1.2. Fuel shares of the world CO₂ emissions in percentage, the total being 24983 Mt.

1.2. Up-to-date wind energy facts

The *rated power* from a turbine (i.e. the maximum obtainable power) is only obtained if the wind speed is higher than a characteristic value, typically around 12 m/s at hub-height. A wind turbine runs below the rated power for approximately 75% of its production time. There is also an upper wind speed above which the turbine is shut down in order to avoid damages to the turbine. The *installed capacity* of wind energy (for a wind turbine park, country or the world) is the sum of the rated power of all considered turbines. Having the above analysis in mind, in order to understand if wind energy has a potential to develop even further, it is essential to understand the world wind resources. Data have been collected during many years in the 30 OECD (Organisation for Economic Co-operation and Development) countries, which includes Sweden

COUNTRY	Installed capacity in 2004 [MW]	Total by end of 2004 [MW]
China	198	764
Denmark	3	3118 (13%)
Germany	2020	16629
Greece	43	468
Italy	357	1265
Japan	434	940
Netherlands	167	1072
New Zealand	132	168
Spain	2061	8263
Sweden	38	442 (5%)
UK	253	900 (14%)
USA	359	6740
Rest of the world	2397	7095
Total	8462	47864 (1.2%)

TABLE 1.1. Installed capacity, data from IEA (2005*b*). Between parenthesis is the off-shore share.

since 1961, and in other areas of the world. The methodology, see for example Grubb & Meyer (1993), is to calculate the available land with an annual average wind speed higher than a chosen threshold value (in the cited case, above 5.1 m/s at a height of 10 m from the ground level). The energy output calculated from the velocity distribution is reduced by 90% when constraints such as high-populated areas, human activities, noise, visual impact, etc. are considered. According to this report, the energy available in the wind in the world is 53000 TWh per year. Furthermore, no off-shore sites were considered by Grubb & Meyer (1993) whereas, today, great attention is focussed also on this area. For instance, the amount of energy which can be produced by off-shore sites in Europe is estimated in the order of 2000 TWh per year.

The statistics for some of the IEA (International Energy Agency) Wind members are shown in table 1.1. It is evident that wind in Europe is mainly a 3-countries business, with Germany and Spain leading the growth. Denmark is focussing more on re-powering old wind turbines and on the off-shore development. The European Union target has been set to 75 GW of installed power by 2010, of which 10 GW will be off-shore, and an additional 100 GW is the aim by 2020. In addition, the Kyoto protocol and the premium for green energy production have pushed for higher private investment in renewable energies. The price for electricity production is rapidly approaching that from other sources thanks to more efficient wind turbines and lower costs. The installation cost depends strongly on the location and size of the project, but a wind turbine alone is between 600 and 900 euros/kW, increasing between 800 and 1100 euros/kW for the complete installation. As an example, Japan has

slightly higher costs because of the complex terrain and service can become expensive during the typhoon season. The investment is roughly divided between the turbine (75%) and the infrastructures necessary to build the power plant. Off-shore costs are higher because of the more challenging environment.

Wind turbines are designed for a 20 years life (or more) and have proven to be very efficient. Some parts (e.g. the brake pads) must be replaced every two-three years, but more important and costly components such as the gear-box might need to be replaced once in a lifetime. The overall wind turbine availability exceeds 98%.

1.3. A view for the future

Regarding my idea for future developments, I hope there will be two main approaches: medium wind turbines with a rated power below 1 MW and larger ones of the order of several MW. The installation of even a single wind turbine in areas where there is none can help to accept more projects. Countries such as Italy or Japan have a large percentage of complex terrain (mountains or hills), and therefore smaller wind turbines are easier to transport and install. It must be remembered that good infrastructures in a mountain area may not be enough: a 750 kW wind turbine blade is approximately 23 m long. Although more costly, the transport of this kind of blade by an helicopter can still be an option. If the size of the turbines will only increase and these turbines will be off the market, this method will be unrealistic. On the other hand, *the bigger, the better* philosophy may be more difficult to accomplish both socially and politically, but its pay-back is highly rewarding in terms of produced energy, so that even the few projects which see and end justify today's efforts in this direction. The Danish approach has proven to be the most reliable and efficient: local communities have a share and participate in the wind farm projects. It is harder to be against wind energy if it helps with the bills.

The development of renewable sources is strictly connected to an energy saving policy. A very interesting example in this direction is the zero emission building headquarters of the RES, Renewable Energy Systems, outside London. A wind turbine and several solar panels provide electricity, which is fed into the network if not used, and a crop field fuels the boiler. Other passive design solutions minimise the energy losses and all the building environment is controlled by a computer system (see <http://www.beaufortcourt.com> for more information). A further insight into future developments of wind energy is the Aero-train project (<http://www.ifs.tohoku.ac.jp/kohama-lab>) currently under development at the Kohama Laboratory, Tohoku University, Japan. The high-speed zero emission train will receive its energy by a cluster of wind turbines, as well as solar panels and fuel cells. The train concept is based on the ground effect between its wings and the U-shaped duct and an unmanned version has successfully been tested. As can be seen in figure 1.3, the wind turbines will most likely be closely spaced together and as a consequence the interaction between wakes and turbines can be crucial. In **paper 2**

an Active Wake Control will be introduced and it is a common goal of the author and of the aero-train researchers to test the method in the Sunrise-Beach facility in Hyuga, Japan.

Future research on wind energy must rely both on experimental as well as numerical studies. In a wind tunnel it is impossible to match the Reynolds number of a real wind turbine, but the flow characteristics are all reproduced: power and drag behaviour, rotation of the wake and tip-vortices. The numerical simulations on the other hand can be used for a wide range of applications in a more efficient and economic way, but they always need experimental data to be validated.

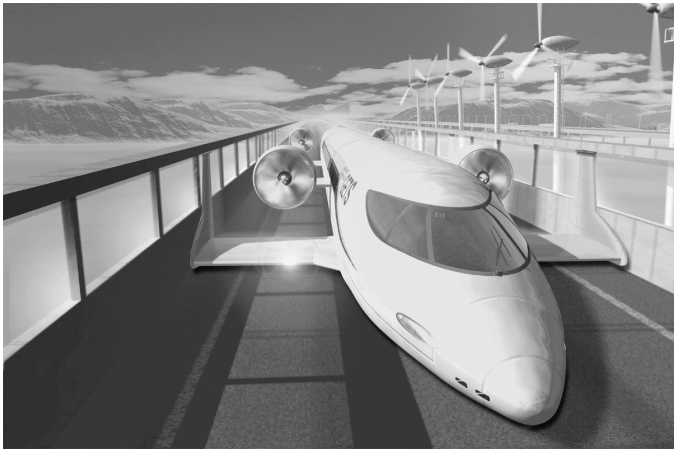


FIGURE 1.3. Zero emission high speed train, courtesy of Dr. Shuya Yoshioka.

1.4. Objectives of the thesis

Wind turbines in a park are often placed in parallel lines, with the distance between the lines of the order of 5 to 9 diameters. The orientation is best when, for the prevailing wind direction, the interaction between the wake from an upstream wind turbine and a downstream one is minimised. The reason is not only that the power extracted is reduced by the velocity defect in the wake, but also the fatigue loads on the structures can become much higher. One objective of the thesis is to give a better understanding of the physical behaviour of both the flow approaching a wind turbine and the behaviour of the wake flow.

Another objective is to investigate the possibility of using the already existing yaw control on turbines in order to deflect the wake away from the downstream turbine. With this, loads on the shadowed turbine can be decreased and power production may be improved. The aim is to understand to what extent the side force created by the yawed turbine affects the wake and how

the structure of the 3-dimensional wake is changed. An interesting observation is that the turbine model wake meanders in a similar way as a bluff body, such as observed for example in field measurements in the Alsvik wind farm, on the island of Gotland. This kind of motion may prove to be very important in wind parks, where interactions between several wakes can take place.

To reach the objectives we have used small wind turbine models and measured the velocity field related to the flow behind the turbines in a wind tunnel. We have used both hot-wire anemometry and PIV techniques and made extensive measurements for a number of configurations of the wind turbines.

Chapter 2 of the thesis gives some fundamentals of wind turbines, both from a historical and modern perspective, whereas chapter 3 gives some basic results for power extraction related to the flow in the wake. Chapter 4 describes the experimental techniques and the turbines used in the present study. Chapter 5 is a summary of the papers which are appended to the present thesis.

CHAPTER 2

Wind turbines design

2.1. Historical development

The need of mechanical energy has pushed for new ideas or improvements to use the natural resources. Before the industrial revolution, water and wind were the most used energy sources¹. This supremacy decreased with the implementation of coal or oil driven machinery, which have the important characteristic of being independent from the local conditions (provided that there is access to the fuel). Nevertheless, technology has never stopped improving the efficiency of water and wind mills and their studies have always been connected by the similar design. In fact, the first windmills may have been a direct application of a water mill, just using a different fluid. Going back in time is always difficult, since the historical sources are not so accurate. Some windmills may possibly be traced back to 2000 years ago in China or to Heron of Alexandria, but this is highly controversial. The first well-documented windmills were developed in the region between modern Iran and Afghanistan around the 10th century. The axis of the rotor was vertical and the torque was generated exclusively by the drag on the sails (Fig. 2.1).

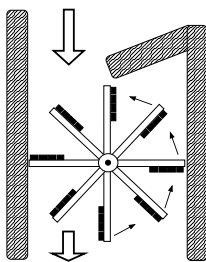


FIGURE 2.1. Vertical-axis Persian wind mill from the 10th century, top view. The rotor was about 6 m high and 4 m in diameter.

The grinding stone was directly below the rotor, or the mill was on top of a well and used to pump water. Although cultural, economical and less friendly (wars) exchanges allowed a prolonged contact with the East, the vertical-axis mill never made it to Western Europe. Instead, another type of mill was developed in the 12th century: the horizontal-axis. The revolutionary idea behind

¹Most of the information presented in this section is adopted from Schepherd (1990).

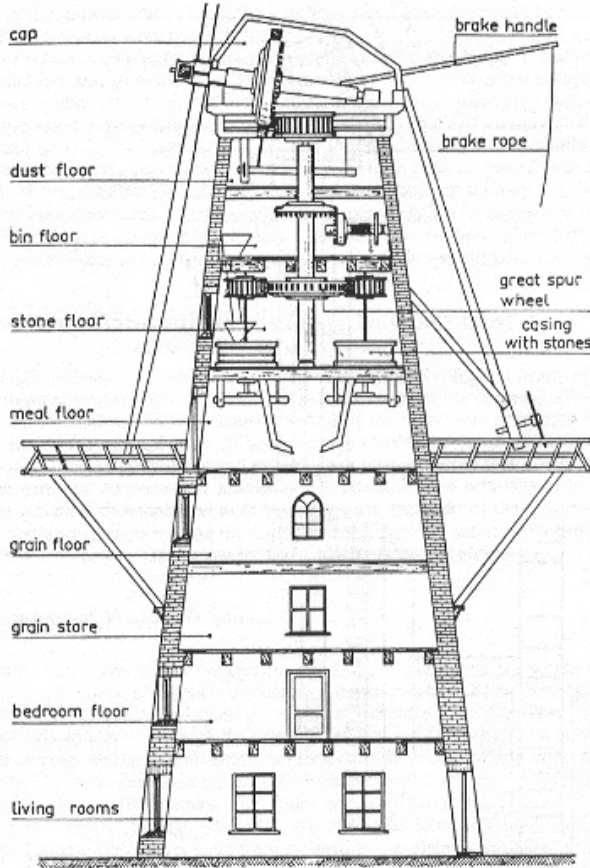


FIGURE 2.2. Sketch of a 12th century tower mill (from Schepherd (1990)). Only the cap on top of the brick tower rotates to face the wind.

its success was the use of the much larger lift instead of the drag to create the torque at the shaft, but it can be argued that not much was known at the time about fluid-mechanics. The most evident change is that the direction of the shaft has turned parallel to the wind. The typical configuration had 4-sails that were inclined with respect to the wind and were most likely thought to be moved by the flow directly impinging on them. It must be remembered that the Newtonian theory was used in many fields (subsonic as well as supersonic) up to the 20th century. The first documented case of a horizontal-axis windmill dates back to 1137 in Northwest Europe, although the mills are reported more as a social than a technical event and few information is given. More is known about the *post-mill* dated 1270, an example of which can be seen also

in the Skansen museum, Stockholm. The post-mill was usually a wooden tower standing on a main post and the entire block was turned accordingly to the wind direction. New engineering problems had to be solved, but many were successfully managed by the Dutch *tower-mill* shown in figure 2.2. This wind-mill is the natural development of the older post-mill and it is first recorded in the beginning of the 15th century in the Turkish town of Gallipoli. Some interesting features can be observed in both the post-mill and the Dutch-mill: the shaft is not perpendicular to the tower, but slightly inclined as for the modern wind turbines. This leaves a good clearance between the tower and the sails. The torque was transmitted to the vertical shaft by a large wheel with pegs. This wheel was large in order to increase the breaking torque of a band around its circumference, since the speed of the millstones was controlled by the miller setting the friction between the band and the wheel. A bearing at the end of the horizontal shaft sustained all the axial drag. The Dutch-mill cap was movable and the platform at the mid-height was used both to activate the brake and to operate the sails. The largest recorded mill of this kind had a tower of 37 m and a rotor of 30 m.

A lot more could be said about the mill development, but it is not in the scope of this thesis. In the end it can be mentioned that many improvements have regarded the sails, the materials used in the construction and the control methods; the latter are described in the next section. Modern windmills are mainly used to produce electricity and they are called wind turbines, but the physical principle has not changed over the years. What is considerably different is the size and the efficiency as compared to wind mills only few decades ago. Off-shore wind turbines have increased up to 120 m in diameter and 5 MW of nominal power. The size of the on-shore wind turbines is generally smaller because of the road constraints for transportation.

2.2. Background

When the air flows around a streamlined body such as a wing profile, the pressure field is modified and therefore a force is generated. The component perpendicular to the flow direction is called *lift*, the component parallel and in the opposite direction to the inflow is the *drag*. The angle of attack between the blades and the direction of the relative wind is not only the result of the wind direction since the blade itself is moving. What happens can be clearly seen in figure 2.3 on one of the wind turbine models used for the experiments. The azimuthal velocity must be added to the wind speed, from left.

Some confusion as regarding the drag can arise. The force that is acting on the entire wind turbine in the same direction of the wind, is called drag as well. The application point of this force is the centre of the rotor, if the turbine is aligned with the uniform flow and the tower is neglected. Since the wind turbine studies are traditionally connected with the propeller area, this force is sometimes also called thrust.

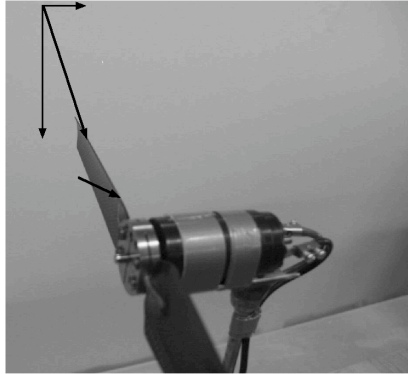


FIGURE 2.3. The angle between the plane of the rotor and the local wind direction is decreasing as moving towards the tip, hence the stall starts from the root. The turbine rotates clockwise.

For good performance of a wing of a wind turbine blade, flow separation on the blade surface should be avoided. This is the reason why wind turbines have twisted blades: the angle of attack is optimised from tip to root, for the most frequent operational condition, by making the blade to turn out of the plane of rotation when moving towards the root. However the so-called *stall control*, one of the main aerodynamic controls on wind turbines, makes the stall to occur gradually from the root as the wind speed increases. The reason is to avoid high loads and also high power production which can cause problems to the electrical components of the wind turbine. This is a passive type of control, since the angle of attack on the blades increases with increasing wind speed.

A second important aerodynamic control present on wind turbines is the *yaw control*. It will be shown how the power is proportional to the cube of the wind speed normal to the rotor plane. To maximize the power output the wind turbine is turned towards the wind by means of electrical motors, which move the entire nacelle (i.e. the top part of the wind turbine including the shaft, the gearbox if present, the generator and the other systems) around the tower. Both the yaw control and the twist of the blades were well known in the past, when windmills produced not electrical but only mechanical energy. The third mostly used control is the *pitch control*. In this active control, the entire blade is turned, to optimise the angle of attack with respect to the wind. If the power output from the generator becomes too high, the system decreases the angle of attack of the blades, in order to obtain less power. This mechanism is the opposite of the *active stall control*, where the blades are instead turned out of the wind to increase the stall, thereby "wasting" the excess energy in the wind.

All the wind turbines have a cut-in wind speed, after which the wind-generated torque is greater than the friction in the system and the rotor starts

to rotate and produce electricity. The cut-off speed is instead the higher limit for the working conditions, above which the loads produced are considered dangerous for the machine. The range of velocities is typically somewhere between 3 m/s and 30 m/s, but depends on the type of wind turbine considered. When the conditions exceed the highest velocity limit, the turbine is stopped first by means of aerodynamic controls, e.g. pitching the blade and causing an extended stall, and then the brakes act on the shaft. Tip ailerons are also used in some models as aerodynamic breaks, or the entire tip itself is tilted.

Some wind turbines run at constant rotational speed, giving a constant frequency of the current produced. Small fluctuations in the frequency are allowed and adjusted with an electronic converter. The reason is that the turbines are connected to an electrical grid with a specific frequency of the current (50 Hz in Europe), which has to be matched by the production plant. Two main concepts are presently on the market: the most common is connecting the shaft with an high speed generator through a gearbox which increases the rotational frequency. Without the gearbox the stator is a large multi-layer ring, where the lower rotational frequency of the rotor is balanced by a greater number of poles in the stator. In this way the frequency of the produced current is increased and the machine can be directly connected to the electrical system. The maximum power of wind turbines has increased from 0.4 MW of a decade ago to the 5 MW machines, manufactured by e.g. Enercon and General Electrics. One example of a modern wind turbine is the Enercon E66 shown in figure 2.4. It has a rated power of 2 MW and a diameter of 70 m.



FIGURE 2.4. Enercon E66. Courtesy of Enercon GmbH.

For a given power output, the choice is then between a large, low speed rotor such as for the Enercon wind turbine, or a smaller, high speed rotor, although hybrid systems have been developed. Ultimately, both have some inconvenience. The weight of the nacelle is of the order of 3-400 tons for the gearless machine, and only about a fifth when the gearbox is present. On the other hand, the gearbox has to stand the large torque from the blades and the fluctuations of the wind speed and direction, which may cause it to break. Also the initial cost is generally in favour of a high speed generator, however the absence of moving parts is a pro-factor for the low speed generator.

In the nacelle a small fixed crane can also be placed to considerably speed up the process of changing internal parts of the wind turbine. When it comes to assembling the machine, some interesting solutions can be seen. On-shore the process is usually easier: the machine is put together *in situ* connecting elements of the tower, of the nacelle and of the service parts (shaft, generator, active power controls, etc.). On the ground, in case of a three-bladed turbine, two blades are connected together and then lifted in front of the nacelle. At the end also the third blade is raised and bolted to the shaft. Off-shore the environment is more challenging. First, the basement of the tower must be built. In a second stage, special-purpose ships with a crane are used and equipped with a number of poles that descend on the sea bottom and anchor the ship. The turbine is put together on-shore and then loaded on the ship, for example in only three pieces: the tower, the nacelle with two blades mounted, and a third single blade. The final assembling process of these parts can take place at sea in typical eight hours, if the weather conditions are good.

2.3. Torque at the shaft

Most of the wind turbines have a horizontal axis rotor because of their higher energy production with respect to the vertical axis. The advantage of the horizontal axis is that, except for the velocity changes in the atmospheric boundary layer, the blades operate at a nearly constant angle of attack. The lift on the profile is always favourable to the rotation. The vertical axis wind turbine has instead a cyclical change in the sign of the angle between the wind speed and the azimuthal velocity, hence the total torque is reduced. Consider a symmetrical wing profile: with the chord parallel to the wind direction only the drag acts on the blade and therefore the torque at this position is opposing the rotation. For both the vertical and horizontal axis wind turbine, the running condition is the balance between the load (breaking torque) on the shaft given by the generator and the driving torque Q created by the rotor. This is related to the mechanical power P by:

$$P = \Omega Q \tag{2.1}$$

The torque of one of the turbines used in this study is shown in figure 2.5 as a function of the rotational speed Ω , with the load depending only on the generator. At a constant wind speed, the rotor accelerates until it reaches

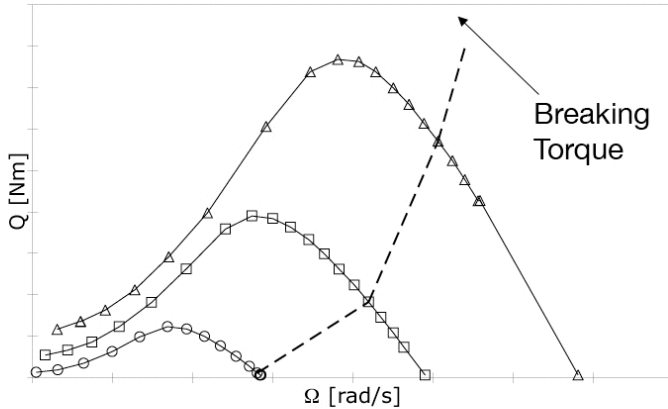


FIGURE 2.5. Rotor torque as a function of the rotational speed for the wind turbine model 2 (see Chapter 4). \circ : $U_\infty=5$ m/s, \square : $U_\infty=8$ m/s, \triangle : $U_\infty=11$ m/s. The dashed line is for a heavy load from the generator, the solid line for a light load.

the rotational speed that balances the load from the generator. If the rotor moves from the equilibrium point, the load restores the original Ω . Suppose that the rotor speed increases, then the breaking torque from the generator is higher (figure 2.5) and slows down the rotor. A steep Q - Ω curve can lead to an unstable equilibrium, i.e. a fluctuating Ω , since there is not a well defined crossing between the torque from the rotor and the load from the generator. The production of current is directly proportional to the torque on the shaft since a DC generator has been used and the variation of the internal losses can be neglected. Curves for different wind speed collapse if the following coefficients are introduced:

$$\frac{P}{\frac{1}{2}\rho A_d U_\infty^3} = \frac{\Omega R}{U_\infty} \cdot \frac{Q}{\frac{1}{2}\rho A_d R U_\infty^2} \Leftrightarrow C_P = \lambda C_Q \quad (2.2)$$

where U_∞ is the wind speed, R is the rotor radius and A_d is the area swept by the blades. The tip-speed ratio λ is defined as tip-speed/wind speed.

A high solidity (σ =blade area/ A_d) turbine means a lower λ , therefore from Eq. 2.2 at constant C_P the torque coefficient is higher. This type of turbine is preferred for water pumps. On the other hand, the starting torque is higher and high σ turbines may need the application of a torque by e.g. an electrical motor to start rotating. Many wind turbines for electrical generation have a control on the loading in order to change the rotational speed and to keep an optimum tip-speed ratio (as close as possible to $C_{P_{max}}$) for a wide range of wind speeds. The optimum λ depends strongly on the blade characteristics and on the lift-to-drag ratio, see figure 2.6. When this ratio tends to infinity, the power coefficient tends to the so-called Glauert limit which will be derived in

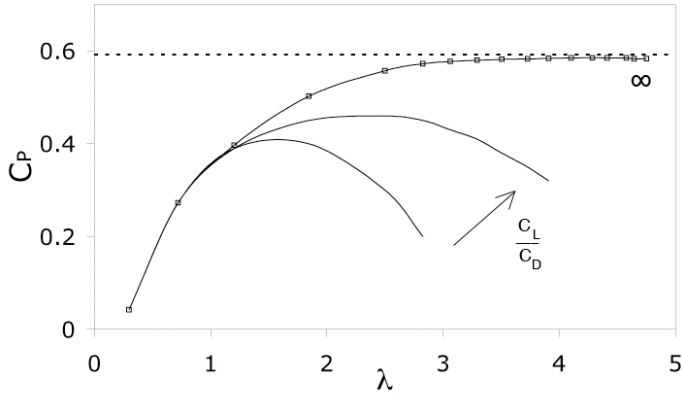


FIGURE 2.6. Power as a function of the rotational speed for different C_L/C_D values.

chapter 3. The Betz limit is the maximum theoretical limit which is approached for $\lambda \rightarrow \infty$ and this will be discussed as well in the next chapter. As for the effect of the number of blades on the power coefficient we refer to **paper 3**. It must be mentioned here that the higher efficiency with the increasing number of blades is referring to an inviscid fluid, while for real wind turbines the increase in lift is counter-balanced by the increased drag and it becomes useless (and costly) to add more blades to the rotor.

CHAPTER 3

Wake principles

3.1. Bluff body wakes

A wind turbine can be viewed as a bluff body, which is defined as any non-streamlined body, because of the large wake generated behind it. This section is aimed at giving a brief summary on bluff body wakes.

A characteristic of bluff body wakes is the self-similarity reached far downstream, see e.g. Johansson *et al.* (2003), where the wake development can be described by an appropriate normalisation. This self-similarity state is reached at a downstream distance of the order of 50 diameters and it is of little interest for practical wind farm application. In addition, the tip-vortices shield the wind turbine wake and delay the turbulent mixing with the free stream. Nevertheless the near wake of bluff bodies has been extensively studied, e.g. by Bevilaqua & Lykoudis (1978). They have compared the wakes of a sphere and of a porous disc with the same drag, finding that the self-similar mechanism depends on the initial conditions. The wake "remembers" the shape of the body in the form of the larger eddies which travel downstream. Connected to the large scale vortex shedding from the body is a wake meandering with frequency f , which is usually normalised with a body length and the free-stream velocity to give the Strouhal number:

$$St = \frac{fD}{U_\infty} \quad (3.1)$$

The normalisation with a geometrical scale gives a Strouhal number which is a function of the aspect ratio of the body, as shown by Kiya & Abe (1999) for the wake behind elliptic discs. Miao *et al.* (1997) found that the wake meandering behind discs has no preferred rotational pattern and that the frequency depends on the Reynolds number. The Strouhal number changes with the inclination of the disc (see Calvert (1967)) and it was proved by Castro (1971) and Higuchi *et al.* (1998) that the large scale oscillation (meandering) of the wake behind two-dimensional plates and discs is influenced by the porosity. These effects are important for studying a wind turbine wake since a wind turbine can be simulated by a porous disc, such as in Sforza *et al.* (1981), since momentum is let through the rotor. The porous disc is largely studied also today as a model for a wind turbine in Sørensen *et al.* (1998), Sharpe (2004)



FIGURE 3.1. The smoke is introduced upstream of the rotor and captured by the tip-vortices shed from the blades, marking the helical wake boundary.

and van Kuik (2003). A wind turbine wake can be thought of as a helical structure shed downstream by the flow (figure 3.1 shows a flow visualisation where the tip vortices are clearly seen). The differences with bluff body wakes are evident, but an analytical approach will be used in the next section to describe in detail the wind turbine wake. A description of the numerical methods used to simulate single wind turbine wakes and their interaction, can be found in Crespo *et al.* (1999). The simulation of a wake in yaw is more difficult. From helicopter models, the change of drag distribution on a rotor disc has been studied by Chaney *et al.* (2001), while an engineering model for the load in yawed conditions is described by Schepers (1999). Snel (1998) finds a restoring yaw moment on the rotor and neglects the vorticity diffusion in the wake by using the Euler equations, because of the high Reynolds number involved.

3.2. Wind turbine wakes

3.2.1. Momentum theory

It is possible from so called actuator disc theory to establish an upper limit on the power production for a turbine. This is called the Betz limit and it is based on the mass and momentum conservation over a control volume which includes the turbine. Usually this is done by considering a streamtube as shown in figure 3.2, where the velocity is assumed to be uniform at each cross section of the tube. In a first approximation the wind turbine can be considered acting like a disc, the *actuator disc*, which has an infinite number of blades creating the needed pressure drop. The velocity along a streamline decreases when approaching the disc and therefore the atmospheric pressure p_∞ rises to the value p^+ , according to Bernoulli to balance the velocity decrease. After the discontinuity surface of the actuator disc over which the pressure drops, the pressure again increases from a lower value p^- to the initial, undisturbed value p_∞ . The difference between p^+ and p^- gives the force acting on the disc.

The inflow and outflow boundaries are taken at such a distance that the pressure has recovered to the undisturbed atmospheric pressure (p_∞). The power output of the turbine can be obtained in two different ways, either as

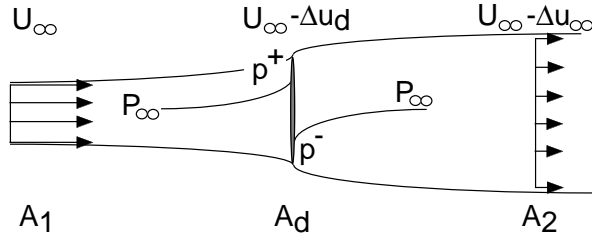


FIGURE 3.2. The wind speed is changed from upstream to downstream due to the presence of the actuator disc, which is represented in the middle of the graph.

the change of kinetic energy per unit time between the inflow and outflow boundaries, or as the force (pressure difference across the turbine times its area) times the velocity at the disc.

However, in the literature it is common that the momentum balance is taken over a streamtube of the form seen in figure 3.2, which in principle is not possible, since also the varying pressure (which is not equal to p_∞) on the mantle area of the streamtube has to be taken into account. It is possible to overcome this problem by considering a much larger streamtube that includes the one passing over the turbine. If the radius of that streamtube is large enough the pressure disturbance on the mantle surface will decay with the distance (r) from the turbine as r^{-2} and there will be no overall contribution from the pressure forces on the momentum balance. This means that the contribution of the pressure forces on the mantle surface in figure 3.2 actually equals $p_\infty \cdot (A_2 - A_1)$, cancelling exactly the pressure force due to the increase in the area at the downstream end of the streamtube.

In order to establish the Betz limit it is necessary to state the equations of conservation of mass and momentum. The mass flow (\dot{m}) which runs through the streamtube enclosing the turbine disc can be written

$$\dot{m} = \rho A_1 U_\infty = \rho A_2 U_2 = \rho A_d U_d \quad (3.2)$$

where A_1 and A_2 are the upstream and downstream areas of the streamtube and A_d is the actuator disc area. Using momentum conservation, the drag D on the turbine can, with the arguments used above, be written as

$$D = \dot{m} U_\infty - \dot{m} U_2 = \rho A_1 U_\infty^2 - \rho A_2 U_2^2 \quad (3.3)$$

By using Bernoulli's equation both upstream and downstream the turbine it is possible to obtain an expression for the pressure difference $p^+ - p^-$ across the turbine such that

$$p^+ - p^- = \frac{1}{2}\rho(U_\infty^2 - U_2^2) \quad (3.4)$$

and the drag on the turbine hence becomes

$$D = \frac{1}{2}\rho A_d(U_\infty^2 - U_2^2) = \rho A_d \left(U_\infty - \frac{\Delta u_\infty}{2} \right) \cdot \Delta u_\infty \quad (3.5)$$

where $U_2 = U_\infty - \Delta u_\infty$, i.e. Δu_∞ is the velocity defect in the wake at the downstream end of the streamtube. Using the same notation, Eq. 3.3 becomes

$$D = \dot{m}(U_\infty) - \dot{m}(U_\infty - \Delta u_\infty) = \dot{m}\Delta u_\infty = \rho A_d(U_\infty - \Delta u_d) \cdot \Delta u_\infty \quad (3.6)$$

where Δu_d is the velocity decrease at the turbine plane. A simple comparison between Eq. 3.5 and Eq. 3.6 gives the result known as Froude's theorem:

$$\Delta u_d = \frac{\Delta u_\infty}{2} \quad (3.7)$$

The total power in the wind, i.e. the kinetic energy passing through a control area A (normal to the wind) per unit time, can be expressed as

$$P_{TOT} = \frac{1}{2}\rho A U_\infty^3 \quad (3.8)$$

The power extracted by the wind turbine on the other hand can be written as

$$P_E = \frac{1}{2}\dot{m}(U_\infty^2 - U_2^2) = \frac{1}{2}\dot{m}[U_\infty^2 - (U_\infty - \Delta u_\infty)^2] \quad (3.9)$$

which after some algebra can be rewritten

$$P_E = \rho A_d (U_\infty - \Delta u_d)^2 \cdot 2\Delta u_d \quad (3.10)$$

The maximum power output is found by searching for the maximum in P_E with respect to the velocity defect at the disc Δu_d . From Eq. 3.10 we obtain

$$\frac{\partial P_E}{\partial \Delta u_d} = 0 \rightarrow (\Delta u_d)_{P_{Emax}} = \frac{U_\infty}{3} \quad (3.11)$$

The maximum power for the actuator disc with no losses, from Eq. 3.10 using Eq. 3.11, can be compared with the energy flux of the wind (Eq. 3.8) in order to obtain the efficiency of a turbine (Betz limit):

$$\frac{P_{Emax}}{P_{TOT}} = \frac{\frac{8}{27}\rho A_d U_\infty^3}{\frac{1}{2}\rho A_d U_\infty^3} = \frac{16}{27} \approx 0.529 \quad (3.12)$$

The power and drag are often expressed in terms of the non-dimensional power coefficient C_P , already defined in Eq. 2.2, and drag coefficient C_D

$$C_D = \frac{D}{\frac{1}{2}\rho A_d U_\infty^2} \quad (3.13)$$

In the Betz limit we find $C_D = \frac{8}{9}$. A measure of the energy extracted from the wind is given by the axial interference factor defined as

$$a = \frac{\Delta u_d}{U_\infty} \quad (3.14)$$

Plugging the result of Eq. 3.7 and the definition in Eq. 4 into Eq. 3.6 we obtain:

$$C_D = 4a(1-a) \quad (3.15)$$

From Eq. 3.10 we have $P_E = D(U_\infty - \Delta u_d)$ and therefore the power coefficient can be rewritten as

$$C_P = C_D(1-a) \quad (3.16)$$

The power and drag coefficients as predicted by the momentum theory as a function of a are shown in figure 3.3. The maximum theoretical C_D is 1, while $C_{P_{max}}$ is the Betz limit. The momentum theory is valid only for $a < 0.5$ or the velocity defect far downstream would be larger than the free-stream velocity: if $a > 0.5$ ($\Delta u_d > 0.5U_\infty$) then $\Delta u_\infty > U_\infty$ as a consequence of the Froude's theorem in Eq. 3.7. For a heavy loading the wind turbine is in the *turbulent-wake state*, with a large backflow region behind the rotor, and for $a > 1$ in the *vortex-ring state*, i.e. a large vortex enclosing the tip of the rotor. In these cases the drag coefficient exceeds 1 and several empirical corrections have been suggested to connect the momentum theory with the experimental data from the vortex-ring state. The correction by Anderson (1979) is plotted in figure 3.3, with the intersection point at $a_T = 0.326$.

The Betz limit is the maximum power for a wind turbine working within the momentum theory model. An apparent contradiction is given by a wind turbine flying on an airplane: the power available to the turbine is $D \cdot U_\infty$, which is the extra work done by the airplane to bring along the turbine. On the other hand, the turbine does work on the fluid with an energy (per unit time) equal to $D \cdot \Delta u_d$ (see Glauert (1926)). Hence the power available to the wind turbine is

$$P_E = D \cdot U_\infty - D \cdot \Delta u_d \quad (3.17)$$

which leads to the result obtained in Eq. 3.16 and therefore to the Betz limit. The air must flow through the actuator disc, otherwise $\Delta u_d = U_\infty$, i.e. $a=1$ and no power can be extracted. In other words, only a porous disc can be used to simulate a wind turbine since for a solid disc it is $C_P=0$.

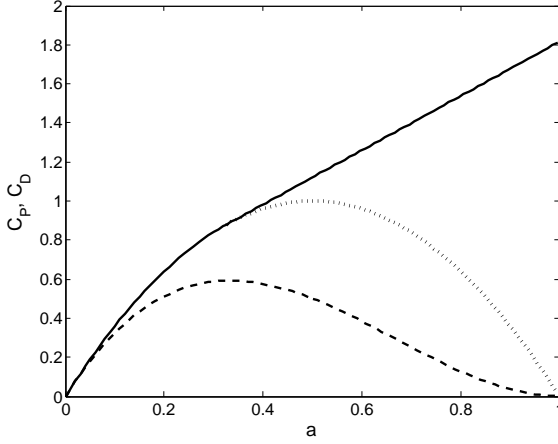


FIGURE 3.3. Results from momentum theory. Solid line: C_D with the correction by Anderson (1979), dotted line: theoretical C_D for $a > a_T$, dashed line: C_P .

Several devices can be used to exceed the Betz limit and among the most interesting is, albeit of difficult practical application, a wind turbine with a frictionless downstream diffuser. The principle is simple: the diffuser can support a force, therefore the pressure p^- downstream of the rotor can be further reduced with respect to the value obtained for the free turbine. The diffuser ensures the pressure recovery at the exit. The velocity at the diffuser exit with cross section A_e can be written as

$$U_e = (U_\infty - \Delta U_d) \frac{A_d}{A_e} \quad (3.18)$$

The drag of the wind turbine with a diffuser is

$$D = A_d \cdot (p^+ - p^-) = A_d \cdot \frac{1}{2} \rho U_\infty^2 \left[1 - \left(\frac{1-a}{\frac{A_e}{A_d}} \right)^2 \right] \quad (3.19)$$

At the Betz limit we have $C_D = \frac{8}{9}$ and $a = \frac{1}{3}$, which means from the equation above that the free wind turbine can be compared to a wind turbine having a diffuser with an aspect ratio of $\frac{A_e}{A_d} = 2$. As for Eq. 3.9, the power extracted by this turbine can be written as

$$P_E = \frac{1}{2} \dot{m} (U_\infty^2 - U_e^2) \quad (3.20)$$

Using Eq. 3.18 and deriving with respect to $U_d = (U_\infty - \Delta u_d)$ it is possible after some algebra to find the maximum power production

$$\frac{P_{Emax}}{P_{TOT}} = \frac{4}{3\sqrt{3}} \approx 0.769 \quad (3.21)$$

A second option is to use a shroud, i.e. an axisymmetric lifting surface, around the rotor. This concept is common between propellers (see e.g. the aero-train in figure 1.3), but it is applicable only to small rotors, thus preventing its use for typical wind turbine sizes. The circulation around the annular wing induces a higher velocity through the turbine, but only if the lift is directed towards the centre of the rotor. A C_P up to 2 is possible according to de Vries (1979), while the calculations by Hansen *et al.* (2000) show that for a shroud which only partially recovers the static pressure is

$$\frac{P_{Emax}}{P_{TOT}} \approx 0.94 \quad (3.22)$$

There are other means to increase the power production: Hütter (1977) considers a flow deflection through the rotor of an angle φ with respect to the symmetry axis. This gives a higher mass flow, and therefore a higher power coefficient, since the velocity through the rotor is $(U_\infty - \Delta u_d)/\cos(\varphi)$. The power gain is quantified by Landahl (1979) for a deflection of $\varphi=35.25^\circ$ as being the double of the Betz limit

$$\frac{P_{Emax}}{P_{TOT}} = \frac{32}{27} \approx 1.185 \quad (3.23)$$

although the practical limitation of such a device are acknowledged by the author himself.

The state-of-the-art of wind turbine technology has increased the power coefficient to values close to 0.5. Future studies can most likely *fine-tune* the wind turbine in order to increase the power production, but the main gain lot more can be done towards the power optimisation from a cluster of wind turbines. The already cited work by Hütter (1977) estimates the turbulent exchange between the outer flow and the wake, predicting a faster wake recovery for heavily loaded wind turbines and a possible reduction of the downstream spacing. On the other hand, for the typical distances between wind turbines in a farm (7 to 9 diameters), a more practical idea may be to extract less energy from an upstream turbine in order to leave more energy for the downstream ones (see Dahlberg (1998) and Corten *et al.* (2003)). Another method is the recently developed Active Wake Control (AWC) by J. Å. Dahlberg and described in detail in **paper 2**. **Paper 1** to **paper 4** focus on wake measurements and aim at improving the power production from a cluster of wind turbines.

3.2.2. Effects of wake rotation on the energy extraction

A complication not taken into account by the momentum theory is that the wake will rotate. This is due to the fact that the flow gives a torque on the turbine, which in turn gives an angular momentum to the flow in the wake, hence the energy extraction creates some kinetic energy related to the wake rotation. In the following we will analyze this effect and show how it affects the possible amount of energy extracted by the turbine.

In a rotating system (with system rotation $\boldsymbol{\Omega}$), the Bernoulli equation can be written

$$p + \frac{1}{2}\rho U_R^2 - \frac{1}{2}\rho (\boldsymbol{\Omega} \times \mathbf{r})^2 = \text{const} \quad (3.24)$$

where the third term on the LHS is the centrifugal body force and \mathbf{U}_R is the velocity vector in the rotating system. The classical Bernoulli equation, i.e. Eq. 3.24 without the rotation term, can be applied along a streamline with $r=\text{const}$. Such a streamline does not exist for a wind turbine, since the streamtube including the turbine is expanding. A more physical interpretation of this equation can be given by considering an absolute reference system (such as the earth) for the wind turbine flow, with $\mathbf{U}_R = \mathbf{U} + (\boldsymbol{\Omega} \times \mathbf{r})$. Substituting into Eq. 3.24 gives

$$p + \frac{1}{2}\rho U^2 + \rho \mathbf{U} \cdot (\boldsymbol{\Omega} \times \mathbf{r}) = \text{const} \quad (3.25)$$

Therefore the energy extraction from the flow, i.e. a change in the total head $H = p + \frac{1}{2}\rho U^2$, is possible only if \mathbf{U} is deflected towards $\boldsymbol{\Omega} \times \mathbf{r}$ during the passage through the rotor. Equation 3.25 states that the azimuthal velocity in the wake is a necessary condition to extract energy, i.e. to obtain the reduction in the total head. The only energy extractor in the flow is the rotating blade(s), which is the only solid surface capable of bearing a torque. Upstream of the rotor there is no energy extractor, therefore no azimuthal velocity and the flow can be considered irrotational.

Glauert (1935) showed that by calculating the torque in each blade section as functions of the local forces assuming an infinite number of blades and a frictionless fluid, it is possible to obtain an expression for the power coefficient which includes the effects of the tangential velocity through the tangential induction factor $a' = v/\Omega r$. The derivation can be found in many text books (see e.g. de Vries (1983)) and it gives the power coefficient as function of the tip-speed ratio λ as

$$C_P = \left(\frac{2}{\lambda}\right)^2 \int_0^\lambda (1-a) a' X^3 dX \quad (3.26)$$

where $X = \lambda r/R$ is the local tip-speed ratio.

A different approach is to use the momentum equations and Bernoulli equation (see de Vries (1979)). It gives the power loss due to the rotation of the wake and it will be shown that the Betz limit derived in Section 3.2.1 can

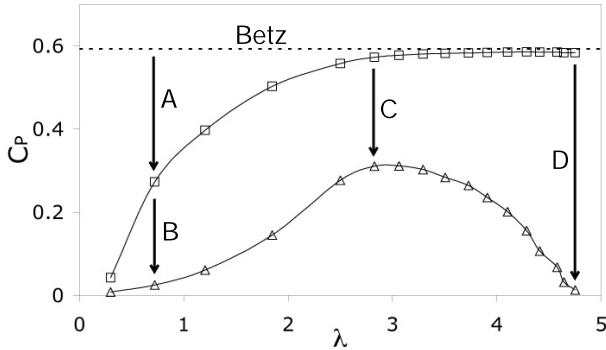


FIGURE 3.4. Power losses. Dashed line: Betz limit, \triangle : C_P for turbine model 3. *A*: rotation effect as from Eq. 3.27, *B*: stall + profile drag + hub losses, *C*: tip-vortex losses + stall at the blade root, *D*: increased profile drag.

be reached only at high λ . For the derivation, we refer to de Vries (1979). The flow is considered axisymmetric and the wake cylindrical, which means a wind turbine with an infinite number of blades, with constant circulation around the blades. We can obtain the maximum power coefficient as

$$C_{P_{max}} = \frac{P_{Emax}}{P_{TOT}} = 4a(1-a)^2 - (1-a) \left(\frac{v_R}{U_\infty} \right)^2 \quad (3.27)$$

The first term is the Betz limit for the one-dimensional momentum theory, while the second is the power loss due to the wake rotation calculated for a cylindrical wake with constant circulation on the blade. It is possible to obtain the v_R from $\Delta H = -\rho\Omega v_R R$, where ΔH is the pressure loss across the rotor. Also the axial induction factor a is obtained directly from the drag on the turbine according to the (non-rotating) momentum theory.

Equation 3.27 can be used to estimate the behaviour of a cylindrical wake with the same total head loss (proportional to the force acting on the rotor) as the turbine model 3 described in Section 4.3.2. The result is plotted in figure 3.4, where the losses from the ideal case ($C_L/C_D = \infty$) are listed. The stall at the blade root for model 3 reduces the power coefficient at $C_{P_{max}}$, but a twisted blade would solve this problem. The contributions of the profile drag and of the hub losses must be included in every point. The increased azimuthal velocity for increasing λ is likely to reduce the stalled blade sections, but in principle the angle of attack on the blade can become negative for high tip-speeds.

3.3. Wind turbine wake meandering

Section 3.1 gives a general introduction on bluff body wakes, while Section 3.2 describes the wind turbine wake from the theoretical point of view. During the measurements described in **paper 2**, a low frequency meandering of the wake was observed. The large scale vortex shedding is well known for discs and spheres, but relatively little is still known about wind turbine wake meandering. Probably the most known case of vortex-induced absolute instability is the Von Karman vortex street behind a two-dimensional cylinder. The ring vortex shed by the disc edge is responsible for the meandering, and Berger *et al.* (1990) observed that a disc oscillating around its axis has a helical mode with a preferred twisting direction opposite to the disc.

A rotating disc can be seen as a wind turbine with an infinite number of blades, or alternatively as a wind turbine with N blades rotating at infinite Ω . The lack of wind tunnel measurements on wake meandering is acknowledged by the already cited work by Crespo *et al.* (1999). Few measurements and all on full-scale turbines have measured the wake meandering. Among the latest, **paper 5** to **paper 7** investigate the influence of the vortex lines shed by a wind turbine wake in controlled conditions. The report by Pedersen & Antoniou (1989) visualised a vortex meandering in the wake of a three-bladed wind turbine and Hassan (1996) mentions a clear low frequency peak in the velocity spectra of the Alsvik wind turbine wakes. More can be understood from the numerical simulations by Okulov & Sørensen (2004), from which figure 3.5 and figure 3.6 are taken. The wind turbine wake meandering seems to be triggered by the interaction between the vortex lines, as it happens for helicopter wakes. The wake pitch is defined as the downstream distance required for one vortex line to complete a 2π rotation. figure 3.6 gives instead the dependency of the stability of the vortex lines on the axial interference factor a and tip-speed ratio λ , both a function of the wake pitch. The axial interference factor depends also on the total circulation of the tip-vortices.

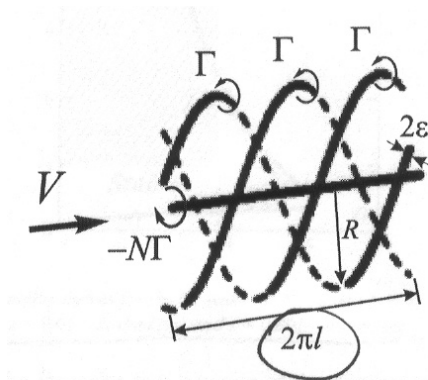


FIGURE 3.5. Scheme of the helical wake from an N -bladed turbine. The vortex core is 2ϵ and the the total circulation is $N\Gamma$.

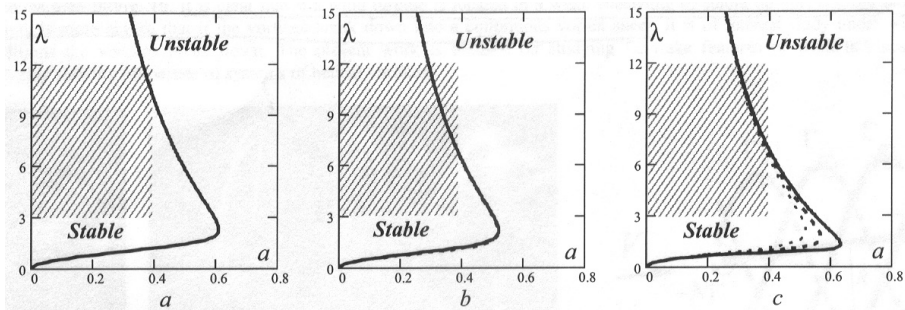


FIGURE 3.6. Neutral stability curves plotted in an axial interference factor vs. λ diagram, from Okulov & Sørensen (2004).
 a): $N = 2$, b): $N = 3$, c): $N = 3$, influence of ϵ .

Experimental Methods

This chapter describes the different experimental techniques as well as the wind turbine models used in the present work in some more detail than has been possible to include in the research papers. Section 4.1 gives a short description of the MTL wind tunnel where most of the experimental work was carried out. Also a short description of LT-5 wind tunnel at FOI is given. The velocity measurement techniques used was both Particle Image Velocimetry (PIV) as well as hot-wire anemometry. Both techniques as they have been implemented in the present work, are described in section 4.2. Several different turbine models have been used during the course of this work and they are all described in section 4.3.

4.1. Wind tunnels

4.1.1. MTL wind tunnel (KTH)

The Minimum Turbulence Level (MTL) wind tunnel at KTH Mechanics, was used in most of the experiments in this work. The tunnel (figure 4.1) is a closed-loop circuit, temperature controlled facility with a velocity speed up to 69 m/s. The test section is 7 m long, 1.2 m wide and 0.8 m high. The roof height of the test section can be adjusted in order to obtain a zero pressure gradient along the test section. The velocity variation achieved along the test section was less than 0.6% of the velocity measured by a Prandtl tube at 8 m/s.

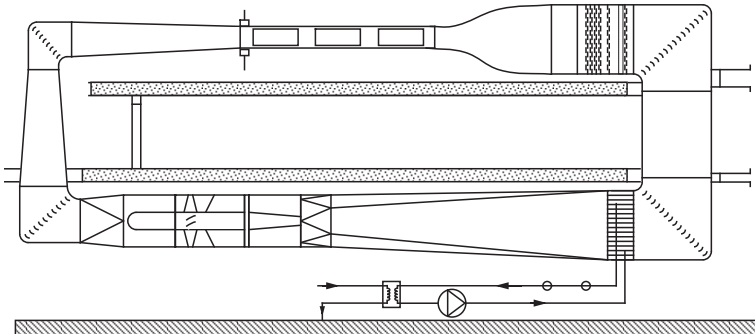


FIGURE 4.1. The MTL wind tunnel layout. The total length is about 25 m and the height is 9 m. The flow is anti-clockwise.



FIGURE 4.2. Test section with traversing system as seen from upstream.

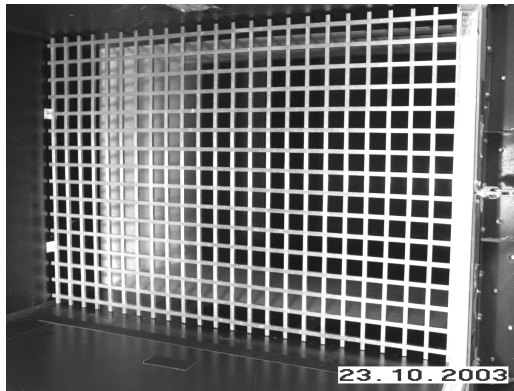


FIGURE 4.3. Turbulence generating grid used in the present experiments.

The Prandtl tube was placed for these experiments at approximately 1 m from the beginning of the test section, and provided the reference velocity for the calibration of the hot wire, as will be described in more detail later. A slot running along the test section length, in the middle of the roof, allows the access of the arm of the traversing system. With the addition of a wing spanning the full tunnel width, 5 degrees of freedom are possible. Added to the spatial x, y, z (i.e. respectively streamwise, vertical and spanwise) are the rotation around the probe axis and the rotation around the y -axis. A photograph of the test section can be seen in figure 4.2.

For some experiments free-stream turbulence was generated by the grid shown in figure 4.3. The grid was fixed to the tunnel walls 0.2 m downstream the start of the test section, creating a turbulence intensity of approximately 4% of the free-stream velocity at the turbine position. The turbulence intensity for the three velocity components as percentage of the free-stream velocity is plotted in figure 4.4 as function of the downstream distance in mm. Without the

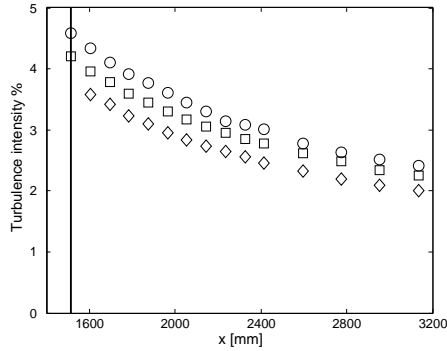


FIGURE 4.4. Turbulence intensity at the test section centre as function of downstream distance for the grid shown in figure 4.3. the grid is placed at $x=200$ mm and the vertical line in the figure represent the position of the turbine. \circ : u_{rms} , \diamond : v_{rms} , \square : w_{rms} .

grid generating the turbulence, the value of the fluctuations in the streamwise direction was less than 0.1% of the velocity at 8 m/s.

A heat exchanger with a feedback control gives a stable temperature with an accuracy of ± 0.5 degrees by means of water cooling. The temperature is set manually at the control panel of the tunnel. Both the tunnel velocity and the traversing system are controlled by Labview programs. Also the data acquisition routines are Labview controlled. For more details about the MTL wind tunnel, the reader is referred to Lindgren (2002).

4.1.2. LT-5 wind tunnel (FOI)

The LT5 wind tunnel at FOI were mainly used for the drag interference measurements reported in **paper 2**. Figure 4.5 shows the test section, the flow is from right to left. This open-loop wind tunnel has a test section 2.5 m long, with a cross section of $0.9 \text{ m} \times 0.675 \text{ m}$. The velocity range is between 5 m/s and 16 m/s, and the tunnel is run by a centrifugal fan downstream of the test section. At the intake section, a grid helps to reduce the turbulence level. After a short contraction, the test section starts and the turbulence level is approximately 0.3% of the free-stream velocity. The wind speed in the centre of the test section is found as the difference between the total pressure in the contraction and the static pressure given by four pressure taps, two upstream and two downstream the model position.

4.2. Measurement techniques

For the wake measurements, two techniques have been used: Particle Image Velocimetry (PIV) and hot-wire anemometry. In the described experiments,

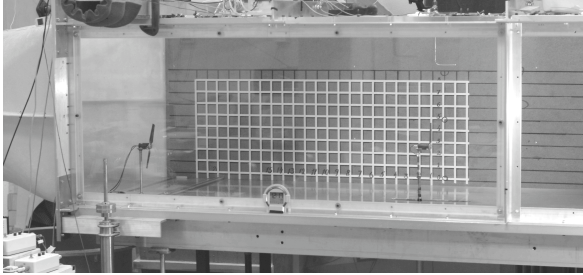


FIGURE 4.5. The test section of the LT5 wind tunnel at FOI.

PIV gave an overall picture of the flow whereas the mean flow statistics were measured with hot-wire anemometry. Below follows a short description of the present set-ups for these two techniques.

4.2.1. Particle Image Velocimetry

The principle of PIV is simple: the speed of a particle is obtained from the distance travelled during a certain time. If particles are added to the flow and they follow the flow, recordings of the particle paths allow us to obtain the velocity field.

In the present experiments the particle motions are recorded with a CCD camera where a laser sheet perpendicular to the camera lights the flow with the particles, i.e. the particles are imaged in one plane. The movements of the particles are registered between two times, t and $t + \Delta t$. In this way the particles are allowed to move somewhere between 0.1 and 1 mm. The post-processing software divides the image in several rectangular regions, the so-called *interrogation areas*. In each of these areas the particle positions between the two recordings are correlated, resulting in the most probable displacement vector (figure 4.6) during the time Δt .

Some of the factors that have to be set for each type of experiment are the choice of the particles and the time delay between the recordings. The particle size, the concentration in the fluid and body forces on the particles (if in very low speed flows) must also be considered in order for the particles to properly track the flow. In our experiment, propylene glycol oil with an average particle diameter of about $2 \mu\text{m}$ has been used to seed the flow, and a 400 mJ Nd:YAG laser has been used as the light source. The time between the two recordings has to be short enough so that only few particles exit the interrogation area. Such a particle has an effect on the signal-to-noise ratio, since its "true" correlated position is not detected. A reliable cross-correlation requires a minimum of 5 particles per interrogation area, and the size of the particles should be at least three pixels on the image in order to pick its correct position. As a rule of thumb the estimated displacement of a particle should not exceed 30% of the side length of the interrogation area. Measuring in regions with large velocity

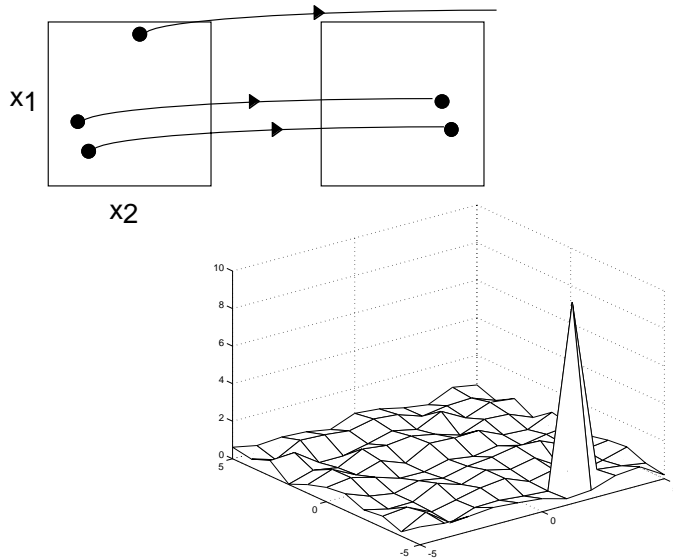


FIGURE 4.6. The correlation principle used in PIV. The sequel of two images from the CCD camera gives the most probable displacement vector in each interrogation area.

gradients can be a source of problems, since the output vector is an average over the interrogation area (therefore the gradient may be somehow smeared) and the time chosen for the capturing should be different for different regions of the layer.

The acquisition frequency is mainly imposed by the frequency of the laser (maximum of 17 Hz), which is also the frequency between each pair of images. The CCD camera has 1018×1008 pixels, and was divided in interrogation areas with 64×64 pixels. The side of each interrogation area depends on the region focused by the camera.

4.2.2. Hot-wire anemometry

Hot-wire anemometry is a technique where a thin wire (e.g. $5 \mu\text{m}$ in diameter and 1 mm long) of platinum is heated up to 100-200 degrees above the ambient temperature. In Constant Temperature Anemometry (CTA) the wire is the fourth arm of a Wheatstone bridge. Depending on the local speed experienced by the wire, its resistance changes, and so does the voltage needed to balance the bridge. The voltage is a function of the velocity value, and the law describing this relation for one-component velocity measurements is known as the *modified*

King's Law, see Johansson & Alfredsson (1982):

$$U = k_1(E^2 - E_0^2)^{\frac{1}{n}} + k_2\sqrt{E - E_0} \quad (4.1)$$

where E is the measured voltage, E_0 the voltage at zero velocity, and k_1 , k_2 , n are the coefficients from the calibration. The wire is soldered to two prongs which are shaped in order to reduce their influence on the flow.

Using two wires placed approximately 45 degrees with respect to the flow direction, the two velocity components can be calculated as combination of the voltages output from the wires. Such a probe is called an X-probe and a photograph of one of the probes used (and built at KTH Mechanics) is shown in figure 4.7. The size of the measurement volume is 1 mm³. In the calibration, the probe is turned to a known angle (from -40° to $+40^\circ$) with respect to the free-stream velocity (from 1 m/s to 18 m/s) measured by a Prandtl tube. Two 2-dimensional fifth order polynomials are fitted to the voltages and the coefficients are calculated with the least square method. A typical calibration map is shown in figure 4.8.

Calibration points were taken down to a free-stream velocity of 1 m/s. If lower velocities need to be measured by the hot-wire, this is not a problem when the modified King's law is used (Eq. 4.1). The polynomials must instead include the velocity range of the measurements. The reason is that the fitting polynomials are not reliable outside the calibration range, since they can diverge to infinity. A solution was found in order to include also the points for velocities lower than the allowed minimum of 1 m/s. The voltages from each wire, having in common the same angle with respect to the wind direction, were fitted to the modified King's law. In this way, the voltage values for lower velocities (namely 0.2 m/s and 0.5 m/s) were extrapolated and inserted in the calibration map of the X-wire. Differences were noticeable with the calibration corrected in this way.

4.3. Turbine models

The main advantage of doing simulation of wind turbines in a wind tunnel, as compared to field measurements, is the controlled flow conditions. On the other hand, the Reynolds number cannot be matched: the difference in chord is evident and wind speed must be kept low to avoid too high rotational speed. The latter may be a source of problem, since the centrifugal forces can modify the boundary layer on the blades and the development of the wake itself. On the other hand, as mentioned by Vermeer *et al.* (2003), measurements at low Reynolds number are suitable for comparison with numerical models as long as an appropriate wing profile is chosen.

The power output of the turbine can simply be measured from the current and voltage across the generator. However in this case the internal friction as well as losses in the generator are not taken into account. By instead calibrating the generator to obtain the torque from the current it is possible to get the aerodynamic power efficiency.



FIGURE 4.7. One of the X-wire used in the experiments. The flow is from right and the measuring volume is a cube with a side length of 1 mm.

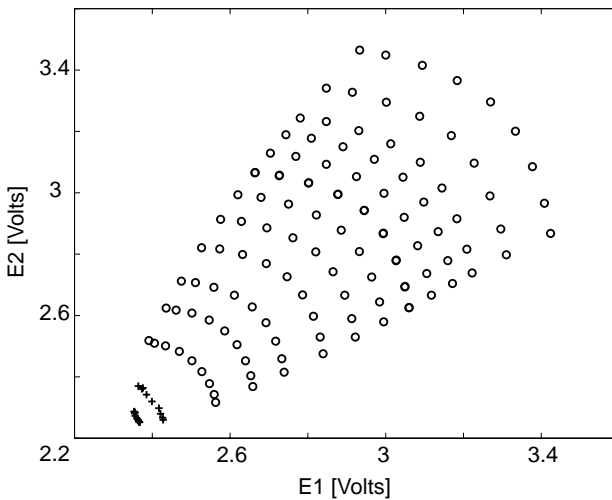


FIGURE 4.8. X-wire calibration map, where the two wires voltages are shown on the abscissa and ordinate, respectively. The circles represent calibration points from 1 m/s to 18 m/s and in 10° intervals with $\pm 40^\circ$. The crosses are the values extrapolated using the modified King's law at 0.2 m/s and 0.5 m/s.

The drag force measurements were carried out using a strain-gauge balance in the support of the model. When a load is applied, the deformation changes the resistance of the strain-gauge. The calibration was made by fixing a known weight acting along the shaft of the generator, where also the rotor acts. The calibration curve can be seen in figure 4.9. The weights were measured by a

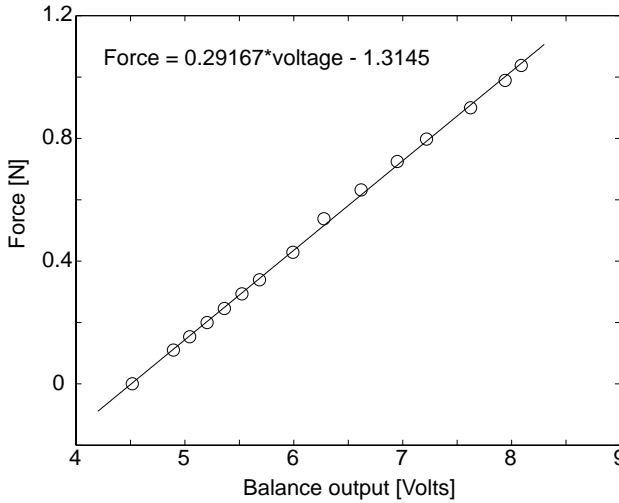


FIGURE 4.9. Drag balance calibration curve with calibration points.

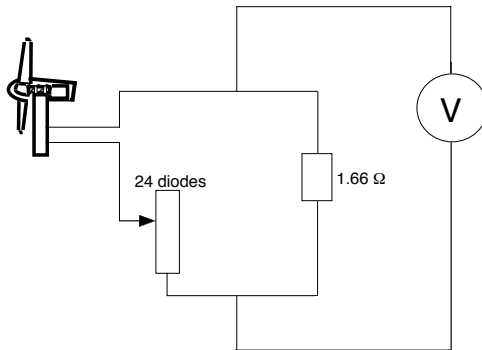


FIGURE 4.10. Scheme of a load circuit connected to the DC generator of the wind turbine.

precision balance, with an accuracy of the order of a milligram. The calibration shows a linear relation between the load and the electrical output from the balance.

A typical loading circuit is shown in figure 4.10. The circuit can have a number of diodes or equally a variable resistor to change the braking torque at the shaft.

4.3.1. *Turbine model 1*

The turbine model 1 is used in **paper 1**. Its diameter is 0.25 m, it has two blades and high solidity (14%). The characteristics of the turbine are shown in table 4.1.

The nacelle accommodates a generator and the turbine was controlled by a load circuit. This system enabled the change of the rotational frequency keeping the free-stream velocity constant. In this case the power output was calculated as product of the voltage and the current from the generator. The rotational frequency was measured using an optical device fixed under the nacelle, giving an electrical impulse at each blade passage. The turbine was tested at different heights from the floor: 0.248 m, 0.305 m and 0.4 m. No differences were noticed between these cases, so the chosen height was that with the turbine in the middle of the test section.

A photograph of the turbine model is shown in figure 4.11. The power coefficient for this turbine is shown in figure 4.12. The turbine tip speed ratio

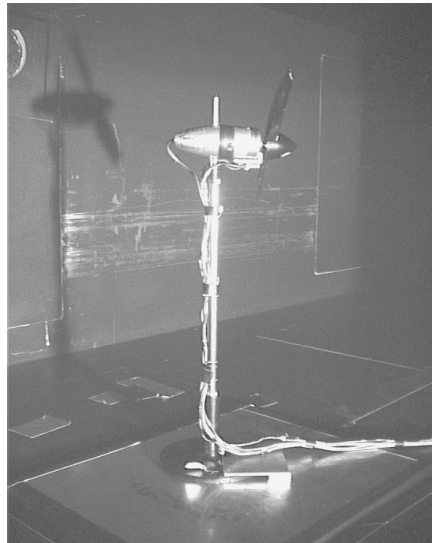


FIGURE 4.11. Turbine Model 1

r/R	Chord [mm]	Twist [deg]
0.25	32	15
0.50	35	11
0.75	31	5
1	25	3

TABLE 4.1. Turbine model 1 characteristics.

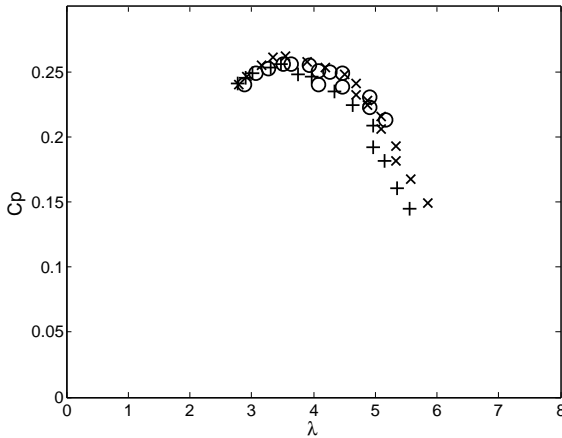


FIGURE 4.12. The power coefficient (C_p) versus tip speed ratio (λ) for three different free-stream velocities. +: $U_\infty=5.65$ m/s, x: $U_\infty=6.7$ m/s, O: $U_\infty=8$ m/s.

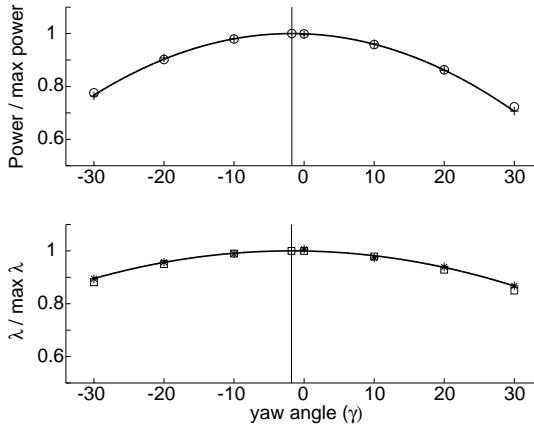


FIGURE 4.13. Power output and tip speed ratio (λ) vs. yaw angle at $U_\infty=6.3$ m/s. The measurement points (+) are normalised with the maximum value obtained from each fitting curve. The squares denotes $\cos \gamma$, the circles denotes $\cos^2 \gamma$.

during the experiments was set such that the turbine operated close to its maximum power coefficient.

When the loading circuit is open, the turbine is free-running: no current flows through the circuit (i.e. no power is produced), and the torque has only

to overcome the internal friction of the rotating parts. Therefore the rotational speed is at the maximum value. The open circuit can be achieved by also increasing the variable resistance to a value where the generator is unable to produce a current through the circuit. The opposite situation is when the resistance is zero, or the circuit is short-circuit.

4.3.1.1. *Yaw dependence*

Another characteristic investigated for this wind turbine is the variation of the power with respect to the flow angle. In figure 4.13 the variation both of C_p and the tip speed ratio is shown for turbine model 1 keeping the loading constant. Both the power curve and the tip speed ratio as function of the yaw angle showed a symmetric behaviour after a small offset was applied. The -1.8 degrees offset may be due to an asymmetry in the turbine behaviour because of the direction of rotation. For this model the variation of the output power is nearly proportional to the square of $\cos \gamma$, whereas the tip speed ratio varies linearly with $\cos \gamma$ when the loading on the turbine was constant.

4.3.2. *Turbine model 2*

A second turbine, built at FOI, was used in other sets of measurements in **paper 2**, **paper 3**, **paper 5** and **paper 7**. Its diameter is 0.18 m, and as the previous one it is two-bladed. For this turbine the blades are straight (i.e. no twist) and they are built out of four layers of carbon fibres giving a final

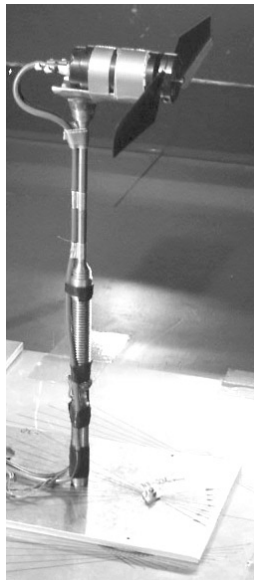


FIGURE 4.14. Turbine model 2.

thickness of 0.5 mm. The profile is based on the Göttingen 417A airfoil, chosen for its good performance at low Reynolds number. The chord at the tip is 16 mm and the maximum chord is 27 mm, at 12% of the radius. The solidity is 13%. The blades are attached by a screw, 3 mm in diameter, to the 23 mm diameter nacelle. These screws allow the setting of the pitch angle of the blades, defined as the line connecting the leading edge to the trailing edge at 85% of the radius. A designated set-up was built at FOI to fix the pitch angle (see Montgomerie & Dahlberg (2003)) and allows an accuracy of ± 0.05 degrees.

The blade pair is connected to a 24V DC motor that works as a generator. In this case the torque was calibrated versus the output voltage and was shown to be a straight line. Hence the aerodynamic power produced by the turbine can be calculated by measuring the generator voltage and the rotational speed.

The other important characteristic for a wind turbine is the drag¹ coefficient. The results e.g. in **paper 3** show how the drag coefficient first increases with the tip speed ratio and then tends to level out at a value which is of the order of 0.9. During the experiments, the running conditions for the turbine, such as power and drag coefficients, were measured and compared before and after. No change was observed, proving that the model had stable characteristics during the maximum 30 hours measurements period. Details on the blade geometry can be seen in the Appendix of **paper 5**.

A development of this turbine is the turbine model 3 shown in figure 4.15 and used in **paper 3**, **paper 4** and **paper 7**. The hub has been built on the same design of the two-bladed turbine to allow the pitch setting of the blades. The power and drag characteristic have been studied for a blade pitch angle from 8° to 12° . The power coefficient increases and the drag coefficient decreases with the pitch only up to 11° .

4.3.3. *Turbine model 4*

This subsection aims at presenting a concept more than a turbine model and it is not reported in any of the appended papers. The measurements followed from an idea by J. Å. Dahlberg and they were inspired by the claim by Enercon that with a large blade root up to the hub, the power was increased by 12-15% (see Enercon (2004)). They aimed at understanding the effect of the hub on the power production. We tested two wind turbine configurations, both two-bladed, in the MTL wind tunnel: rotor A was based on the blades built at FOI, described in subsection 4.3.2. The second configuration (rotor B) consisted of a twisted blade, built for airplane models and available in hobby stores. The diameters of the rotors were 199 mm and 187 mm respectively. A rod 4 mm in diameter was connecting the two blades, allowing the flow through the centre of the rotors. By means of a 70 mm long sting, the rotors could be connected to the generator and therefore loaded with a negligible aerodynamic influence of the breaking apparatus. The turbine with the twisted blades is shown in figure 4.16. Power and drag measurements were performed both on the turbines

¹As already mentioned the drag of the turbine is sometimes denoted as thrust.



FIGURE 4.15. Turbine model 3.

in the *no-hub* configurations described above, but also after adding a hub in the form of half a table-tennis ball with a diameter of 40 mm. The characteristics of the turbines as a function of the tip-speed ratio are shown in figure 4.17. Rotor B has a consistent gain in the power coefficient of the order of 4% in the region of the maximum, whilst the non-twisted blade rotor performs worst with the hub. More investigations were therefore carried out on the flow. The set-up is the same as described in **paper 4**: the PIV measurements were made the turbines at their $C_{P_{max}}$. The results show a considerable change in the radial velocity field, but very little changes in the streamwise velocity: the flow is accelerated only close to the root because of the presence of the hub. It will be shown in **paper 3** that the flow at the root of the FOI non-twisted blade is separated, therefore the flow close to the hub does not influence the power production.



FIGURE 4.16. Model 4, rotor B as seen from upstream, *no-hub* configuration.

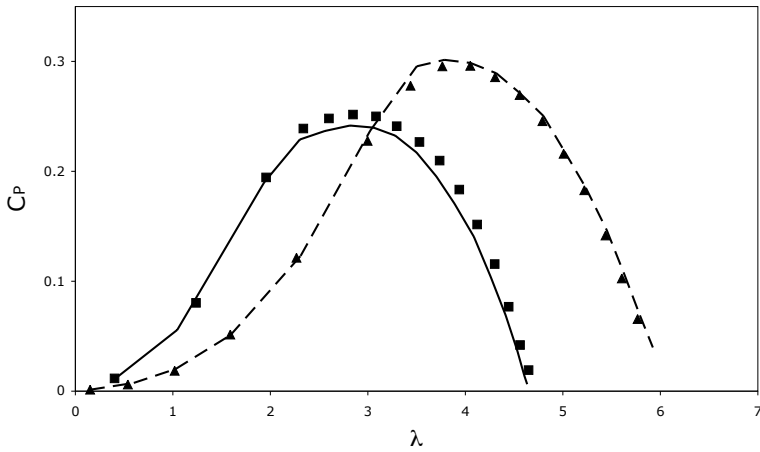


FIGURE 4.17. Power as a function of the tip-speed ratio, the solid symbols are for the configuration with the hub. ■: twisted blade, ▲: non-twisted Göttingen 417A airfoil.

CHAPTER 5

Summary of papers and authors contributions

The thesis is based on the following seven papers.

Paper 1

Parkin, P., Holm, R. and Medici, D. “The application of PIV to the wake of a wind turbine in yaw”, Proc. 4th International Symposium on Particle Image Velocimetry, Göttingen, 2001.

The experiment was led by PP and RH. The data processing and analysis was done by DM supervised by PP. The paper was written by PP and RH, whereas DM analysed the data.

Paper 2

Dahlberg, J. Å. and Medici, D. “Potential Improvement of wind turbine array efficiency by active wake control (AWC)”, Proc. European Wind Energy Conference, Madrid, 2003.

The work was equally divided between the authors. The original idea of AWC was by JÅD.

Paper 3

Medici, D. “Influence of the number of blades on the wake of a wind turbine model”.

Paper 4

Medici, D. “The upstream flow of a 3-bladed wind turbine model in yaw”.

Paper 5

Medici, D. and Alfredsson, P.H. “Measurements on a wind turbine wake: 3D effects and bluff-body vortex shedding”, Wind Energy. Published online.

The measurements were performed by DM, as well as the data analysis. The paper was written together with HAL.

Paper 6

Medici, D. and Alfredsson, P.H. “Wind Turbine Near Wakes and Comparisons to the Wake Behind a Disc”, AIAA-paper-205-0595.

The measurements were performed by DM, as well as the data analysis. The paper was written together with HAL.

Paper 7

Medici, D. “A note on the frequency of wind turbine wake meandering”.

5.1. Summary of papers

In **paper 1** the near wake downstream a rotating wind turbine model is studied using PIV, both with the turbine normal to the free stream direction and under yawed conditions. It is shown that yawing the turbine makes the wake deflect towards the side of the downstream blade, in response to a force perpendicular to the wind direction. The PIV used in the experiment allowed several instant pictures of the flow, and in specific of the tip vortices. The vortices, together with the rotation of the wake, seem to make the difference with the wake from another bluff body, as if the wake can be frozen until these vortices are particularly strong and easily detectable. The effect of yawing can be seen in the mean velocity values, which are known every few millimetres thanks to the technique used for the measurements. The velocity in a chosen point can even double when the wake moves away.

In **paper 2** various effects on a single turbine under yaw is studied as well as the interaction between two turbines by traversing one turbine in the spanwise direction downstream an undisturbed turbine. In this way a direct measure of the power interference can be obtained, showing itself in terms of “power wakes”. The effect of yaw on the power deficit is studied and a model for a wind farm is used to predict the effect of active yaw control. It is shown that for a six turbine station an increase in power of about 4% can be achieved.

Paper 3 describes in detail the changes in the wake as a consequence of the number of blades. Wind turbines with two and three blades have been studied in connection with their commercial production, while the one-bladed turbine has a more fundamental importance: the helical wake can be clearly visualised since the vortex lines shed by the blade tip are far from each other. The multi-bladed turbine, although with the same pitch, shows on the other hand a high mixing in the wake. The velocity field has been measured up to 9 diameters downstream for some chosen conditions and at $x/D = 1$ as a function of the tip-speed ratio. The shape of the wake seems to change dramatically in the central region and becomes deeper for high λ .

All the previous papers dealt with the near or far wake, while **paper 4** focus on the flow immediately upstream of the rotor. The 3-bladed turbine has been yawed and the flow is proved to be two-dimensional up to typically 3-4 mm from the blades, where the viscosity induces the rotation of the flow. The reduction of the power with the yaw angle goes with the cube of the wind speed, but this coefficient is highly dependent on the number of blades. The paper shows that the momentum theory can be successfully applied upstream of a rotating wind turbine.

In **paper 5** the wind turbine wake is studied using two component hot-wire measurements. It is shown that the wake from a single wind turbine exhibits a large degree of non-symmetry with respect to the central axis when yawed. The effect of free stream turbulence is also studied. An unexpected and interesting phenomenon was observed during the measurements, namely a large scale motion of the wake which reflects itself in low frequency variations as detected by the hot wire measurements. The frequency, if expressed as a Strouhal number, is similar to what one would expect for shedding behind a solid disc and it was concluded that the turbine sheds vortices in a similar way as a disc. It was hypothesized that the meandering of the wake observed behind full scale turbines is due to such vortex shedding.

Paper 6 compares the meandering frequencies of the two-bladed model of paper 5 to the meandering behind porous discs. It was observed that the Strouhal number depends on the tip-speed ratio and tends to the values given by porous discs. A turbine in yaw increases the low-frequency shedding in a similar way as a solid disc. In this respect, the vortex ring behind a disc can be seen as the limit for $\lambda \rightarrow \infty$ of the vortex structures behind a wind turbine. The meandering frequency behind a disc disappears for high porosity, as showed also by Castro (1971).

In order to further investigate the parameters influencing the meandering, the measurements presented in **paper 7** were performed in the wake of turbines with different number of blades, blade pitch and tip-speed ratio. The meandering frequency was observed to change for the different configurations, although a connection with the drag coefficient was not established. At the same time, the low frequency showed to be dependent on the number of blades, suggesting a link to the blade passage frequency. This finding is in agreement with the theory, according to which the wake meandering depends on the wake pitch (a measure of the distance between the vortex lines), on the axial interference factor and on the vortex strength.

Acknowledgements

This work was mainly financed under the Vindforsk program of the Energy Agency of Sweden (STEM) and for the final crucial months by Elforsk, for both of which I am very grateful.

I want to thank first my supervisor Prof. Henrik Alfredsson for his advice and help during my course of studies. His contributions have always taught me something important.

Jan-Åke Dahlberg has had a crucial role during these years. Thank you for your help, enthusiasm and friendship. My work would not have been possible without your assistance. Sven-Erik Thor and Björn Montgomerie are also acknowledged for their many fruitful discussions and help. I also want to thank Prof. Jens Sørensen for his comments and for many discussions on wake meandering.

Prof. Y. Kohama and Dr. S. Yoshioka are acknowledged for the assistance and the welcome provided during the 21st Century COE internship at the Tohoku University, Sendai, Japan.

Marcus Gällstedt and Ulf Landén always made my ideas a reality. Dr. Nils Tillmark is acknowledged for his assistance and help with many problems.

Luca F. and Marco have become true and important friends. A special thanks goes to Leandro for his friendship and for the Wednesdays lunches.

Many other people need to be mentioned: Luca B., Ramis the runner, Mike, Fredrik, Jens and everybody in the Lab and at the Department. Jun and Kristian: thank you for the great time in Stockholm and in Tokyo.

My Swedish journey started seven years ago and I will never forget all the friends that made my time here worthwhile. The months during my Nippo-Kiwi-Aussie journey were unforgettable, thanks to everyone who made it so special and sharpened my English listening!

Last but not least, I would like to mention the same people who have been there for me over the years. Despite the distance, we are even closer. Thanks to my brother Dario, to Cesare, Luca S. and Guido.

Grazie alla mia famiglia per il supporto durante tutti questi anni.

Bibliography

- ANDERSON, M. B. 1979 Horizontal axis wind turbine in yaw. In Proc. First BWEA workshop, Cranfield, pp. 57–67.
- BERGER, E., SCHOLTZ, D. & SCHUMM, M. 1990 Coherent vortex structures in the wake of a sphere and a circular disk at rest and under forced vibrations. *J. Fluids Struct.* **4**, 231–257.
- BEVILAQUA, P. M. & LYKODIS, P. S. 1978 Turbulence memory in self-preserving wakes. *J. Fluid Mech.* **89**, 589–606.
- CALVERT, J. R. 1967 Experiments on the flow past an inclined disk. *J. Fluid Mech.* **29**, 691–703.
- CASTRO, I. P. 1971 Wake characteristics of two-dimensional perforated plates normal to an air-stream. *J. Fluid Mech.* **46**, 599–609.
- CHANEY, K., EGGERS, A. J., MORIARTY, P. J. & HOLLEY, W. E. 2001 Skewed wake induction effects on thrust distribution on small wind turbine rotors. *J. Solar En. Engng.* **123**, 290–295.
- CORTEN, G. P., SCHAACK, P. & EECEN, P. 2003 Heat and flux. In *Proc. European Wind Energy Conference and Exhibition*, Madrid, (published on CD).
- CRESPO, A., HERNÁNDEZ, J. & FRANSEN, S. 1999 Survey of modelling methods for wind turbine wakes and wind farms. *Wind Energy* **2**, 1–24.
- DAHLBERG, J. Å. 1998 Möjligheter och risker med stora vindfarmer till havs (in Swedish). Presented at *Vind-98*, CTH, Göteborg, Sweden.
- ENERCON 2004 Wind blatt, issue 03/2004. Enercon Magazine.
- GLAUERT, H. 1926 *The elements of airfoil and airscrew theory*. Cambridge University Press.
- GLAUERT, H. 1935 Windmills and fans. In *Aerodynamic Theory* (ed. F. W. Durand). Springer.
- GRUBB, M. J. & MEYER, N. I. 1993 *Renewable Energy Sources for fuels and electricity*. Island Press, Washington DC.
- HANSEN, M. O. L., SØRENSEN, N. N. & FLAY, R. G. J. 2000 Effect of placing a diffuser around a wind turbine. *Wind Energy* **3**, 207–213.
- HASSAN, G. 1996 Dynamic loads in wind farms ii. Final report Joule Project, JOU2-CT92-0094.
- HASSAN, G. 2005 Wind Guangdong. Greenpeace scientific report.
- HIGUCHI, H., ZHANG, J., FURUYA, S. & MUZAS, B. K. 1998 Immediate and near wake flow patterns behind slotted disks. *AIAA Journal* **36**, 1626–1634.
- HÜTTER, U. 1977 Optimum wind-energy conversion systems. *Annu. Rev. Fluid Mech.* **9**, 399–419.

- IEA 2005*a* Key world energy statistics. Technical Report, IEA statistics.
- IEA 2005*b* Wind energy annual report 2004. Technical Report, IEA statistics.
- JOHANSSON, A. V. & ALFREDSSON, P. H. 1982 On the structure of turbulent channel flow. *J. Fluid Mech.* **122**, 295–314.
- JOHANSSON, P. B. V., GEORGE, P. B. V. & GOURLAY, M. J. 2003 Equilibrium similarity, effects of initial conditions and local Reynolds number on the axisymmetric wake. *Phys. Fluids* **15**, 603–617.
- KIYA, M. & ABE, Y. 1999 Turbulent elliptic wakes. *J. Fluid Struct.* **13**, 1041–1067.
- VAN KUIK, G. A. M. 2003 An inconsistency in the actuator disc momentum theory. *Wind Energy* **7**, 9–19.
- LANDAHL, M. T. 1979 Momentum theory analysis of unconventional wind extraction schemes. FFA technical note, AU-1499 part 10.
- LEMONICK, M. D., FONDA, D. & DOWNIE, A. 2005 The future of energy. Time magazine, October 2005.
- LINDGREN, B. 2002 Flow facility design and experimental studies of wall-bounded turbulent shear-flows. PhD thesis, TRITA-MEK Tech. Rep. 2002:16, Dept. Mech., KTH, Stockholm, Sweden.
- MIAU, J. J., LEU, T. S., LIU, T. W. & CHOU, J. H. 1997 On the vortex shedding behind a circular disk. *Exp. Fluids* **23**, 225–233.
- MONTGOMERIE, B. & DAHLBERG, J. Å. 2003 Vortex system studies on small wind turbines. FOI scientific report, ISRN FOI-R-0936-SE.
- OKULOV, V. L. & SØRENSEN, J. N. 2004 Instability of the far wake behind a wind turbine. In *Proc. XX ICTAM*, Warsaw, Poland.
- PARFIT, M. 2005 Future power. National Geographic magazine, August 2005.
- PEDERSEN, T. F. & ANTONIOU, I. 1989 Visualisation of flow through a stall-regulated wind turbine rotor. *Wind Engng.* **13**, 239–245.
- SCHEPERS, J. G. 1999 An engineering model for yawed conditions, developed on the basis of wind tunnel measurements. AIAA paper 99-0039, 18th ASME Wind Energy Symp., and 37th AIAA, Aerospace Sciences Meeting and Exhibit, Reno, also published in *Collection of Technical papers* (A99-17151 03-44).
- SCHEPHERD, D. G. 1990 Historical development of the windmill. NASA paper DOE/NASA/5266-1.
- SFORZA, P. M., SHEERIN, P. & SMORTO, M. 1981 Three-dimensional wakes of simulated wind turbines. *AIAA J.* **19**, 1101–1107.
- SHARPE, D. J. 2004 A general momentum theory applied to an energy-extracting actuator disc. *Wind Energy* **7**, 177–188.
- SNEL, H. 1998 Review of the present status of rotor aerodynamics. *Wind Energy* **1**, 46–69.
- SØRENSEN, J. N., SHEN, W. Z. & MUNDUATE, X. 1998 Analysis of wake states by a full-field actuator disc model. *Wind Energy* **1**, 73–88.
- VERMEER, L. J., SØRENSEN, J. N. & CRESPO, A. 2003 Wind turbine wake aerodynamics. *Prog. Aerospace Sci.* **39**, 467–510.
- DE VRIES, O. 1979 Fluid dynamic aspects of wind energy conversion. AGARD publication, AGARDograph 243.
- DE VRIES, O. 1983 On the theory of the horizontal-axis wind turbine. *Annu. Rev. Fluid Mech.* **15**, 77–96.

Part 2

Papers

Paper 1

The application of PIV to the wake of a wind turbine in yaw

By P. Parkin, R. Holm and D. Medici

KTH Mechanics, SE-100 44 Stockholm, Sweden

Proc. 4th International Symposium on Particle Image Velocimetry, Göttingen, 2001.

PIV has been used in a wind tunnel study of the wake of a 0.25 m diameter two bladed model horizontal axis wind turbine (HAWT). Velocity fields of the wake from one to five rotor diameters downstream of the wind turbine model are shown, both with the turbine aligned in the flow and yawed. Data analysis is mainly based on time averaged velocity profiles of the wake for a range of yaw angles $[0^\circ, \pm 10^\circ, \pm 20^\circ, \pm 30^\circ]$ in a plane parallel to the flow. Results show the size and persistence of the velocity deficit and tip vortices in the wake, and the wake deflection in yaw. It is shown that active control of turbine yaw angles could be an advantage for overall maximization of power output from wind farms.

1. Introduction

Wind power is now an established alternative to more conventional electrical power generation. To economise the utilisation of wind power, it is usual to group several units together in parks. Design criteria have to be developed for the interspacing of turbines to minimise interference between nearby turbines. Thus an understanding of wind turbine wakes is important. Even with careful placement of wind turbines within a wind park some interference, particularly at non-predominant wind directions, is inevitable. When a wind turbine is yawed the wake is deflected. Therefore, with the further understanding of wind turbines wakes in yaw, there is the possibility of actively controlling the yaw angle of an upstream turbine to steer the wake away from downstream turbines, thereby maximising the power output from the wind farm as a whole.

Wind turbines extract energy from the wind, therefore there is a consequential momentum loss downstream. In addition, previous gross wake investigations (e.g. Pedersen & Antoniou (1989)) have shown the wake to be dominated by tip vortices trailing from the blades, which later break down creating turbulence. Several aspects determine the wake development, such as the turbine operating conditions, the turbulence level in the flow field, the boundary layer shear and the distance to the ground plane. Hot-wire experiments by Alfredsson & Dahlberg (1979) investigated the velocity deficit in the wake from

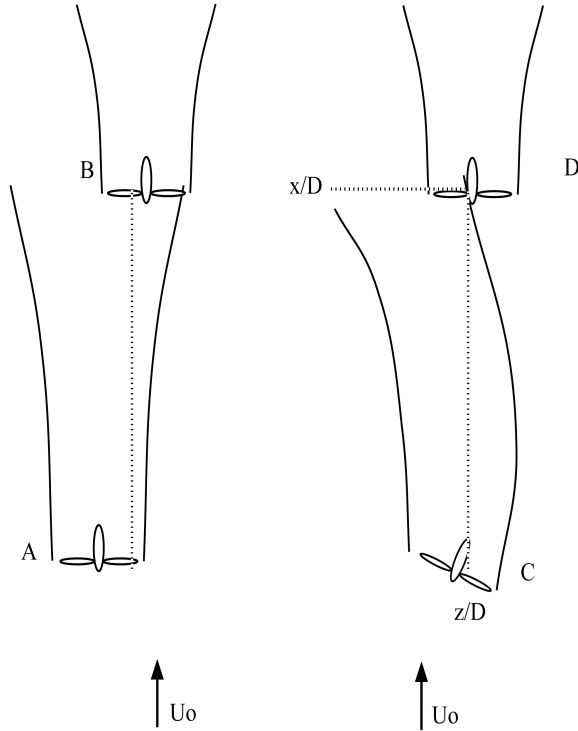


FIGURE 1. Turbine B is heavily disturbed by an unyawed turbine A. On the other hand, by yawing turbine C turbine D can work under much more favorable conditions compared to turbine B.

two to six diameters downstream in different free stream turbulence intensities, whilst Alfredsson & Dahlberg (1981) made interference measurements with two and three turbines in a wind tunnel. These and studies by Vermeulen (1980), Sforza *et al.* (1981), Ross & Milborrow (1985) and Smith & Taylor (1991) enabled simple interspacing models for wind farms to be formed. No experiments were performed with turbines operating in yaw, however.

The gross wake deflection in yaw was shown by Clayton & Filby (1982), who performed hot-wire measurements in the wake of a wind turbine at a number of downstream positions. PIV measurements in the near wake (up to one diameter downstream) by Grant *et al.* (1997) and Grant & Parkin (2000) have enabled a detailed understanding of vortex formation and expansion both in yawed and unyawed conditions, as well as the initial skew angle of the wake of a yawed turbine. This kind of detail in the very near wake is important for wake-vortex theories for performance predictions, but is less relevant when

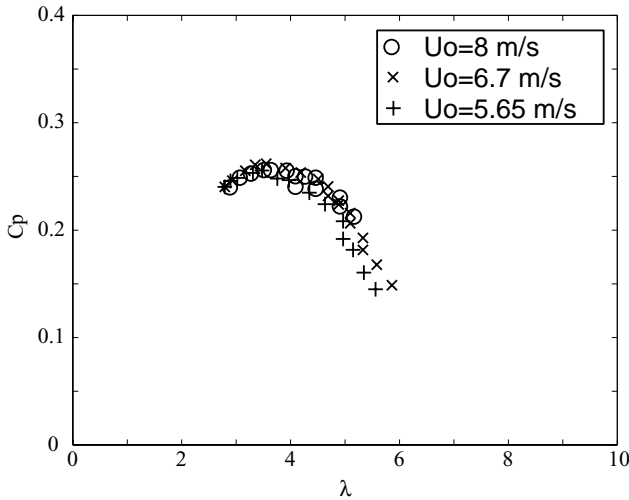


FIGURE 2. Power coefficient vs. tip speed ratio (λ) for different freestream velocities for the model wind turbine. The collapsing of the curves gives the unique tip speed ratio for the maximum power output.

considering interactions between machines. The present experimental study aims to advance the understanding of the development of non-axisymmetric wakes of horizontal axis wind turbines (HAWT) further downstream to enable better modelling and active control of wind turbine interactions in arrays.

PIV images have been obtained in the wake of a two bladed HAWT from one to five diameters downstream at a range of yaw angles. The study can be considered as a fundamental study of the behaviour of wakes behind deflecting bodies, but also has a clear application to actively control and maximise the power output from wind farms. A possible feature of the result may be concluded from figure 1.

2. Experimental set up and data processing

Experiments were carried out in the 0.8m×1.2m MTL low turbulence wind tunnel at the Royal Institute of Technology (KTH), Stockholm, Sweden. A 0.25 m diameter two bladed model wind turbine (further details given in Alfredsson & Dahlberg (1979)) was positioned in the centre of the tunnel on a tower standing on the tunnel floor. The wind turbine was controlled using a generator and load circuit. Rotor frequency, torque and thrust were measured to obtain power and force curves for the wind turbine at different tip speed ratios (see figure 2). The tip speed ratio is the ratio between the tip velocity of the blade and the freestream velocity. The turbine was then run at optimum tip speed ratio in a freestream wind velocity of 6.3 m/s. Using a laser sheet

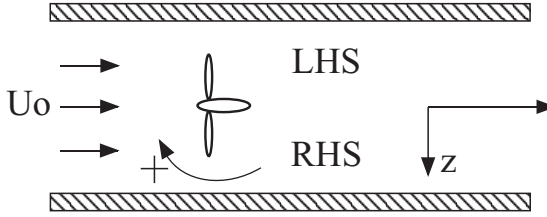


FIGURE 3. Experimental set-up, top view, showing yaw angle notation.

parallel to the flow, cutting through the centre of the turbine wake, PIV images were obtained at a series of positions - from approximately one diameter to five diameters - downstream of the rotor, at a number of different yaw angles. In the present study, a positive yaw angle indicates that the right hand side (RHS) blade of the turbine was yawed upstream when viewed in the downstream direction, see figure 3. Wake measurements were carried out for the following yaw angles $[-30^\circ, -20^\circ, -10^\circ, 0^\circ, 10^\circ, 20^\circ, 30^\circ]$ with each PIV image covering an area of approximately $0.17\text{m} \times 0.17\text{m}$. At least 250 images were collected at each position with a spatial resolution of around 2.7 mm.

The PIV system included a two-cavity (400mJ each) Nd:YAG laser (Quanta Ray), with a wavelength, after frequency doubling, of 532 nm and pulse frequency of 14 Hz. The duration of the laser beam was 8.0 ns. A digital high-resolution Kodak ES 1.0 CCD-camera (1008×1018 pixel) was used. This was equipped with a 60 mm lens. The processor and software was delivered by DANTEC Measurement Technology, Denmark. The seeding was introduced downstream of the test section and re-circulated round the closed circuit wind tunnel producing uniform seeding in the test section. Seeding was achieved using smoke generated from 1,2-Propanediol diluted with 30-40% water with an approximate particle size of 2.0-2.5 μm volume median diameter (VMD). The PIV data post processing was evaluated using an in-house written Matlab code. The post processing used the Peak Value Ratio (PVR) - validation criteria, set to ≥ 1.2 . The velocity range was chosen up to $1.6 \times$ freestream velocity in the streamwise direction and $\pm 0.8 \times$ freestream velocity in the spanwise direction. The measurements provided sufficient data for further analysis without the requirement for filling or smoothing.

3. Results and discussion

Figures 4 and 5 show the composed velocity surface plots of the wake for a series of downstream positions of the wind turbine at zero and 30 degrees yaw respectively. The average velocity has been subtracted so the flow features can be seen more easily. In these particular data sets there was no data acquired along the centre line since the outer part of wake was of interest. The colour scale represents the sum of the velocity vectors, with red representing downstream and positive spanwise (to RHS) directed velocity components and, at the other end of the scale, blue denoting upstream and negative spanwise directed components. The resultant of the freestream velocity only consists of the downstream component and is denoted by yellow, thus representing the mid range vector sum. The laser sheet was positioned parallel to the flow direction, thus cutting through the helical vortices trailing from the blade tips. The intersection between the laser sheet and the helical vortex is seen as a series of isolated vortices at approximately 0.6 diameters from the centre of the wake, diverging and becoming more erratic downstream as the wake expands and the vortices break down. The velocity decreases towards the centre of the wake but, as more of the free stream is drawn into the wake, this inner-wake flow deficit is reduced and the velocity increases towards the freestream velocity. In the zero yaw case the wake travels straight downstream of the rotor, as expected. When the turbine is positively yawed the wake is deflected towards the LHS of the rotor. The inner wake deficit is less pronounced as the rotor is less effective in extracting the energy from the wind.

Figure 6 shows a close up of the intersection between the laser sheet and one of the trailing vortices, with the velocity vectors superimposed onto the colour plot. This figure shows the presence of data close to the core of the vortex. However, the centrifugal force in the centre of the vortex excludes tracer particles from this part of the flow thus the velocity vectors are seen to reduce and shows one of the problems of PIV in highly circulating flows.

In figure 7 the average streamwise velocity profiles are presented for different downstream positions showing the wake deflection due to yawing the turbine [0° 10° 20° 30°]. The yawing effect is clearly shown. At approximately $x/D=4.5$, at 30 degrees yaw, the wake is deflected approximately 30% of the rotor diameter. In each velocity profile there is a systematic velocity excess of 5% of the freestream velocity in the outer region, which is thought to be due to the solid blockage effect also corresponding to 5%. A similar result was seen in Alfredsson *et al.* (1980) when studying the wake downstream of a turbine.

Figure 8 shows the skew angle of the centre of the wake, calculated by taking the midpoint of the wake and comparing to zero yaw, for different yaw angles. Comparison is made with results by Grant *et al.* (1997). Since the curves flatten off at higher yaw angles, the gain in deflection by going to higher yaw angles is minimal. The results by Grant *et al.* (1997), where a larger rotor with different blade profiles was used, shows slightly higher wake skew angles but the shape of the curve is the same.

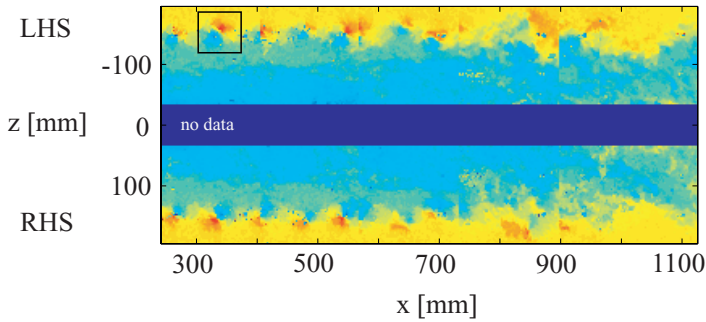


FIGURE 4. Composed velocity plot of a series of downstream image areas showing the wake development at zero yaw angle. The colour scale represents the sum of the velocity vectors, with red representing downstream and positive spanwise (to the RHS) directed velocity components and, at the other end of the scale, blue denoting upstream and negative spanwise directed components. The resultant of the freestream velocity only consists of the downstream component and is denoted by yellow, thus representing the mid range vector sum.

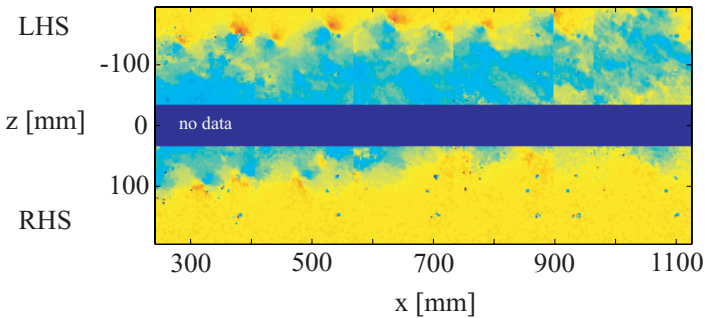


FIGURE 5. Composed velocity plot for 30 degrees yaw.

When analysing the wake development the comparison to field condition is always desirable but complicated. There are a number of non-dimensional groups of parameters that may influence the wake behaviour, such as the power coefficient, drag coefficient, tip speed ratio, aspect ratio (chord/blade length), Reynolds number etc. The ambient flow, which in nature is an atmospheric boundary layer, is of course also an important factor for the wake dispersion, especially the ambient turbulence level. The present study was performed at a

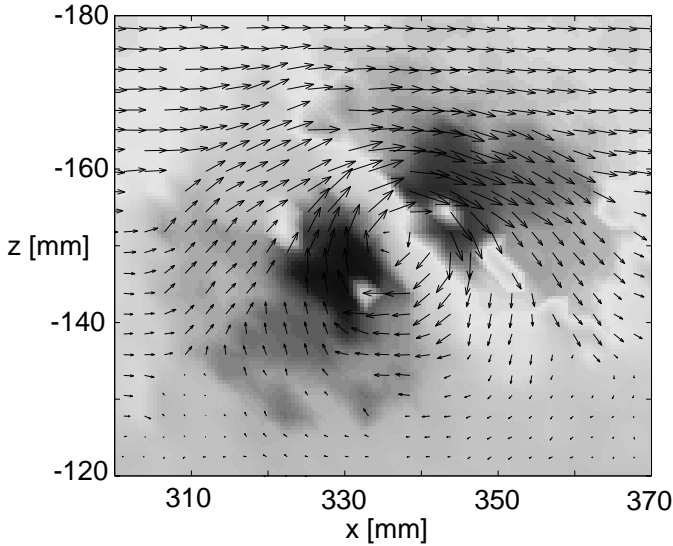


FIGURE 6. A close up of a vortex with velocity vectors, giving the centre of the vortex. The upper part of the figure represents the free stream and the lower part the inner wake region.

low turbulence level and therefore the wake dispersion would be smaller than in nature. The strength and stability of the tip vortices is another important factor that may affect the spreading of the wake. However the qualitative feature of wake deflection would still be valid and future work will include free stream turbulence and mean shear gradients.

The application of this study to the active control of wind turbine wakes in wind farms is illustrated in figure 9 and figure 10. Here the wake streamwise velocity, expressed as a fraction of the freestream velocity, is plotted versus yaw angle for a number of axial positions for a particular distance downstream. Only the streamwise velocity component is considered as the spanwise component in the outer part of the wake was negligibly small and in the inner part, where it was possible to contribute, was less than 10%. So, if we were to position a second turbine at this distance downstream from the first turbine, it would be desirable for the wind speed to be as near to the free stream as possible. The figure shows what yaw angle of the upstream turbine is required to give a particular wind speed at various span positions with respect to the upstream turbine of a downstream turbine. For example, if the blade of the downstream turbine was directly downstream of the upstream rotor a freestream velocity could be achieved by yawing the upstream rotor by 30 degrees. In reality this is unlikely to optimise the energy output from both turbines as yawing

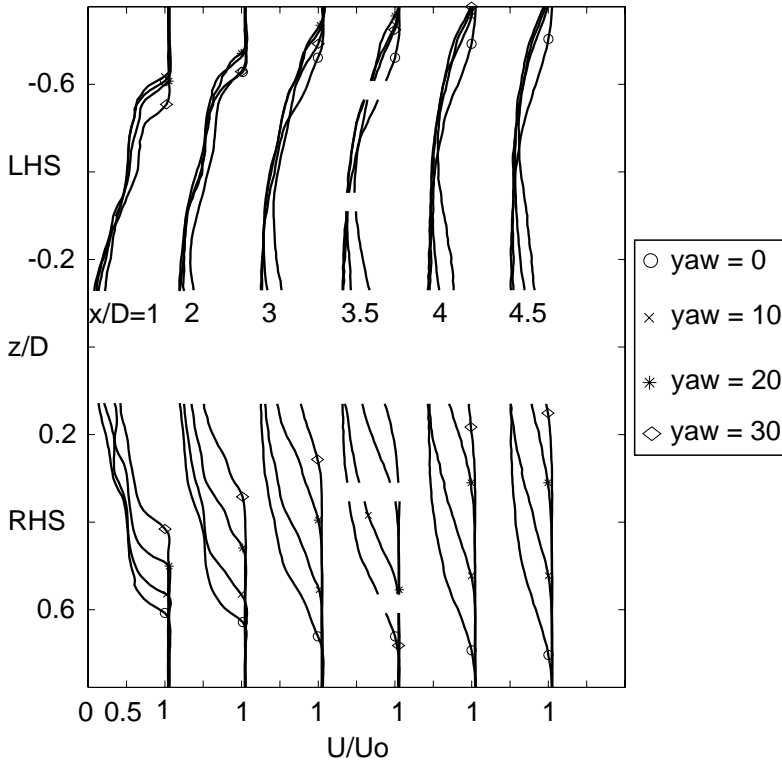


FIGURE 7. The mean velocity profiles of the streamwise flow component for different downstream positions and yaw angles [0° 10° 20° 30°].

a turbine by 30 degrees will give a significant reduction in energy output. A more realistic example is if the downstream turbine was at a span position of 0.4. The upstream turbine could be yawed by 10 degrees to get 95% of the free stream, or by 20 degrees to get the freestream wind velocity.

4. Conclusions

The results presented show a clear picture of the wake of a wind turbine, both aligned into the wind and at a range of yaw angles, up to approximately 5 diameters downstream. The positions of the trailing tip vortices are shown and vortex dissipation downstream illustrated. When the turbine is yawed the wake is deflected and this effect seems to increase further downstream. The

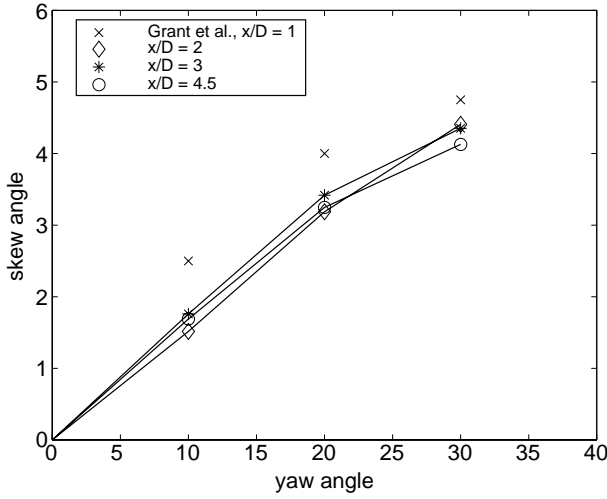


FIGURE 8. The wake skew angle at different downstream positions, calculated from the displacement of the midpoint between the two sides at 95% of the freestream velocity.

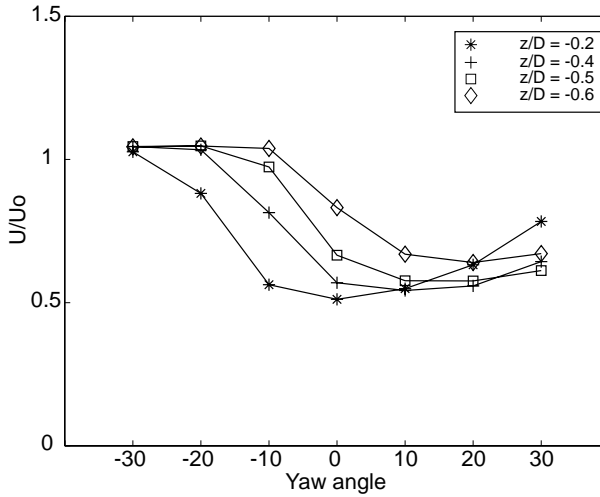


FIGURE 9. The essence of the wind tunnel tests. The influence on the streamwise velocity value, and thus a second wind turbine D , at a downstream position of $x/D=4.5$ from turbine C at different yaw angles. The parameter is the spanwise position (z/D) for turbine D , see figure 1.

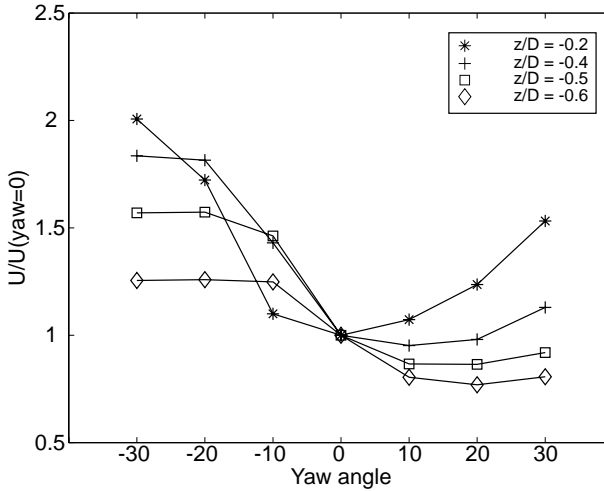


FIGURE 10. Figure 9 normalized with the data for zero yaw angle.

wake deflection effect in yaw will be used in continued studies to investigate the possibility of active control of the wake paths in wind farm applications and the feasibility of this has been illustrated in present study.

5. Acknowledgements

The authors would greatly acknowledge the Swedish National Energy Administration for financially supporting this project. The authors are also very thankful for the support of equipment and fruitful discussion with the staff at the Wind Energy Department at the Swedish Defence Research Agency (FOI/FFA) in Stockholm and finally thanks to the colleges and technicians at the Department of Mechanics at KTH.

References

- ALFREDSSON, P. H. & DAHLBERG, J. Å. 1979 A preliminary wind tunnel study of windmill wake dispersion in various flow conditions. FFA Technical Note AU-1499, part 7.
- ALFREDSSON, P. H. & DAHLBERG, J. Å. 1981 Measurements of wake interaction effects on the power output from small wind turbine models. FFA Technical Note HU-2189, part 5.
- ALFREDSSON, P. H., DAHLBERG, J. Å. & BARK, F. H. 1980 Some properties of the wake behind horizontal axis wind turbines. In *Proc. Third Int. Symp. on Wind Energy Systems*, Copenhagen, BHRA Fluid Engineering, paper J5, pp. 469–484.
- CLAYTON, B. R. & FILBY, P. 1982 Measurement effects of oblique flows and change in blade pitch angle on performance and wake development of model wind turbines. In *Proc. 4th BWEA Wind Energy Conference*, Cranfield, BHRA Fluid Engineering, pp. 214–224.
- GRANT, I. & PARKIN, P. 2000 A DPIV study of the trailing vortex elements from the blades of a horizontal axis wind turbine in yaw. *Exp. Fluids* **28**, 368–376.
- GRANT, I., PARKIN, P. & WANG, X. 1997 Optical vortex tracking studies of a horizontal axis wind turbine in yaw using laser-sheet flow visualisation. *Exp. Fluids* **23**, 513–519.
- PEDERSEN, T. F. & ANTONIOU, I. 1989 Visualisation of flow through a stall-regulated wind turbine rotor. *Wind Engng.* **13**, 239–245.
- ROSS, J. N. & MILBORROW, D. J. 1985 Laser velocimetry applied to the study of model wind turbines. *Optical Measurements in Fluid Mechanics*, Inst. of Physics Pub. Inc. (ISBN: 0-85498-1683), Institute of Physics Conf. **77**, pp. 27–31.
- SFORZA, P. M., SHEERIN, P. & SMORTO, M. 1981 Three-dimensional wakes of simulated wind turbines. *AIAA J.* **19**, 1101–1107.
- SMITH, D. & TAYLOR, G. J. 1991 Further analysis of turbine wake development and interactive data. In *Proc. 13th BWEA Wind Energy Conference*, Swansea.
- VERMEULEN, P. E. J. 1980 An experimental analysis of wind turbine wakes. In *Proc. Third Int. Symp. on Wind Energy Systems*, Copenhagen, BHRA Fluid Engineering, paper J3, pp.431–450.

Paper 2

2

Potential improvement of wind turbine array efficiency by active wake control (AWC)

By J. Å. Dahlberg[†] and D. Medici[‡]

[†] FOI, Aeronautics Division, FFA, Department of Wind Energy Research,
SE-172 90 Stockholm, Sweden

[‡] KTH Mechanics, SE-100 44 Stockholm, Sweden

Proc. European Wind Energy Conference, Madrid, 2003.

The concept of Active Wake Control (AWC) has been tested by experiments with several turbine models in two wind tunnels. The basic idea of AWC is to use ordinary control methods to influence (reduce or eliminate) the interaction between its wake and a downstream turbine. A wind turbine extracts energy causing a loss of momentum in the airflow; consequently a thrust force acts on the turbine disc. The velocity deficit and shape of the wake are mainly controlled by the magnitude and direction of this thrust force. By yawing the turbine the thrust force vector is deflected from the main flow direction. The wake will move in the opposite direction, according to Newtons First Law. The consequence for the yawed turbine will be a reduction in power. Results from Particle Image Velocimetry and hot-wire measurements have clearly shown that the wake can be displaced significantly. This means that the power output decrease of a downstream turbine can be limited. The direct interaction between two turbines has also been examined by traversing a turbine through the wake of an upstream turbine for different configurations and yaw operation. These results have been used to predict the feasible energy gain in a small farm consisting of six turbines. The study shows that there is most to gain (up to 10% if two turbines are considered and 2-3% for the whole farm) for shorter turbine separations and that the energy yield is highly dependent on the power reduction for the yawed turbine.

1. Introduction

Wind energy is of increasing importance in electrical power production. The key for even further enhancing its role is to make the cost per produced energy unit competitive with other sources. Common approaches to control and therefore to optimize the power output include tip speed variation, stall, variable blade pitch, and yaw. The aerodynamic efficiency is one side of the problem, the other being the interaction between two or more turbines. This paper focuses on the possible increase in power output from a wind farm using an Active Wake Control (AWC) method.

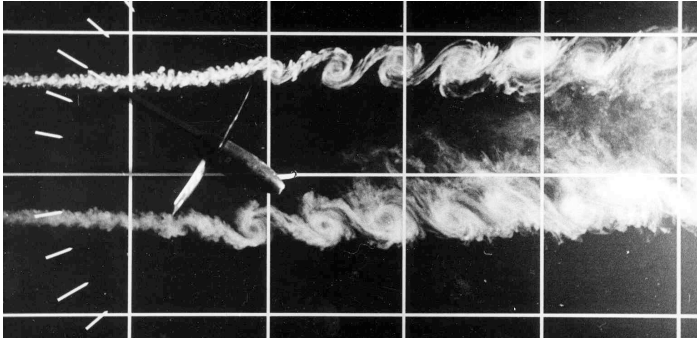


FIGURE 1. Flow visualisation of wake deflection from a turbine yawed 30° conducted at the Royal Institute of Technology (KTH), January 1987.

Comprehensive studies on the wake characteristics of single turbines are available in the literature. Comparisons between tunnel tests and full-scale turbines (e.g. Magnusson & Smedman (1999) Whale *et al.* (1996)) are a typical example. Near wake measurements (Grant *et al.* (1999), Magnusson (1999)) have been performed using, for example, hot wire and laser techniques. The airflow behind wind turbines has also been investigated (Alfredsson *et al.* (1980), Vermeulen (1980)). Studies of wakes by Ronsten *et al.* (1994) visualised the wake deflection when the turbine was yawed. Smoke was injected in the airflow at two positions at hub height such that the smoke trails touched the blade tip paths on both sides of the turbine. A photo taken from the test is presented in figure 1. The two-bladed turbine was yawed 30 degrees and operated close to maximum power. The vortices emerging from each blade passage are clearly visible. Note the vortex core path on each side. Both the sides of the wake are deflected upward, although the lower side more noticeably.

Numerical simulations on a porous surface were investigated also in yaw, based on the actuator disc theory, after measurements with no yaw in a wind tunnel (Sforza *et al.* (1981)). Blade element theory is very popular when dealing with rotor performance analysis. For yawed conditions, free wake models based on induction velocities and prescribed wake models have been used (Coton & Wang (1999)). Engineering models are also based on wind tunnel measurements (Schepers (1999)). For a more detailed discussion about single turbine studies, extensive review literature is available (Hansen & Butterfield (1993), McGowan & Connors (2000), Leishman (2002)). Starting from a single wind turbine, the interaction between elements bundled into a wind farm has been investigated. The farm configurations depend strongly on the site, ranging from linear arrays to more complex geometries. Models for prediction of power production from wind farms have been implemented and compared with experiments (Landberg

(1999)), as well models to calculate wind and turbulence characteristics inside a wind farm (Ivanova & Nadyozhina (1998)).

However, little information has been given about the mechanisms that influence the wake in connection with the power production. The aim of this study is to demonstrate the possibility of controlling the operational characteristics of a turbine and thereby controlling the development of the wake. Yawing the turbine implies that the relatively large thrust force, which essentially acts perpendicularly to the rotor plane, has been given an angle with respect to the wind. This side force causes the wake to change direction proportionally to its magnitude. Using controls installed in a large majority of wind turbines, the magnitude and direction can be modified. Pitch, tip speed ratio and yaw are believed to provide the desired changes on the wake and therefore on the output; consequently not only wake measurements will be discussed in the paper, but also power production from one wind turbine model as tested in a wind tunnel, and production from a bundle of turbines. The advantages will be reduced wake loads and increased power for the downstream turbine; the consequences for the controlled turbine will be reduced power and eventually increased loads. Although performance measurements for several pitch settings and tip speed ratio have also been made, the changes due to the modified magnitude of the thrust were not studied.

2. Experimental methods

An investigation by models in two wind tunnels was carried out to understand to what extent the development of the wake could be influenced by active wake control (AWC). The wake measurements were performed in the MTL (Minimum Turbulence Level) wind tunnel at KTH Mechanics. The tunnel test section is 1.2 m wide and 0.8 m high, for a total length of 7 m and an adjustable ceiling used to obtain a zero pressure gradient when empty. The coordinate system is x, y, z for the streamwise, wall-normal, and spanwise directions, respectively.

Used only in a first set of measurements, the 2-velocity component Particle Image Velocimetry (PIV) consists of seeding the flow with propylene glycol oil smoke and then taking a rapid sequence of two images with a CCD camera, while a pulsed laser sheet lights the flow. The PIV post-processing program was the Dantec software system FlowManager 2.12, by means of which the captured area of 1018×1008 pixels was divided in a mesh of 62×62 cells with no overlap. The cross correlation of the position of the smoke particles between the images resulted in a velocity vector in each of the cells, since the elapsed time between the two images was known. The side length of the captured images was 170 mm, giving a resolution for the velocity field of approximately 2.7 mm. A sketch of the experimental set-up can be seen in figure 2. A positive yaw angle was defined when the right hand side of the turbine as viewed from upstream, corresponding to positive z -values, was rotated downstream. Measurements were made in the horizontal (i.e. xz) plane; the camera was equipped with

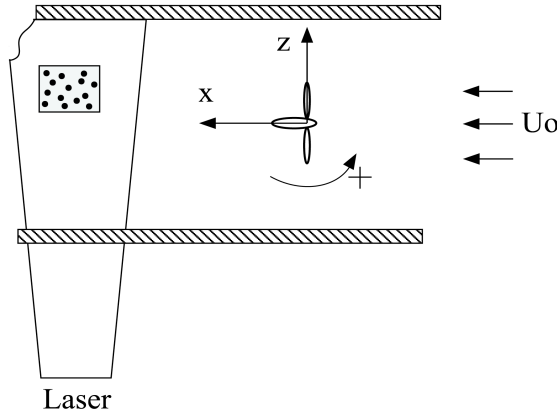


FIGURE 2. Experimental set-up for the PIV, top view. The region targeted by the camera under the floor is shown, with a sketch of the seeding particles (dots).

a 60 mm lens and fixed under the wind tunnel floor, looking up through a plexiglass panel. The flow was seen as coming from bottom to top of the captured area, therefore a positive yaw angle caused the flow to move toward the left side of the picture, i.e. to positive z -values.

The turbine was a 2-bladed model with a diameter ($D=2R$) of 250 mm, and the hub of 40 mm was large enough to accommodate a power generator. The turbine was placed in the middle of the test-section and the running point was chosen as the one giving the maximum power coefficient from the generator. The freestream velocity as measured by a Prandtl tube in the beginning of the test section was 6.3 m/s. Approximately 250 images were taken for each downstream position (from 1 to 4.5 diameters) and each yaw angle ($0^\circ, -10^\circ, -20^\circ, -30^\circ$). This number of images was not enough to calculate reliable statistics, consequently only the mean velocity components were derived.

A second turbine model was built at the Aeronautical Research Institute (FOI) of Sweden: the blade was based on the Göttingen 417A airfoil, because this thin airfoil has good performance at low Reynolds numbers. The blades were produced in a mould of carbon fibres reinforced epoxy. The outer 77% of the blades were tapered such that the tip chord was 16 mm and the maximum chord at 12% radius was 27 mm. This gave a solidity (blade area/swept area) of 13%. Each blade was attached to a 23 mm diameter hub by means of a screw glued parallel to the 25% chord line, giving a total diameter of 180 mm. Any pitch angle could be fixed within an accuracy of 0.05° . The hub was then directly attached to the shaft of a DC motor having the same diameter.

The generator had a straight torque-current relationship that was determined through calibration, when the reaction torque on the housing of the

generator was measured with strain-gauges. Three pair of blades were tested: the couple chosen for the experiment was the one giving the best performances in terms of power coefficient. A strain-gauge moment balance, close to the bottom of the 180 mm support, was used to measure the streamwise force and therefore the thrust coefficient. For this measure it was assumed that the resultant of the forces acting on the blades was located in the centre of the rotor, with an accuracy considered acceptable for non-yawed conditions.

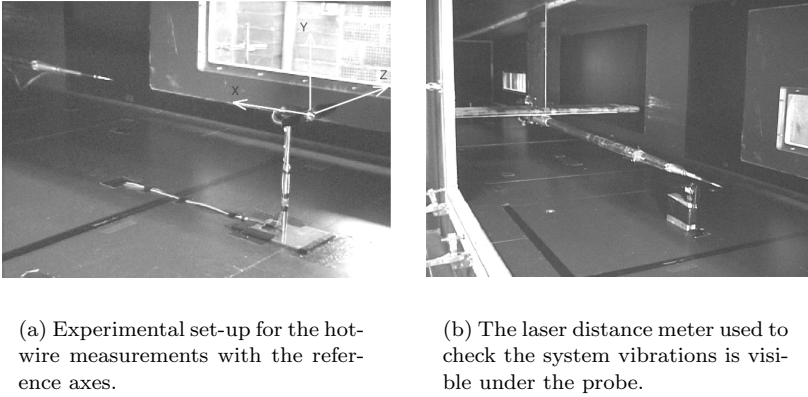


FIGURE 3. Experimental set-up and traversing system.

Power (P) and thrust (T) as function of rotational speed have been measured in the MTL wind tunnel, using the wind turbine model presented above; the coefficients were defined as:

$$C_P = \frac{P}{\frac{1}{2}\rho\pi R^2 U_\infty^3} \quad (1)$$

$$C_T = \frac{T}{\frac{1}{2}\rho\pi R^2 U_\infty^2} \quad (2)$$

$$\lambda = \frac{\Omega \cdot R}{U_\infty} \quad (3)$$

where Ω is the angular velocity and λ the tip speed ratio. The velocity wakes were then investigated with hot-wire anemometry. A picture of the experimental set-up is shown in figure 3(a). The X-wire probe was built for the experiment and connected to the traversing system in order to have five degrees of freedom. As can be noticed in figure 3(b), the probe was placed at one end of a shaft to minimize the disturbances. On the other hand, this reduced the maximum measurable distance to 15 diameters downstream of the turbine. The prongs of the probe were edged to minimize the disturbances with the flow and their separation was approximately 1 mm, which was also the side length of the cubic measurements volume. The platinum wires were 5 μm in diameter.

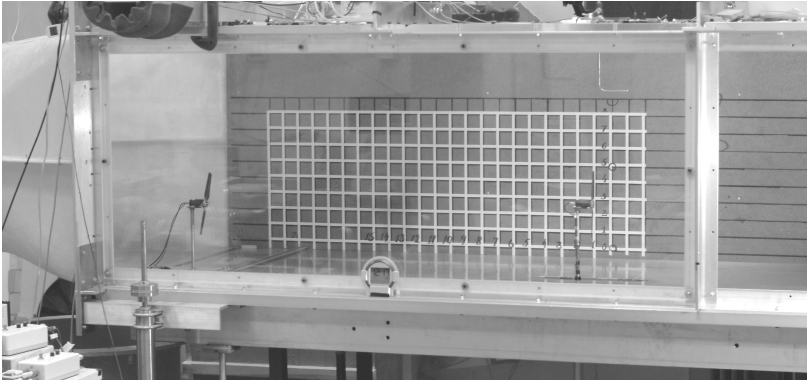


FIGURE 4. The test section of the LT5-II wind tunnel with two turbines mounted. The wind is blowing from right to left. The right turbine is fixed whilst the left turbine can be traversed from side to side.

The velocity components of interest (axial and radial) were the ones lying on the xz -plane, which therefore was the plane containing the wires. With a pitch angle for the two blades of 8° , three velocities were tested: 5, 8, 11 m/s at a constant thrust coefficient. Differencing the pitch angle to $7^\circ/9^\circ$ and $6^\circ/10^\circ$ between the two blades, additional sets of data were captured at 8 m/s. Data were acquired for 30 seconds at 6 kHz in each grid point for all the investigated conditions.

For the two lowest velocities tested, the anemometer voltages at the wake centreline were below the minimum calibration point. Since the two 5th degree polynomials used for the fitting of the values cannot be used outside the calibration velocities, a different approach was considered. The calibration points for the X-wire probe ranged between 3 m/s and 15 m/s, the seven angles between $\pm 30^\circ$. The anemometer voltages that had in common the probe calibration angle were interpolated with the modified King's law. Thanks to the nature of the Kings law, the expected voltage at 1 m/s was extrapolated and inserted as a calibration point. The polynomials so obtained could then be used in the new range 1 m/s to 15 m/s.

The power wakes measurements, expressing the power relatively to undisturbed conditions, were conducted in the LT-5, NPL-type wind tunnel at FOI. The tunnel (figure 4) has a 2.5 m long test section with a cross-section of 0.9×0.675 m and a velocity range from 5 m/s to 16 m/s. The wind speed in the centre of the test section was measured as the difference between the total pressure in the contraction and the averaged static pressure from four taps, two located upstream of, and two downstream of, the test section. The purpose of

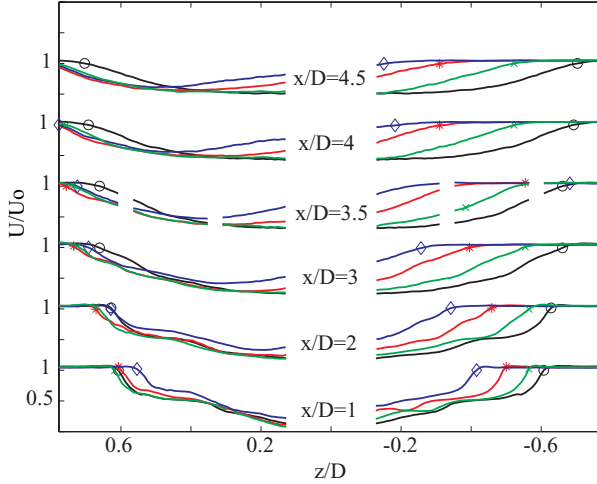


FIGURE 5. Mean velocity profiles (PIV), axial component. Different yaw angles are investigated: 0° (\circ), $+10^\circ$ (\times), $+20^\circ$ ($*$) and $+30^\circ$ (\diamond).

measuring the static pressures both up- and downstream of the turbine is to take the wake blocking effect into account when estimating the wind-speed.

By traversing a turbine through the wake of an upstream turbine at a fixed streamwise position in the test section, the interactions have been examined. The upstream turbine was positioned in the centre of the wind tunnel at fixed distances of 3, 5, 7 and 9 diameters. This model was yawed in 10° steps from -30° to $+30^\circ$. The test was carried out such that the upstream turbine was operating at a fixed tip speed ratio, which gave nearly optimum C_P . The traversing turbine was as well connected to a load circuit, which for uniform flow would have kept the tip speed ratio constant. The downstream turbine was slowly traversed back and forth during 9 minutes, which enabled the turbine to complete four sweeps. All relevant data were continuously recorded at 17 Hz. The processing of data involved the conversion to physical values and sorting the data into 1 cm bins, with the position of the traversing turbine as the independent variable. The C_P values in each bin were normalised with the corresponding C_P value for undisturbed conditions.

Slowly rotating the turbine back and forth between -35° and $+35^\circ$ and continuously recording the data was the method used to calculate the reduction in power due to yaw operation. A positive yaw angle was defined when the right hand side of the turbine, corresponding to positive z -values, was rotated upstream. The turbine was connected to a load circuit that kept the turbine in near constant TSR operation.

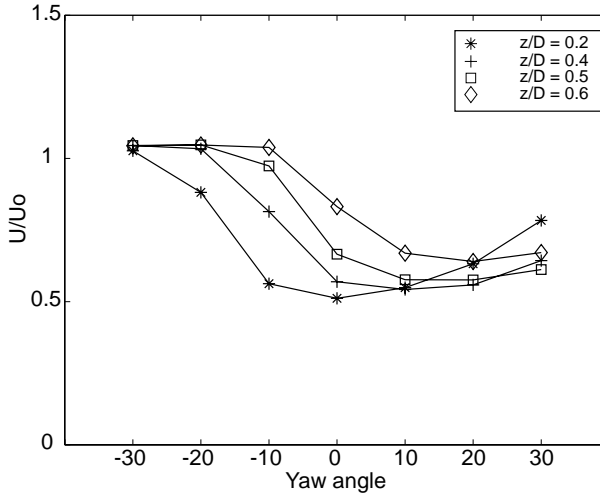


FIGURE 6. Velocity gains in a fixed position as function of the yaw angle, for different spanwise positions.

3. Results

The data can be divided into three main groups: measurements performed on one wind turbine, on the interactions between two turbines, and finally on a model describing a wind farm of 6 elements. The wake measurements were limited to the single turbine test, the performances and force data to all the cases.

Single turbine study: a wind turbine working in yawed conditions ranging from 0° to $\pm 30^\circ$ was investigated with PIV. The displacement of the wake is plotted in figure 5 for different yaw angles. From the velocity field, once the downstream position was chosen and a point at a known spanwise distance from the centre of the turbine was selected, the local velocity value could be calculated, as shown in Fig. 6. In this case the relative velocity value as a function of the yaw angle is shown for $x/D=4.5$.

The operational conditions such as pitch angle and tsr for the 180 mm diameter wind turbine were selected to give a thrust, and thereby a wake, which resembled conditions for full-scale turbines. A more detailed description involving two turbines will be given in the next section. The performances of the models were measured at constant wind speed and by manually loading the turbine with different resistors. For each load-case the wind speed, rotational speed, torque and thrust were recorded for 10 seconds. The power coefficient C_P and thrust coefficient C_T versus tip speed ratio could be plotted as function of the blade pitch angle. The performance characteristics for the turbine model can be seen in figure 7 and figure 8. The power coefficient C_P is relatively low, whilst the thrust values expressed as C_T reaches values that are realistic for full-scale turbines. The low C_P values are probably caused by non-optimal airfoil performance at low Reynolds number with a relatively high airfoil drag. Some

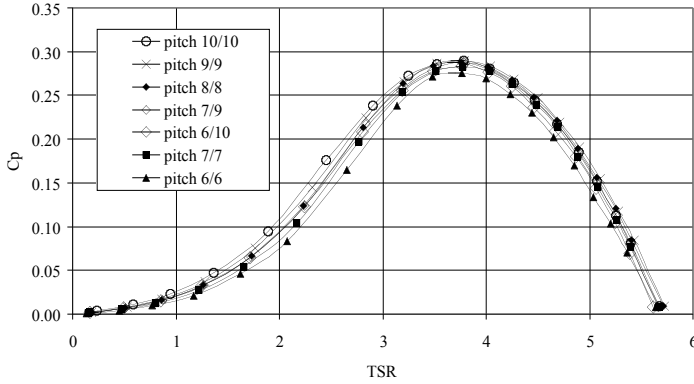


FIGURE 7. Power coefficient C_P versus λ (TSR) for different pitch settings. Note that the C_P curves with different pitch settings on the two blades, $7^\circ/9^\circ$ and $6^\circ/10^\circ$, are very similar to the curve with the pitch set to 8° on both blades ($8^\circ/8^\circ$).

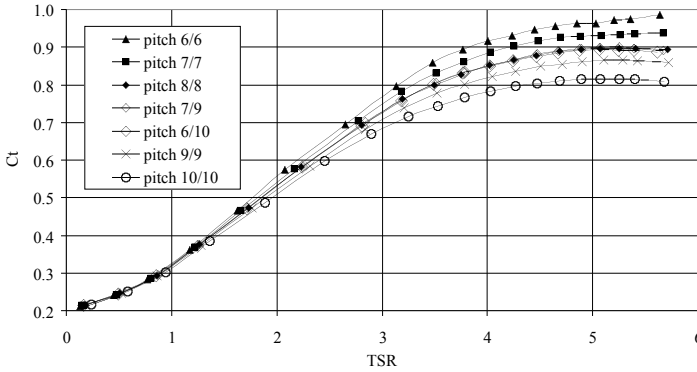


FIGURE 8. Thrust coefficient C_T versus λ (TSR) for different pitch settings. Note that the C_T curves with different pitch settings on the two blades, $7^\circ/9^\circ$ and $6^\circ/10^\circ$, are very similar to the curve with the pitch equals to 8° on both blades ($8^\circ/8^\circ$).

reduction in performance can also be attributed to the non-twisted blades. As regarding the performances in yaw, the data sorted into two degree bins are presented in figure 9 with the pitch set to 8° and the turbine operating close to maximum C_P . The following expression:

$$\frac{P}{P_0} = [\cos(\beta - \beta_0)]^{exp} \tag{4}$$

was fitted to the binned data and showed to give a good representation of the power versus yaw angle characteristics.

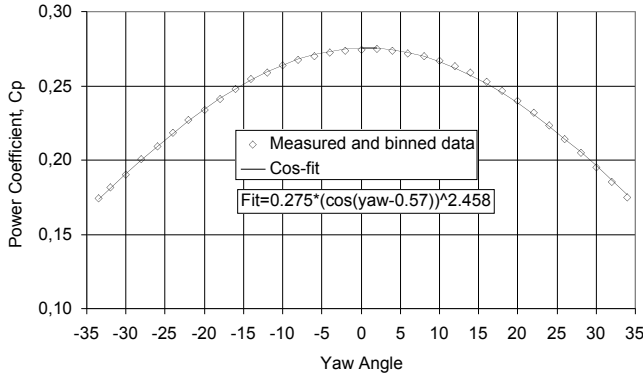


FIGURE 9. C_P as function of yaw for turbine model with pitch set to 8° and operating at C_{Pmax} .

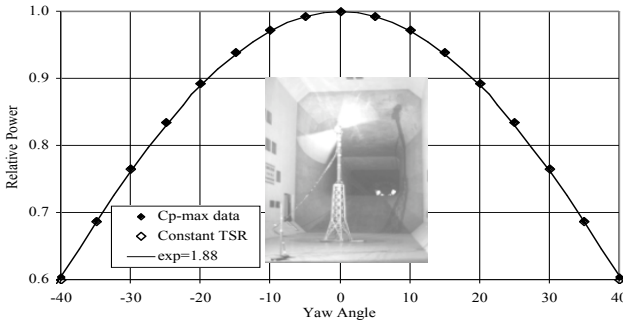
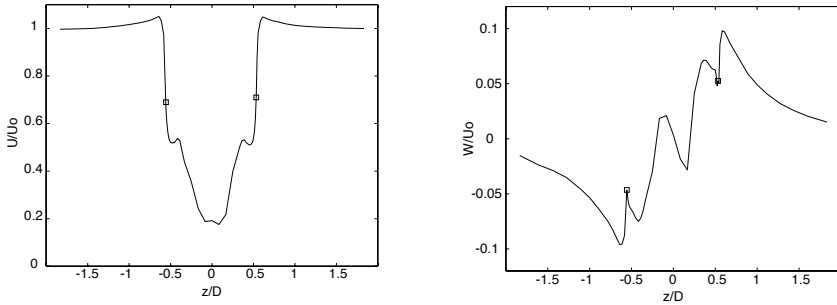


FIGURE 10. Relative power vs. yaw angle, derived from tests on a 5.35 m diameter wind turbine in CARDC 12×16 meters low speed wind tunnel 1994, China (from Ronsten *et al.* (1994)).

The exponent here used will now on be referred to as the cosine-loss-exponent. The relative power P/P_0 was defined as the ratio between the actual performance and the performance in non-yawed condition. As indicated in table 1, the power coefficients and fitted exponents changed for different pitch settings and operational conditions. The offset values β_0 varied in the range 0.2° - 0.7° and the effect was probably due to the presence of the tower. The exponents found from these tests are believed to be too high to represent full-scale conditions. One reason could be that the load circuit did not manage to keep the tip speed ratio at optimum C_P for the yawed condition. The exponent for the PIV experiment was 2, whereas a similar yaw test carried out on a 5.35 m diameter turbine gave a corresponding exponent of 1.88. The result from the mentioned experiment is recalled in Fig. 10.

Pitch angle	λ (TSR)	Power Coefficient	fitted exponent	note
6	3.14	0.233	2.316	
6	3.70	0.264	2.322	C_{Pmax}
6	4.18	0.246	2.254	
8	3.18	0.252	2.475	
8	3.72	0.274	2.458	C_{Pmax}
8	4.21	0.257	2.541	
10	3.21	0.259	2.639	
10	3.75	0.275	2.684	C_{Pmax}
10	4.21	0.250	2.894	

TABLE 1. Turbine parameters.



(a) Axial mean velocity component.

(b) Radial mean velocity component. The profile has been shifted 0.015 down.

FIGURE 11. Velocity components at $U_0=8$ m/s and $x/D=0.5$. The squares mark the centre of the vortices at $z/D=\pm 0.555$.

The wake was also measured with hot wire anemometry in the axial (u) and radial (w) velocity components, as shown in figure 11(a) and figure 11(b). In figure 12 the radial component for downstream positions up to 9 diameters and for 8 m/s are described. The rms for the axial velocity is presented in figure 13, up to 5 diameters downstream. The profiles above $x/D=5$ are decreasing in absolute value, but not changing in shape. The freestream velocity was used to normalise the quantities.

The turbine was run at essentially the same thrust coefficient also during the active wake control investigations. The blade pitch angle was differentiated between the two blades, first to 7° and 9° , and then to 6° and 10° . The axial velocity was affected by the control, as plotted in Fig. 14, more noticeably in the centre.

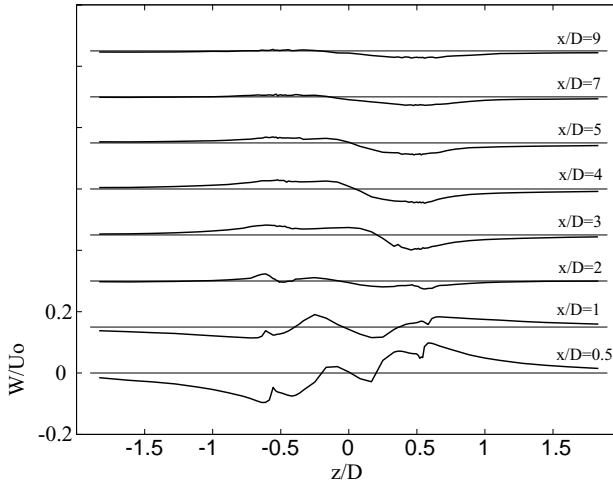


FIGURE 12. Spanwise mean velocity profiles for several downstream positions. The change of sign is evident from two diameters downstream. The profiles for $U_0=5$ m/s and $U_0=11$ m/s are similar.

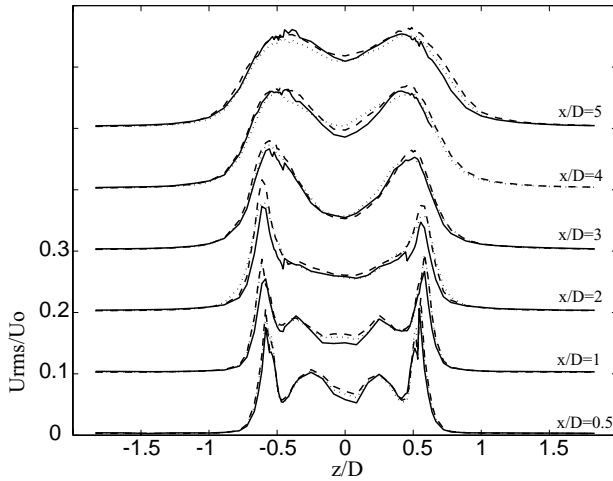


FIGURE 13. u_{rms} profiles from $x/D=0.5$ to $x/D=5$: solid (5 m/s), dotted (8 m/s), and dashed line (11 m/s).

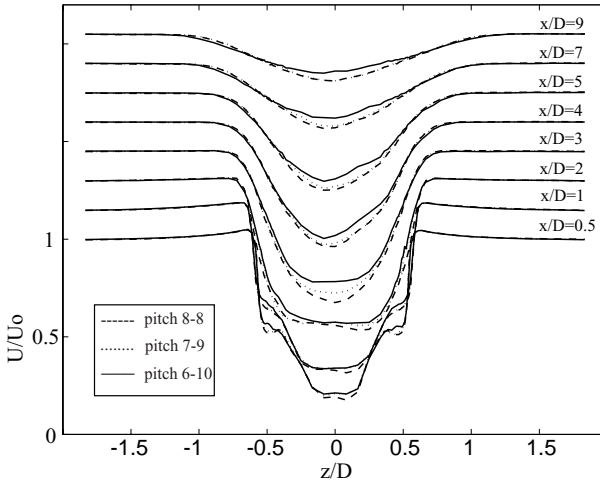


FIGURE 14. Streamwise mean velocity component. The pitch angles for the two blades are 8°/8° (dashed), 7°/9° (dotted), and 6°/10° (solid line).

Two turbines study: the relative power for one turbine, i.e. the power output normalised with the power for the undisturbed conditions, has been used to quantify the interferences caused by the wake from an upstream turbine. As mentioned above concerning the choice of the running conditions for the turbines, a comparison of the power wakes from the models and wake data measured at a small wind farm in Alsvik, consisting of four 180 kW turbines, are presented in figure 15. The farm is situated close to the shoreline and the flow comes from the open sea. This gives a very low turbulence intensity of about 5%, based on 1-minute data. The layout of the farm is such that one turbine is exposed to wakes from upstream turbines that are separated by 5, 7 and 9.5 diameters, depending on the wind direction. Data from the power wake survey for 3 and 9 diameters are shown in figure 16 and figure 17.

Wind farm model: the power wakes resulting from traversing the wind turbine, have been used to demonstrate the possibility of increasing the array efficiency by using AWC in a simulated wind farm. Five turbines were equally distributed on a circle around a centred turbine as depicted in figure 18, where the wind direction was considered clockwise from the top-to-bottom line. The layout of the wind farm was selected such that essentially no more than two individual pairs of turbines were influencing each other simultaneously. This enabled direct interpolation in the measured database matrix for yaw operation from -30° to $+30^\circ$ and downstream distance between 3 and 9 diameters. Wind direction sector, direction steps, radius of the circle as well as cosine-loss-exponent were given as input to the calculations. For each wind direction the relative power of each turbine was determined by interpolation in the database.

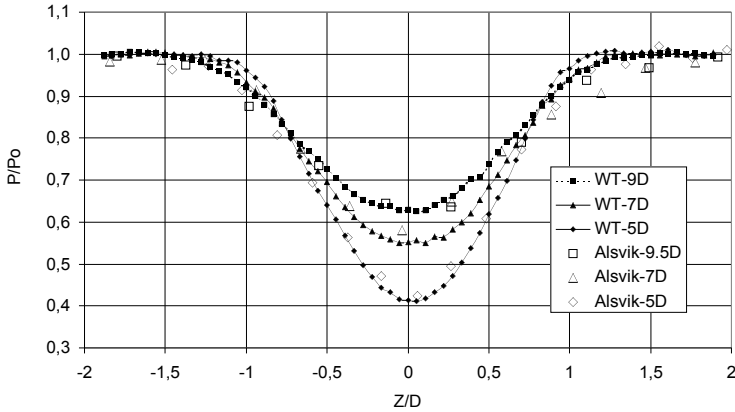


FIGURE 15. Comparison between LT5 measurements (wind tunnel, WT) and Alsvik power curves.

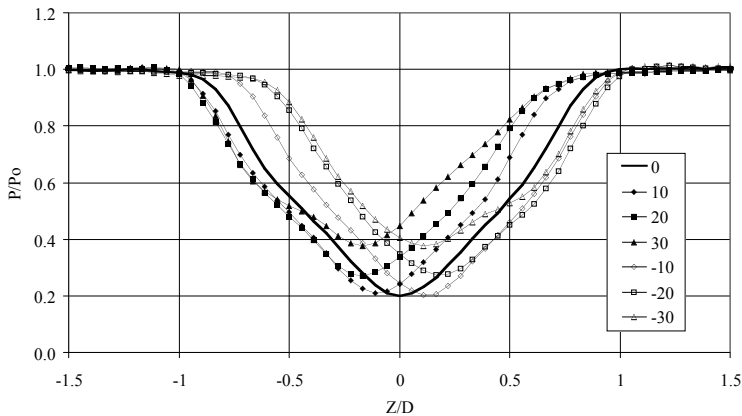


FIGURE 16. Relative power versus relative side position for the downstream turbine. The power-wakes are obtained by traversing the downstream turbine through the wake from the upstream yawed turbine. The turbine distance is $3D$.

This was done with and without AWC. When AWC was used, the optimum yaw angle was searched to give the maximum total power for all turbines involved. The optimisation process took into account the increase in power for the downstream turbine(s) due to AWC as well as the reduction in power for the yawed turbine. The calculations were performed for circle radii (distance between turbine T1 and T2:T6) of 3, 4 and 5 diameters and cosine-loss-exponents in 0.5 steps from 0 to 3. Figure 19 exemplifies, for conditions when T6 operated in

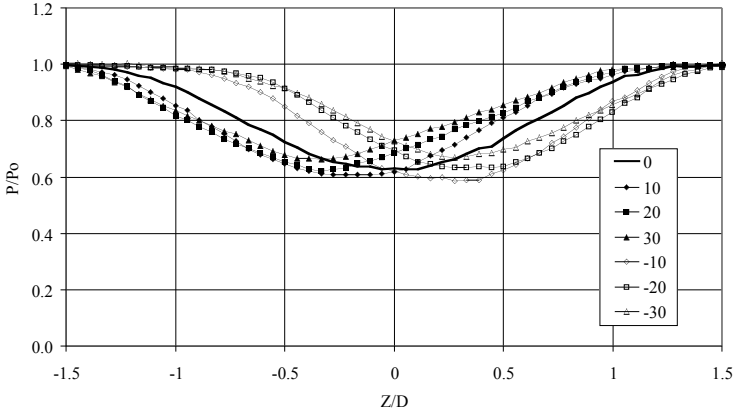


FIGURE 17. Relative power versus relative side position for the downstream turbine. The power-wakes are obtained by traversing the downstream turbine through the wake from the upstream yawed turbine. The turbine distance is $9D$.

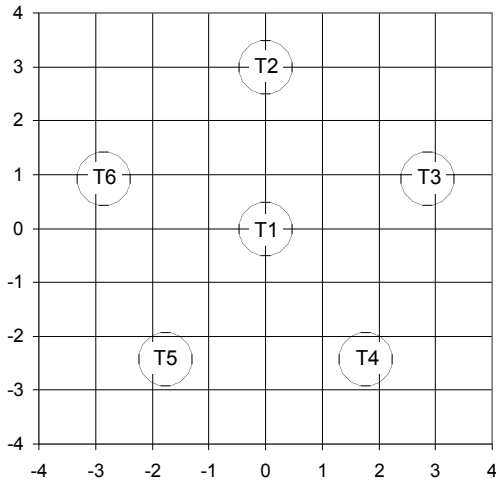


FIGURE 18. Wind farm used for the simulations.

the wake from T2, the reduction in power for the yawed turbine (T2) as well as the increase for the downstream turbine (T6) with AWC. In this example the radius in the farm is 3 diameters, the linear distance between the turbines is approximately $3.5D$, and the cosine-loss-exponent is set to 2. The optimum yaw angle for T2 can also be seen in figure 19. The corresponding percentage

gain for the two turbines is presented in figure 20. Maximum gain exceeds 11%. Note that the curves in these figures are not fully symmetric. This is caused by the direct use, by linear interpolation, of the measured data. The detailed percentage gain in power for the whole farm, for one fifth of the wind rose, and at different cosine-loss-exponents is presented in figure 21. The values for $exp=0$ give the total available increase, since no losses for the upstream turbines were considered. Reasonable values of the exponent for full-scale turbines are believed to fall in the 1.5-2.0 range.

In table 2 the possible increase in power for the whole farm exposed to equally distributed wind directions is shown. The total averaged gain in energy yield is then 2 to 4% for the supposed full-scale exponents. Turbines extract about 75% of the total energy below the rated power; therefore AWC could be applied during most of the production time in order to improve the overall efficiency of the park. It is obvious that there is more to gain at shorter distances for a given yaw angle, since the velocity/power deficit decreases with distance. This is the reason why the shorter turbine separation gives the highest gain.

radius	exponent	no AWC	AWC	% gain
3	0	0.836	0.910	8.9
4	0	0.888	0.943	6.3
5	0	0.918	0.961	4.7
3	1.5	0.836	0.868	3.9
4	1.5	0.888	0.914	3.0
5	1.5	0.918	0.939	2.3
3	2	0.836	0.862	3.1
4	2	0.888	0.910	2.5
5	2	0.918	0.936	1.9
3	2.5	0.836	0.857	2.5
4	2.5	0.888	0.907	2.2
5	2.5	0.918	0.933	1.7
3	3	0.836	0.854	2.2
4	3	0.888	0.905	1.9
5	3	0.918	0.932	1.5

TABLE 2. Array efficiency.

4. Discussion

This paper deals with the possible effects of active wake control on wind turbines, studied experimentally in wind tunnels. An aspect that should also be considered when dealing with wind turbine wakes is the tip vortex path. A

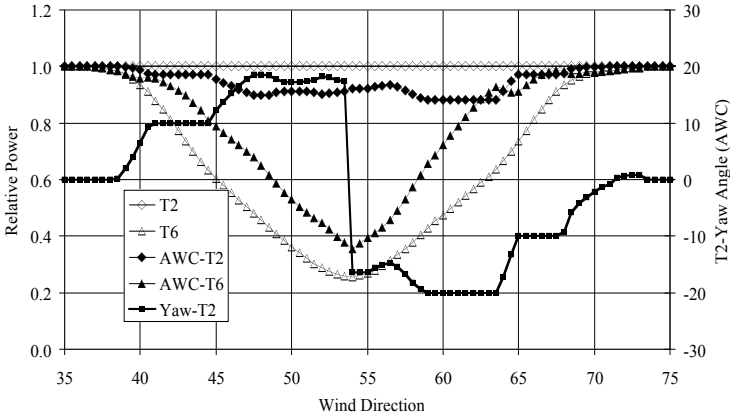


FIGURE 19. The relative power from T2 and T6 is plotted. The yaw angle for T2 was applied by the AWC code. The distance between the turbines is $3.5D$ and an exponent 2 was used as cosine-loss-coefficient.

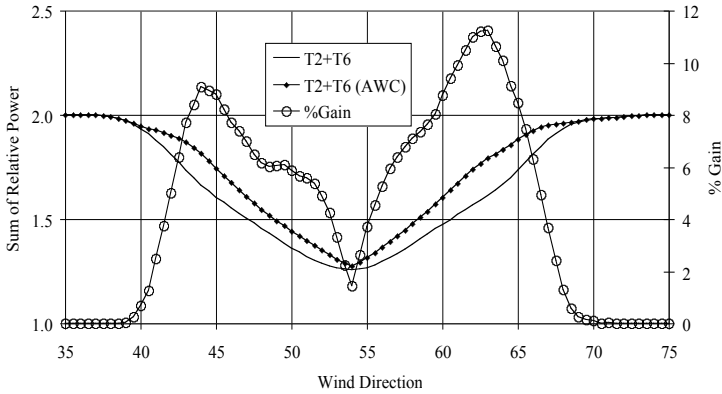


FIGURE 20. Relative power with/without AWC, and gain as from figure 19. The radius of the wind farm is $3D$ and the cosine-loss exponent is 2.

clear result from the hot wire measurements of the wake (figure 11(a) and figure 11(b)) is that the position of the centre of the vortex has, already at 0.5 diameters, moved out with respect to the blade tip. The centre can be detected not only as the mid-point between the overshoots (downwind and upwind) in the axial velocity, but also as a sudden dip in the radial velocity. It can be

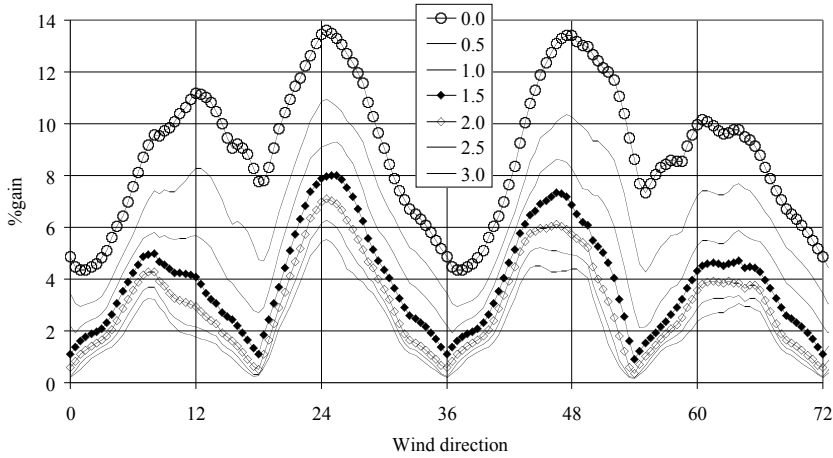


FIGURE 21. Power increase for the entire wind farm, with assumed losses due to yaw operation. The radius of the wind farm, i.e. the radius of the circle on which turbines T2 to T6 are positioned, is $3D$.

noted from figure 12 that the wake is first expanding, identified as a radial velocity directed outwards due to the effect of the reduction of speed through the turbine. Soon however the entrainment of flow from the free stream to the wake takes over. The position corresponding to two diameters is probably when the vortex effect is less strong than the turbulence created by the wake: not only the peak identifying the centre of the vortex has almost disappeared, but also the radial velocity changes sign.

The position of the vortex can be of crucial importance when applying AWC, since structural problems might be taken into account when choosing the control parameters. As seen in figure 13, the vortex positions at approximately $z = \pm 100$ mm for $x/D = 0.5$ correspond to a very high peak in the rms values. It is believed that the two inner peaks are due to the higher velocity gradient in the wake, and then they merge with the vortex peaks between two and three diameters. It can also be observed, both from the smoke visualization in figure 1 and from a spectral analysis, that this distance corresponds to the grouping in pairs of the vortices, with no free stream turbulence.

The development of the wake is mainly affected by the magnitude and direction of the thrust force. The tip speed ratio and blade pitch angle control the magnitude. If the pitch angle is fixed, a change in the TSR always produces a change both in the power and in the thrust coefficients, as seen in figure 7 and figure 8. On the other hand, if the average blade pitch angle of the blades is kept constant (as for the $8^\circ/8^\circ$, $7^\circ/9^\circ$, and $6^\circ/10^\circ$ cases), the coefficients are

unaffected. However, although the thrust coefficient is the same, the shape of the wake can be different, as can be seen in figure 14. The AWC applied to the pitch had a consistent effect on the velocity profiles: the larger the pitch difference between the blades, the smaller the velocity deficit in the centre of the wake. Since the thrust coefficient was the same, the total area derived from the momentum thickness should be the same. At a larger radius, even a very small velocity error has a large effect on the integral; therefore the calculations were not performed. On the other hand, it can be seen that the velocity deficit is higher in the controlled case (with a different pitch angle on the blades) for the outer region, compensating for the decrease in the centre of the wake.

In yaw, the other control method analyzed, a dependence on the model used for the experiment is noticed for the power output, figure 9 and figure 10. The cosine-loss-exponent is still unknown for full-scale turbines, but the loss is lower than that expected from theoretical considerations (the power should be proportional to the cube of the velocity component perpendicular to the actuator disc). The velocity profiles obtained with PIV, figure 5, show how large the displacement of the wake in yawed conditions can be. The nature of the data allows to know the velocity profiles in any position from 1 to 4.5 diameters with a step of 2.7 mm. It can also be noted how effective the AWC is on the side of the turbine with the blade moved upstream, as shown in the introduction from the smoke visualization. For example at 4.5D and 20° of yaw, the wake has been moved a distance approximately 30% of the diameter. If a downstream turbine was shadowed by the wake of the non-yawed turbine, the same control could have avoided any interaction. Figure 6 clearly states how, once the point is selected, the upstream turbine should be yawed to obtain a desired velocity change. From Fig. 16 and figure 17, the yawing of the upstream turbine can give a power gain for the downstream turbine of, for instance, 30% for 20° and $z/D=0.5$. The interesting quantity is the relative total gain, which takes into account also the power loss from the yawed turbine. In figure 19 and figure 20 it is shown that the gain can be of the order of 10% for the controlled case, if applied to two wind turbines. In this case, the considered downstream distance is three diameters and the cosine-loss-exponent is 2. For the wind farm of radius 3D simulated in the study, the maximum power gain for favourable wind directions ranged between 5% and 8% if a cosine-loss-exponent representative for full-scale turbines is considered (figure 21). The cosine-loss-exponent is a crucial data for the final result, but it is believed that a value of 1.5-2 can be applied for full-scale turbines.

Models resembling the running conditions of full-scale turbines have been successfully used to demonstrate that array efficiency can be improved by using Active Wake Control. The wake has been modified in its shape using pitch control, and deflected using yaw. It should be noted that this study has not addressed any fatigue or load issues. The turbine in yawed conditions undergoes larger stresses, but the downstream turbine can be relieved from the loads due to the presence of the oncoming wake.

References

- ALFREDSSON, P. H., DAHLBERG, J. A. & BARK, F. H. 1980 Some properties of the wake behind horizontal axis wind turbines. In *Proc. Third Int. Symp. on Wind Energy Systems*, Copenhagen, BHRA Fluid Engineering, paper J5, pp. 469–484.
- COTON, F. N. & WANG, T. 1999 The prediction of horizontal axis wind turbine performance in yawed flow using an unsteady prescribed wake model. In *Proc. Instn. Mech. Engrs.*, **213** Part A, pp. 33–43.
- GRANT, I., MO, M., PAN, X., PARKIN, P., POWELL, J., REINECKE, H., SHUANG, K., COTON, F. & LEE, D. 1999 An experimental and numerical study of the vortex filaments in the wake of an operational, horizontal-axis, wind turbine. *J. Wind Engng. Ind. Aerodyn.* **85**, 177–189.
- HANSEN, A. C. & BUTTERFIELD, C. P. 1993 Aerodynamics of horizontal-axis wind turbines. *Annu. Rev. Fluid Mech.* **25**, 115–149.
- IVANOVA, L. A. & NADYOZHINA, E. D. 1998 Wind flow deformation inside the wind farm. *J. Wind Engng. Ind. Aerodyn.* **74-76**, 389–397.
- LANDBERG, L. 1999 Short-term prediction of the power production from wind farms. *J. Wind Engng. Ind. Aerodyn.* **80**, 207–220.
- LEISHMAN, J. G. 2002 Challenges in modelling the unsteady aerodynamics of wind turbines. *Wind Energy* **5**, 85–132.
- MAGNUSSON, M. 1999 Near wake behaviour of wind turbines. *J. Wind Engng. Ind. Aerodyn.* **80**, 147–167.
- MAGNUSSON, M. & SMEDMAN, A.-S. 1999 Air flow behind wind turbines. *J. Wind Engng. Ind. Aerodyn.* **80**, 169–189.
- MCGOWAN, J. G. & CONNORS, S. R. 2000 Windpower: a turn of the century review. *Annu. Rev. Energy Environ.* **25**, 147–197.
- RONSTEN, G., DAHLBERG, J. A., GIUQING, J. & DEXIN, H. 1994 An experimental investigation of the performance and wind tunnel wall interference for a wind turbine operating in yaw. FFA scientific report, FFA TN 1994-13.
- SCHEPERS, J. G. 1999 An engineering model for yawed conditions, developed on the basis of wind tunnel measurements. AIAA paper 99-0039, 18th ASME Wind Energy Symp., and 37th AIAA, Aerospace Sciences Meeting and Exhibit, Reno, also published in *Collection of Technical papers* (A99-17151 03-44).
- SFORZA, P. M., SHEERIN, P. & SMORTO, M. 1981 Three-dimensional wakes of simulated wind turbines. *AIAA J.* **19**, 1101–1107.
- VERMEULEN, P. E. J. 1980 An experimental analysis of wind turbine wakes. In *Proc. Third Int. Symp. on Wind Energy Systems*, Copenhagen, BHRA Fluid Engineering, paper J3, pp.431–450.
- WHALE, J., PAPADOPULOS, K. H., ANDERSON, C. G., HELMIS, C. G. & SKYNER, D. J. 1996 A study of the near wake structure of a wind turbine comparing measurements from laboratory and full-scale experiments. *Solar Energy* **56**, 621–633.

Paper 3

3

Influence of the number of blades on the wake of a wind turbine model

By **D. Medici**

KTH Mechanics, SE-100 44 Stockholm, Sweden

The velocity field in the near wake behind a wind turbine models equipped with 1, 2 or 3 blades has been investigated. The paper illustrates the effects on the flow field when the tip-speed ratio λ and the number of blades N of the turbine are changed. The turbine characteristics of drag and power coefficient for the different turbines have been evaluated as function of the tip-speed ratio and are consistent with the behaviour of full-scale wind turbines. The streamwise and radial velocities have been measured at one diameter downstream the turbines as function of the tip-speed ratio for all three turbines. The wake for $N = 3$ at $C_{P_{max}}$ has been studied up to 9 diameters downstream and compared with the wake from the one-bladed turbine with the same wake pitch. In another comparison the wake behind the two and three-bladed turbines are compared at the same C_D , and it is shown that these wakes show a different recovery behaviour.

1. Introduction

The typical number of blades of horizontal-axis wind turbines has varied over time but also geographically. A good summary of the major historical development can be found in the report by Scheperd (1990). Following the development of the Danish model, the 3-bladed wind turbine has become dominant, although the 2-bladed is common in the American market. Because of the relation between power (P) and torque (Q), $P = \Omega Q$, where Ω is the angular rotational speed, at constant power a higher number of blades means a lower rotational speed. The influence on the mechanical stability of the rotor is not considered in this paper, but for more insights see de Vries (1979). A factor in the choice of the number of blades is the additional cost of extra blades. For small turbines (of the order of 1 kW) it is common to find up to 8 blades.

A wind turbine is a complicated and costly machine, therefore as for many other disciplines computer simulations are used to predict the performance and the aerodynamic behaviour. Recent developments have described the wind turbine rotor together with the hub, see Okulov & Sørensen (2005) and for more details on the numerical models refer to Vermeer *et al.* (2003). Most, if not all, numerical methods used nowadays need experimental data for testing and tuning. However, extensive measurements are still rare. Data are needed for

different wind turbines and for as many running conditions as possible. The present study aims at partly filling this gap. The knowledge of the wake development can also help to understand the inflow conditions that a downstream wind turbine may experience. Under these circumstances, the Active Wake Control described by Dahlberg & Medici (2003) can be used to increase the power production of a wind farm, or the wake loading can be changed in order to minimise the interference (see Dahlberg (1998) and Steinbuch *et al.* (1988)).

In addition, the recently observed wake meandering (Medici & Alfredsson (2005)) is starting to interest the wind energy community and there are few experimental data, although low frequency peaks in the velocity spectra at Alsvik were measured (Hassan (1996)) for wind speeds up to 9 m/s. More is known for helicopter wake stability and tip-vortex behaviour, see e.g. Leishman (1998). The tip-vortices stability depends on the vortex core, tip-speed ratio ($\lambda = \text{tip speed/wind speed}$) and axial interference factor (Okulov & Sørensen (2004)). These parameters are used to represent among others the wake pitch, defined as the streamwise distance travelled by the tip vortex in a full blade rotation. The tip-vortices start to interact when the pitch is small enough, i.e. the vortex lines are closely spaced, which influence the near-wake development.

2. Experimental set-up and methods

The experiments were performed in the MTL (Minimum Turbulence Level) wind tunnel at KTH Mechanics, Stockholm in order to evaluate the effect of the number of blades N (1, 2 or 3) on the near wake development. The closed-circuit wind tunnel has a maximum speed of 69 m/s and the turbulence level at 8 m/s is less than 0.1% the freestream velocity. The air temperature is controlled by a heat exchanger positioned immediately after the fan. The test section is 1.2 m \times 0.8 m and 7 m long. The adjustable ceiling is used to correct for the boundary layer growth along the empty test section and to create a zero-pressure gradient.

The wind turbine rotor is centred in the origin of the reference system (figure 1) and the blade azimuthal angle θ is defined to be zero with a blade vertical and in front of the tower. The diameter of the rotor is 0.18 m, including the 0.025 m hub, and the height of the centre of the hub above the floor is 0.24 m. The non-twisted blade is based on the Göttingen 417A airfoil and has been built at FOI (Swedish Defense Research Agency), Stockholm. Details on the blades can be found in Montgomerie & Dahlberg (2003) and in Medici & Alfredsson (2005). The maximum chord is 27 mm at 12% of the radius, and the tip chord is 16 mm. The blades were set at a pitch of 11° within an accuracy of a few seconds of a degree. The drag was measured by a calibrated strain-gauge fixed on the turbine tower and the power was given by a generator which also provided the necessary loading torque on the rotor. The load was determined by the number of electrical diodes connected to the generator, from short circuiting to free-running (open circuit) conditions. The one-bladed rotor

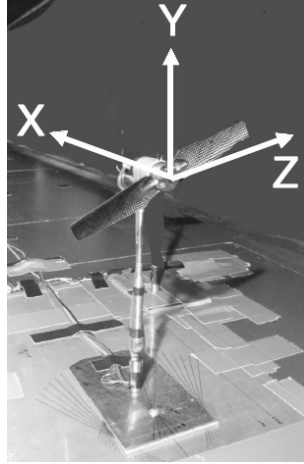


FIGURE 1. The two-bladed wind turbine model mounted in the tunnel with the coordinate system indicated.

was obtained from the two-bladed by removing one of the blade and statically balancing the rotor, with an added weight of small dimensions.

The freestream velocity was measured by a Pitot tube positioned upstream of the wind turbine models and it was approximately 8.0 m/s in all experiments. The streamwise (U, u : mean and fluctuating component) and radial (W, w : mean and fluctuating component) velocities were measured with hot-wire anemometry. An X-probe was used with a measuring volume of approximately 1 mm^3 . The traversing system on which the probe was mounted has 5 degrees of freedom: downstream, spanwise and vertical (x, y, z) and rotation around the y -axis and x -axis (α, ϕ), each controlled by a dedicated servomotor.

The data were recorded for 30 s at 5 kHz and simultaneously acquired on 3 channels: two for the X-probe and one for a photodiode, the latter was illuminated by a laser beam intersecting the area swept by the blades. The circuit connected to the photodiode had a voltage step every time a blade crossed the $\theta=0$ position and shielded the laser beam.

The probe was traversed to 18 radial grid points. The grid points were not equally spaced but chosen to be closer together at $r/D = 0.6$ in order to have a better resolution around the tip-vortices. The measurements were performed at $x/D = 0.5, 1, 2, 4, 9$ and for 7 radial directions, although the results here presented are only at hub-height.

3. Results and discussion

3.1. Wind turbine characteristics

The power and drag coefficients for the turbines with 1, 2 and 3 blades are presented in figure 2. The curves show that by increasing the number of blades the maximum power coefficient $C_{P_{max}}$ is obtained at a lower tip speed ratio (λ) and also that drag coefficient levels off and even decreases at high tip speed ratios. The generated power depends on the torque at the rotor, but it does not increase linearly with the number of blades. The filled symbols mark the maximum power coefficient points for the three turbines. The same λ as $N = 3$ at $C_{P_{max}}$ has been used for one set of measurements with $N = 1$ (figure 2, "*" symbol). Measurements were also made for $N = 3$ at the same drag coefficient as $N = 2$, $C_{P_{max}}$ ("+" symbol in figure 2). An additional resistor connected in series with the diodes has been used to fine-tune the value of the tip-speed ratio. See table 1 for the detailed running conditions.

The location of the maximum power coefficient is a crucial characteristic in a wind tunnel test, although the value itself is usually smaller than for a large scale wind turbine. The power coefficient obtained with this blade profile, chosen for its good performances at low Reynolds number, is slightly lower than expected (Montgomerie & Dahlberg (2003)) and, as it will be shown later in the paper, it may be a consequence of the flow separation at the blade root.

The drag coefficient for $\lambda \rightarrow 0$ approaches different values depending on the number of blades. This is in agreement with the idea that for low tip-speed ratios the flow "feels" the turbine as a slowly rotating plate and the drag on the turbine for low λ is close to that for a rectangular plate (see Medici & Alfredsson (2005)). The blockage of one blade is approximately 7% of the rotor area and the drag coefficient for a rectangular plate normalized with the swept area is 0.08. This is close to the value that is aimed by the C_D curve for $\lambda=0$ and $N = 1$. The values for $N = 2$ and $N = 3$ are close to the double and triple of the value obtained for the $N = 1$ case.

	λ	C_D	C_P
$N = 1 \max C_P$	4.41	0.50	0.20
⁽¹⁾ $N = 2 \max C_P$	3.82	0.75	0.29
$N = 3$ same C_D as ⁽¹⁾	2.23	0.74	0.23
⁽²⁾ $N = 3 \max C_P$	2.94	0.85	0.32
$N = 1$ same λ as ⁽²⁾	2.93	0.37	0.12

TABLE 1. Experimental conditions.

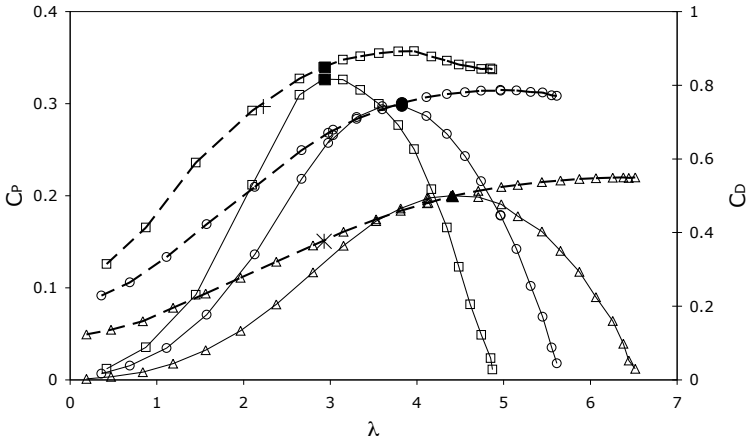


FIGURE 2. Drag (---) and power (—) coefficients as function of the tip-speed ratio λ . $U_\infty=7.90$ m/s. \triangle : $N = 1$; \circ : $N = 2$; \square : $N = 3$.

3.2. Effects of tip-speed ratio on the near wake

The normalised mean streamwise and radial velocities (U/U_∞ , W/U_∞) measured at $x/D = 1$ at hub-height are plotted as function of the tip-speed ratio in figure 3 and figure 4, respectively. The wake boundary is (arbitrarily) defined at $U/U_\infty = 0.98$ and it is only marginally affected by the increase in λ in thereby C_D . The streamtube must expand under the influence of the reduced momentum in the wake, but it is clear from figure 3 that most of the change occurs in the centre of the wake. The velocity decreases rapidly for increasing λ but it tends to become constant at higher values of λ , thus following the trend of the drag coefficient. Compared to the behaviour of the drag in figure 2 it is clear how this dependency is not linear, but the centrifugal forces in the wake may play a greater role at high tip-speed ratios.

The radial velocity W , which is seen to be negative in figure 4, shows that the flow is directed towards the centre of the wake and therefore the wake tends to recover by gaining speed from the higher momentum region. For $N = 3$ this trend is clear already at lower tip-speed ratios than for the wake behind the two-bladed turbine. The contour line for $W = 0$ intersects the wake boundaries (plotted as a dashed line in figure 4) at $\lambda = 1.3$ for $N = 2$ and $\lambda = 2.8$ for $N = 3$.

A massive separation is likely to occur on the blades at low tip-speed ratio. This can be detected not only by the inspection of the hot-wire signal, but also from the behaviour of the mean values. Consider the case for $N = 3$ approaching $\lambda = 1$ from the low tip-speed ratio side. Both the streamwise and radial velocities show a change in tendency. The contour of $U/U_\infty = 0.5$ in figure 3 suggests that the wake at the root is stronger, then the velocity

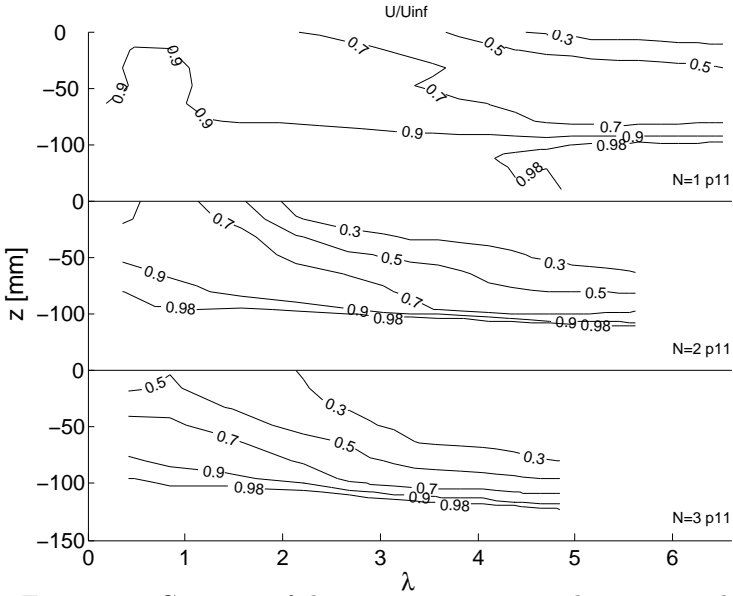


FIGURE 3. Contours of the mean streamwise velocity normalized with the freestream velocity (U/U_∞) as function of λ for (from top) $N = 1, 2, 3$ at $x/D = 1$.

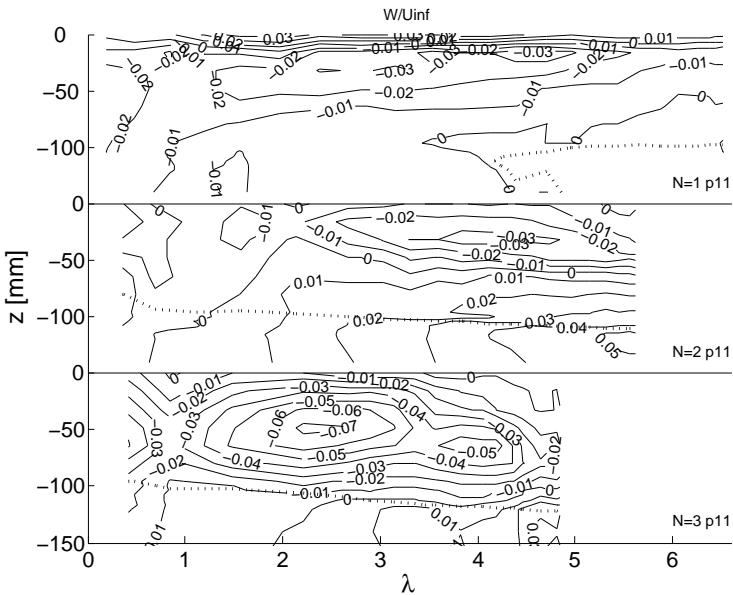


FIGURE 4. Radial velocity normalized with the freestream velocity (W/U_∞) as function of λ for (from top) $N = 1, 2, 3$ at $x/D = 1$. The dashed line represent the contour at $U/U_\infty = 0.98$.

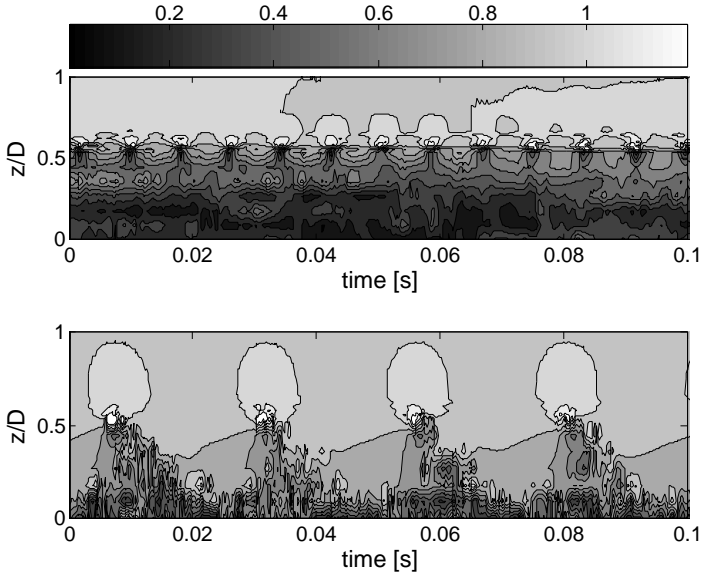


FIGURE 5. Time signal of the normalised streamwise velocity $(U + u)/U_\infty$ in the z -direction at $x/D = 0.5$. All the time signals are triggered at $\theta = 0$. upper: $N = 3$, measurement taken at $C_{P_{max}}$, $\lambda = 2.94$; lower: $N = 1$, $\lambda = 2.93$.

through the rotor increases for $\lambda \rightarrow 1$: the flow on the blades has reattached due to the increased azimuthal velocity. The velocity begins to decrease again for $\lambda > 1$, meaning that the rotor extracts energy more efficiently, i.e. without a massive separation on the blades. This is connected with the saddle in the contour of the radial velocity for $\lambda = 1$ in figure 4. A similar behaviour is seen for $N = 1$ and $N = 2$.

The effect of the blade number on the near wake ($x/D = 0.5$) is illustrated in figure 5 where the 1- and 3-bladed turbines are run at the same tip speed ratio. The velocity signals from all the 18 radial positions have been synchronised so that the blade passage at $\theta=0$ corresponds to $t = 0$ and thereby it is possible to reconstruct the wake. The time axis for the plots have been chosen such that the plots are close to the real geometrical scale.

The 3-bladed turbine gives rise to wake meandering which is clearly seen in the free stream for $z/D > 0.7$ at $t = 0.04$. Figure 5 shows clearly how the interaction between the tip-vortices is much stronger for the 3-bladed turbine, as expected by the consideration that the wake pitch is the same and two vortex lines have been added from the $N = 1$ case. The regularly spaced 9 contour levels are used between $U/U_\infty = 0$ and $U/U_\infty = 0.9U$. The free

stream is set at $U/U_\infty = 0.98$. The helical shape of the wake for $N = 1$ is also visible almost to the centre of the wake. The centre of the wake is transported downstream slower than the outer part of the wake and therefore it reaches the measuring position at $x/D = 0.5$ later than the faster regions of the wake. In other words, the wake can be seen as moving from right to left in all the plots which are a function of time. The tip-vortex can be reconstructed well because of its deterministic nature, whereas the inner turbulent region can only be reproduced without the real-time synchronisation, which would instead require the simultaneous sampling of the velocity in all the radial points.

3.3. Effects of the number of blades on the wake development

Contours of the streamwise velocity in the xz -plane taken at hub-height for $N = 2$ and $N = 3$ is shown in figure 6. The wake for $N = 2$ is taken at $C_{P_{max}}$ and the data for $N = 3$ is taken at the same C_D . It is clearly seen that the wake behind the three-bladed turbine recovers much faster than that behind the two-bladed despite the fact that for both cases C_D is the same. This clearly shows that not only the drag of the turbine is important for the wake development but also the initial wake structure.

In order to further illustrate the difference between the two cases the velocities for $N = 3$ is subtracted to the values obtained in the same positions for $N = 2$ at $C_{P_{max}}$, normalised with the corresponding values at $z/D = 1.78$. In

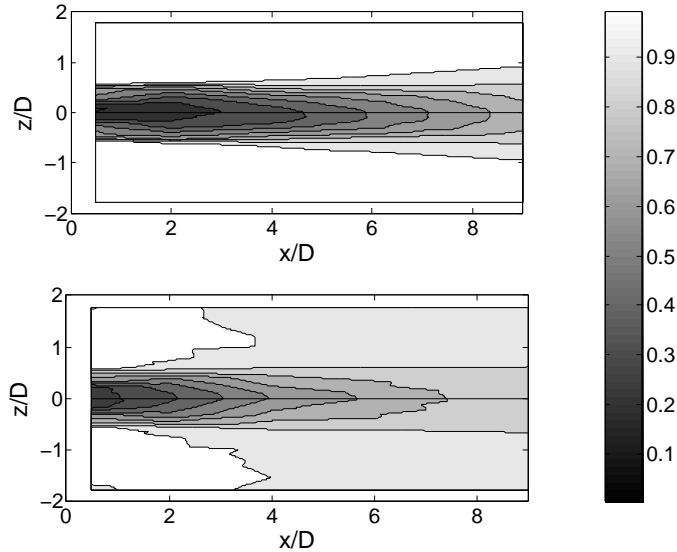


FIGURE 6. Contour of the normalised mean streamwise velocity in the radial (z/D) and downstream (x/D) directions: upper: $N = 2$ at $C_{P_{max}}$, lower: $N = 3$ at same C_D as upper figure.

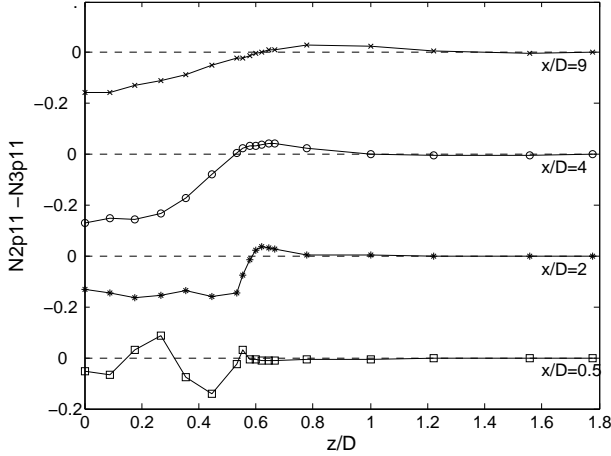


FIGURE 7. Streamwise velocity difference: $U_{(N=2,maxC_P)}/U_\infty - U_{(N=3,sameC_D)}/U_\infty$. A negative difference means that the local mean streamwise velocity for the $N = 3$ case is higher than for the $N = 2$ case, i.e. a faster wake recovery. The data have been normalised with the value at $r/D = 1.78$.

this way the offset (approximately 2%) resulting from the measurement of the freestream velocity has been corrected for. The result is plotted in figure 7. A negative difference means that the velocity for $N = 3$ is higher than for $N = 2$. At $x/D = 0.5$ the integral along z should be zero, since the drag coefficient is the same. It is extremely difficult to evaluate this integral since a very small error at a large distance from the centre has a pivotal effect and in addition the spacing between the points is not optimised for this purpose. The central region for the $N = 3$ wake is considerably faster, but the positive values on the outer region show that the wake expands more.

The effect of the number of blades was also investigated for turbines with the same tip-speed ratio, i.e. the same tip-speed since the freestream velocity was constant. Matching the same λ of $N = 3$ at $C_{P,max}$ with a one-bladed turbine gives the mean streamwise velocity contour of figure 8. It is clearly seen how the wake behind the one-bladed turbine does not expand significantly. By comparing the spectra for the two cases it is clear that for the one-bladed turbine the wake still persist at $x/D=9$ whereas no peak is found in the spectrum for the three-bladed turbine at this position. This indicates that the helical vortices confine the wake and hinders its spreading.

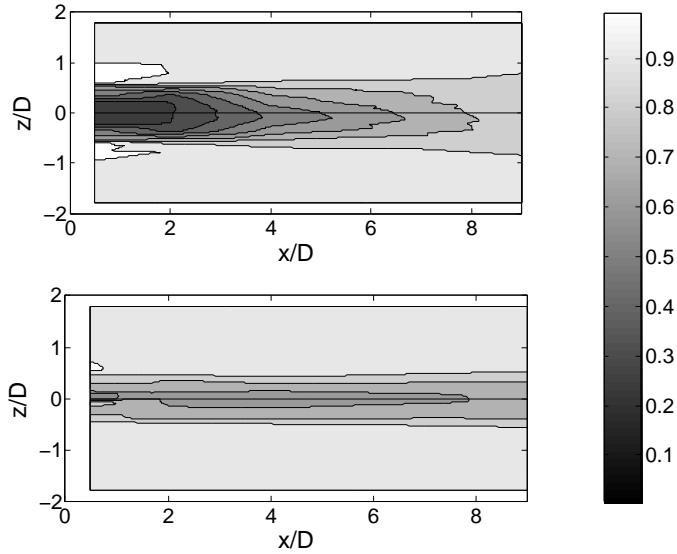


FIGURE 8. Contour of the normalised mean streamwise velocity, upper: $N = 3$ at $C_{P_{max}}$, lower: $N = 1$, same λ as for the upper figure.

3.4. Wake as function of the azimuthal angle

The interest for the one-bladed turbine is not in the possible commercial application, but in the reconstruction of the wake behind the rotating blade. The helical wakes produced by each blade in a multi-bladed turbine interact strongly with each other and merge quickly together. The screw thread of the wake becomes virtually indistinguishable and running the two or three-bladed turbine at very low λ in order to separate the helical wakes of the blades is likely to stall the flow.

The dependency of the streamwise velocity $(U + u)/U_\infty$ on the azimuthal angle can be seen in the ensemble average shown in figure 9 for $N = 1$ at $C_{P_{max}}$, $x/D = 0.5$. All the data have been synchronised with the blade passage and then averaged for equal θ . The use of the ensemble average gives the cyclical contributions of the wake, without the time averaging performed usually in the measurements. The rotational frequency is 61.9 Hz, hence a blade complete the 2π rotation in 0.016 seconds. The passage of the tip vortex is in relation with an increased streamwise velocity in the centre of the wake. The reason may be that the wake is shed by the turbine blade simultaneously with the tip vortex, but the central region moves downstream with a lower velocity and therefore it reaches $x/D = 0.5$ at a different azimuthal angle. The contour of the *rms* of the streamwise velocity is plotted in figure 10. The plots show a region of low

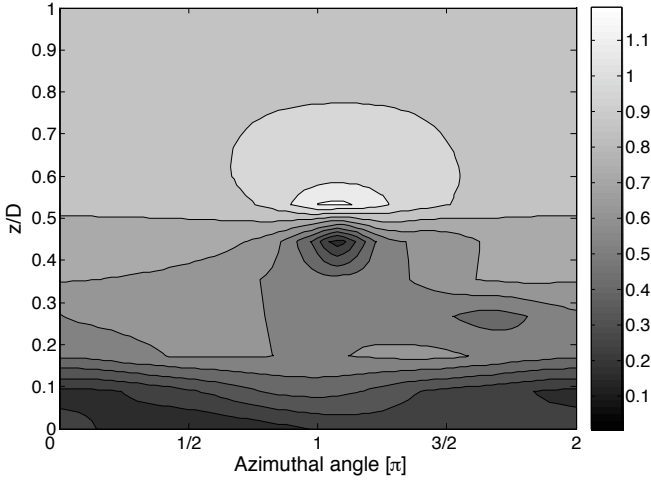


FIGURE 9. Normalised streamwise velocity for $N = 1$ as a function of the azimuthal angle, ensemble average at $x/D = 0.5$.

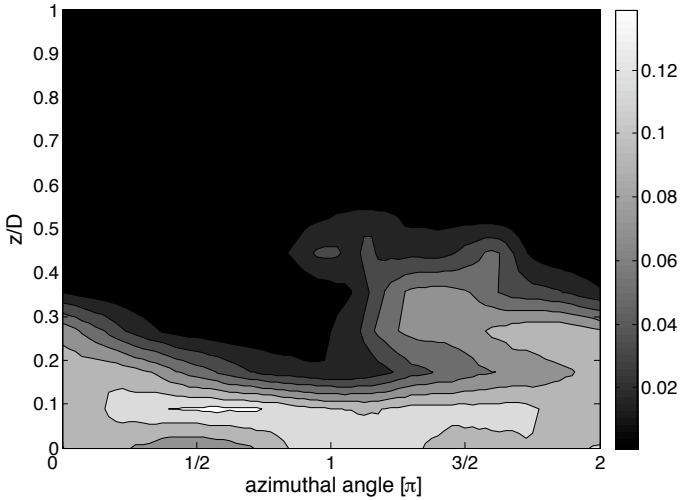


FIGURE 10. Normalised rms of the streamwise velocity for $N = 1$ as a function of the azimuthal angle, ensemble average at $x/D = 0.5$.

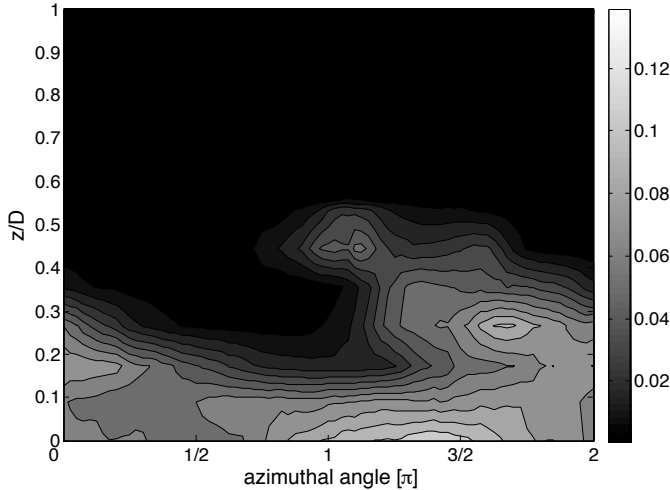


FIGURE 11. Normalised *rms* of the spanwise velocity for $N = 1$ as a function of the azimuthal angle, ensemble average at $x/D = 0.5$.

velocities and high fluctuations in the centre of the wake, where the effect of the hub and of the stalled flow at the blade root is strongest. The helical wake is best seen also in the ensemble average of the fluctuating component of the radial velocity (figure 11). The highest peak is found in the centre of the wake for $\theta \approx 1.37\pi$.

The ensemble average at $x/D=9$ shows the cyclical passage of the wake in the form of a small *rms* peak (both of the streamwise and radial velocities), but the mean values are not periodic any more.

4. Conclusions

The wake behind a wind turbine as measured in a wind tunnel looks quite different from the simulated result in some numerical models, see Crespo *et al.* (1999). The reason is that the turbulence mixing and the presence of the hub tend to see the merging of the helical wakes that are shed by the blades. Running at low tip-speed ratio is likely to stall the flow on the blades, as can be seen from the contours of the velocity as function of λ . One way to visualise the helical wake was to run a one-bladed turbine at high tip-speed ratio. Although the non-twisted blade had a separation region at the root, the deterministic passage of the wake at $x/D = 0.5$ was reconstructed by triggering the measurements with the blade azimuthal position. The measurements spanned over typical wind farm distances, up to 9 diameters downstream, finding the end of the near wake between 2 and 4 diameters and the maximum streamwise velocity gradient at $x/D = 4$. By nearing the vortex lines on the boundary of the wind turbine wake (either with an increased rotational velocity or with the

addition of more blades), an increasing interaction between the vortices was observed.

References

- CRESPO, A., HERNÁNDEZ, J. & FRANDBSEN, S. 1999 Survey of modelling methods for wind turbine wakes and wind farms. *Wind Energy* **2**, 1–24.
- DAHLBERG, J. A. 1998 Möjligheter och risker med stora vindfarmer till havs (in Swedish). Presented at *Vind-98*, CTH, Göteborg, Sweden.
- DAHLBERG, J. A. & MEDICI, D. 2003 Potential improvement of wind turbine array efficiency by active wake control (AWC). In *Proc. European Wind Energy Conference and Exhibition*, Madrid, (published on CD).
- HASSAN, G. 1996 Dynamic loads in wind farms II. Final report Joule Project, JOU2-CT92-0094.
- LEISHMAN, J. G. 1998 Measurements of the aperiodic wake of a hovering rotor. *Exp. in Fluids* **25**, 352–361.
- MEDICI, D. & ALFREDSSON, P. H. 2005 Measurements on a wind turbine wake: 3d effects and bluff-body vortex shedding. *Wind Energy*, published online.
- MONTGOMERIE, B. & DAHLBERG, J. A. 2003 Vortex system studies on small wind turbines. FOI scientific report, ISRN FOI-R-0936-SE.
- OKULOV, V. L. & SØRENSEN, J. N. 2004 Instability of the far wake behind a wind turbine. In *Proc. of the XX ICTAM*, Warsaw, Poland.
- OKULOV, V. L. & SØRENSEN, J. N. 2005 Modelling of the far wake behind a wind turbine. Presented at the IEA Annex 11/20 meeting, Pamplona.
- SCHEPHERD, D. G. 1990 Historical development of the windmill. NASA paper DOE/NASA/5266-1.
- STEINBUCH, M., DE BOER, W. W., BOSGRA, O. H., PETRS, S. A. W. M. & PLOEG, J. 1988 Optimal control of wind power plants. *J. Wind Eng. Ind. Aer.* **27**, 237–246.
- VERMEER, L. J., SØRENSEN, J. N. & CRESPO, A. 2003 Wind turbine wake aerodynamics. *Prog. Aerospace Sci.* **39**, 467–510.
- DE VRIES, O. 1979 Fluid dynamic aspects of wind energy conversion. AGARD publication, AGARDograph 243.

Paper 4

4

The upstream flow of a 3-bladed wind turbine in yaw

By **D. Medici**

KTH Mechanics, SE-100 44 Stockholm, Sweden

Presented at the International Energy Agency Annex XI/XX Symposium 2005,
CENER, Pamplona, Spain.

An extensive set of velocity data are measured with Particle Image Velocimetry upstream a three-bladed 180 mm wind turbine rotor. The normal and radial velocities to the rotor are measured for different inclinations (yaw angles) of the turbine to the freestream velocity: $\alpha=0^\circ$, 10° , 20° . Since the wake is not axisymmetric in yaw, the measurements span the entire rotor and show the different induced velocities between the upwind and downwind sides. The flow is deflected already at a considerable distance upstream towards the downwind side as a reaction to the side force created on the yawed turbine. The formation of the tip-vortex is seen at the rotor as a peak in the radial velocity and its position moves towards the downwind side with increasing yaw angle. The pressure on the upstream side of the rotor is estimated from the velocity field for all the yaw angles and the momentum theory is used to calculate the drag coefficient.

1. Introduction

Wind energy utilisation is expanding and although its growth raises new questions, some basic problems still have to be answered. The researchers and developers are challenged to reduce the spacing between wind turbines in a farm in order to optimise the land and the offshore areas. The problem of the interaction between a wake and a turbine or between wakes (Carlén & Dahlberg (2005) and Corten *et al.* (2003)) is difficult to estimate, but computer simulations can be very useful for these studies. In such a perspective, the relatively simple actuator disc model can simulate a wind turbine, see e.g. Sørensen *et al.* (1998), van Kuik (2003) and Sharpe (2004). The majority of the previous studies such as the one by Alfredsson *et al.* (1980) focus on the wake or the application of the experimental results on a number of numerical models, which are well described by Vermeer *et al.* (2003). The measurements have been made with several techniques: optical methods, laser, pressure probes, hot-wire anemometry just to mention the principal methods. Among the laser techniques is the Particle Image Velocimetry (PIV), which has been used to estimate the strength and to track the vortex development (such as in Grant

& Parkin (2000)) or to measure the wake at different yaw angles, e.g. Parkin *et al.* (2001). A number of measurements have been taken in wind tunnels on the flow approaching a wind turbine, but focussed only on a few points (for comparisons with data from meteorological masts), or on the flow close to the blades, such as for the NREL measurements (see Schreck (2002)) which provided valuable data of the aerodynamic coefficients as a function of the angle of attack. The latter experiment was also aimed at measuring the local inflow conditions on the blades.

The present study on the other hand determines experimentally the flow approaching the wind turbine in a large region upstream the turbine. Wind turbines can be misaligned for a considerable time with respect to the wind direction as a result of cross winds or of the recently developed concept of Active Wake Control (see Dahlberg & Medici (2003)), therefore the wind turbine in this study is yawed up to 20° . Since the flow field with the turbine in yaw is not axisymmetric, the measurements span the entire diameter of the turbine at hub-height. To the knowledge of the author, similar results have not been presented before and it is believed that they can offer a unique set of data for the understanding of the flow approaching a wind turbine or an actuator disc. These results can also be relevant in comparison with the momentum theory.

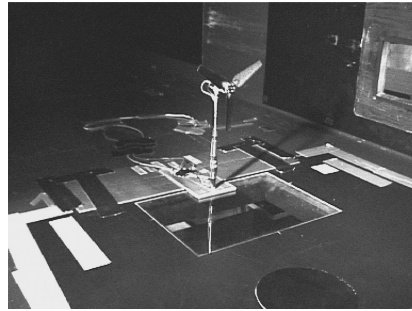
2. Experimental set-up and methods

The experiment was performed in the MTL (Minimum Turbulence Level) wind tunnel at KTH Mechanics. The test section has a width and height of 1.2 m and 0.8 m respectively, and its length is 7 m. The ceiling is adjustable, which makes it possible to provide a constant velocity in the streamwise direction despite the boundary layer growth on the test section walls. The maximum speed achievable in the tunnel is more than 60 m/s, however for the present study a typical freestream velocity was 8 m/s. The wind tunnel provides stable flow conditions and the air temperature is controlled by means of a heat exchanger.

The three-bladed turbine is shown in figure 1(a), it has a diameter of 0.18 m and it is mounted on the wind tunnel floor along the centreline, 1.45 m from the test section inlet. The blockage of the model is less than 3% of the wind tunnel cross-section. The hub diameter is 25 mm and its centre is 0.24 m above the floor. The non-twisted blade is based on the Göttingen 417A airfoil (see Riegels (1961)) and consists of a four-layered structure of reinforced epoxy with a constant thickness of about 0.5 mm. The maximum chord is 27 mm at 12% of the radius, and the tip chord is 16 mm. Details on the blades and their construction can be found in Montgomerie & Dahlberg (2003) and in Medici & Alfredsson (2005). The rotor was connected to a 24 V DC generator that provided the breaking torque. The tip speed ratio (λ =tip speed/wind speed) was changed keeping the wind speed constant and by connecting a number of electrical diodes to the generator, from short circuiting to free-running (open circuit) conditions. An high loading from the generator requires a low rotational frequency. On the other hand, the turbine is free-running with the open circuit:



(a) Wind turbine model as seen from upstream.



(b) The laser fires through the window on the RHS, while the camera looks up through the tunnel floor.

FIGURE 1. Experimental set-up.

Yaw angle	U_∞ [m/s]	λ	C_P	C_D
0°	7.8	2.803	0.308	0.834
10°	7.9	2.802	0.295	n.a.
20°	7.8	3.613	0.242	n.a.

TABLE 1. Experimental conditions.

no aerodynamic torque is required at the rotor because there is no current (i.e. no loading) in the circuit.

The experimental set-up is shown in figure 1(b). The experimental conditions of the wind turbine model are summarised in table 1 for all the three yaw angles ($\alpha=0^\circ$, 10° , 20°). The coordinate system is centred in the middle of the rotor. From upstream, the x -axis is directed in the undisturbed wind direction, the y -axis points upwards and the z -axis is positive towards the right hand side. The yaw angle is defined positive when the left hand side of the turbine is turned upstream (rotation around the positive y -axis).

The PIV system included a two-cavity (400mJ each) Nd:YAG laser, with a wavelength, after frequency doubling, of 532 nm and pulse frequency of 17 Hz. The laser was synchronised with a digital high-resolution Kodak ES 1.0 CCD-camera (1008×1018 pixel) equipped with a 60 mm lens. The processor and software was delivered by DANTEC Measurement Technology, Denmark. The seeding was introduced downstream of the test section and re-circulated around the closed circuit wind tunnel producing even seeding in the test section. The laser fires twice in a very short time interval, typically $\Delta t=80 \mu\text{s}$, while the camera records one image at each laser shot. The position of the smoke particles is acquired by the software. Each frame is divided into the so called *interrogation areas*, i.e. the full image is split into 62×62 sub-sections. The position of the particles at time t is cross-correlated with the new position assumed at

$t + \Delta t$ in each interrogation area, giving the most probable displacement. The streamwise (U, u : mean and fluctuating component) and radial (W, w : mean and fluctuating component) velocities in the x and z -direction are therefore obtained after dividing by the time interval between the shots. The map with 3844 vectors is stored in the computer memory after each calculation. A large number of vector fields (approximately 1600) has been recorded for each measurement, with a resolution of 1.24 mm for a side length of the image of 76 mm.

The laser illuminates the flow from outside the wind tunnel test-section at the hub-height (plane xz), through the plexiglass window visible on the right side of the turbine model. The camera is placed under the tunnel floor and looks up at the rotor plane. The turbine is on the bottom of the image and the flow is top-to-bottom. Therefore the flow direction is defined positive from top to bottom for the streamwise velocity and towards the RHS for the radial velocity (respectively towards positive x and z -axis). In order to measure the drag D on the wind turbine, the tower was mounted on a strain-gauge balance that was always perpendicular to the rotor. The strain-gauge was calibrated by applying a known force in the centre of the hub.

3. Results and discussion

The application point of the forces is in the centre of the hub only for $\alpha=0^\circ$. For this condition, the drag and the power coefficients of the wind turbine as function of the tip speed ratio are shown in figure 2. The PIV measurements were performed at the $C_{P_{max}}$ with a blade pitch angle (angle between the blade chord and the rotor plane) of 11° and for a constant wind speed of 8 m/s. The C_D at high λ decreases with increasing tip-speed since the sections of the blade approach the zero-lift angle of attack.

3.1. Stagnation point and normal velocity

The non-rotating turbines as seen by the camera for $\alpha=0^\circ$ and $\alpha=20^\circ$ are shown in figure 3. These images are used to find the position of the blades in the laser plane and to find the origin of the reference system. The solid line around the wind turbine is considered to enclose the overlapping region. The camera was fixed and the turbine support was moved alongside the z -axis since the lens used for the experiment allowed a good spatial resolution, but a relatively small image. Several experiments were combined to obtain the final images here presented. The data for $\alpha=0^\circ$ were measured for one side only of the rotor and then mirrored to obtain the values for negative z . For $\alpha=20^\circ$ the turbine had to be moved also in the x -direction in order to compensate for the displacement along the streamwise axis.

The mean velocity vectors (U, W) close to the hub can be seen in figure 4 for $\alpha=0^\circ$. The lines bounding the turbine model show part of the hub (from $z = -5$ to $z = +12.5$) and the root of the blade. The streamlines are plotted with a Matlab toolbox. The stagnation point can be found at $z = +0.6$ and $x = +6.9$ by following the streamline which connects the vectors with zero

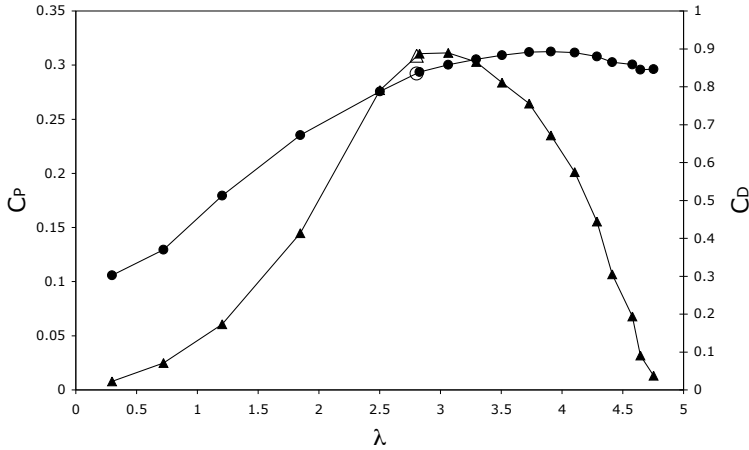
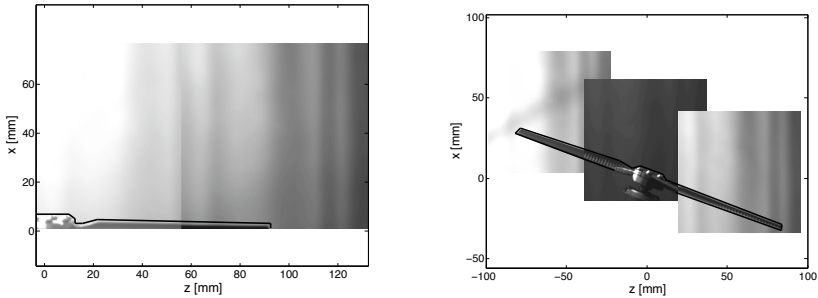


FIGURE 2. Drag (●) and power (▲) coefficients as function of the tip-speed ratio λ for $U_\infty=8$ m/s. The empty symbols mark the PIV measurements at $C_{P_{max}}$.



(a) Camera view for $\alpha=0^\circ$. (b) Camera view, $\alpha=20^\circ$. Note the different axis limits than figure 3(a).

FIGURE 3. Images used to obtain the position of the wind turbine in the field of view of the camera. The flow is from top to bottom and the laser is from the right.

radial velocity to the hub. This result agrees well with the expected position at the centre of the rotor, within the accuracy granted by the resolution of the interrogation areas. To lock the blades in place, the hub had six screws (see also figure 1(a)) that shadowed the centre of the hub from the laser light. Therefore the actual stagnation point is at $x = +5$, after subtracting the height

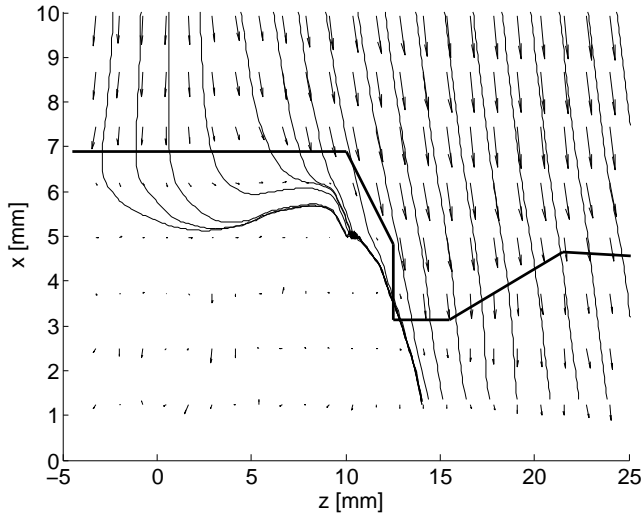


FIGURE 4. Streamlines at yaw = 0° for the region close to the hub. The stagnation point is found at the intersection between the streamline at $z=+0.6$ mm and the hub.

of the heads of the screws. The velocity vectors overlapping with the hub are the result of background noise in the PIV images. The streamlines and the velocity vectors overlap also with the area swept by the blades since the laser was not triggered by the blade passage, but shot instead at random blade azimuthal angles (i.e. at different positions of the blade on the rotor plane). The mean vectors upstream are not affected by the azimuthal angle and it will be shown later that only close to the blades there is an influence of the rotation in the form of an out-of-plane velocity component. The contours of the velocity normal to the rotor for $\alpha=20^\circ$ in figure 5 show a region with higher velocity along the blade turned upstream, which therefore must contribute more to the torque at the shaft. The rotor is consequently unbalanced, but nothing can be said about the velocity distribution outside of the laser sheet. It can be observed that the normal velocities are measured in the wake and only for a small area behind the blades. These data offer an indication of the large extraction of momentum from the flow across the rotor. The wake is deeper at the downwind side, where the vortex lines are closer and therefore accordingly to the Biot-Savart law the induced velocities are higher.

3.2. Radial velocity

The x and z -axis are normal to the tunnel walls since the camera is fixed, but the radial velocities are referred to the rotor itself and are considered positive towards the downwind side (positive z) of the rotor.

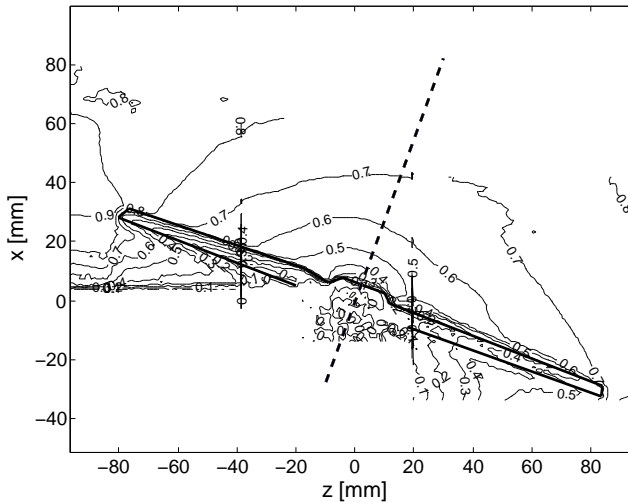


FIGURE 5. Normal velocity for yaw = 20° . The dotted line is the rotor axis of symmetry and highlights the differences in the flow field between the RHS and the LHS of the turbine.

For $\alpha=0^\circ$ the velocity contours are shown in figure 6. The zero-contour line is at $z = +0.6$ and corresponds to the streamline plotted in figure 4. An interesting feature can be observed: the tip vortex leaves a trace of its formation in the xz plane in the form of the radial velocity peak, if the blade is not overlapping with the laser sheet. The peak is clearly visible for $\alpha=0^\circ$ at $z = +84$ (i.e. 93% of the rotor radius).

It is well known (e.g. Dahlberg & Medici (2003)) that a wind turbine in yaw reacts with a force on the flow and therefore the wake moves towards the downwind side of the turbine. The flow at $\alpha=10^\circ$ in figure 7(a) is deflected already at a large distance upstream and only close to the rotor it turns towards the negative- z side, as can be seen from the position of the zero-contour line indicated by the arrow. At $\alpha=20^\circ$ (Fig. 7(b)) the contour lines are positive everywhere, both upstream and downstream of the rotor. The side force increases with the yaw angle and as a consequence the flow approaches the turbine only from the upwind side. The radial flow speeds up at the blade tips as for the non-yawed cases, but in yaw the values are considerably higher on the negative- z side. The peak in the region swept by the blades moves towards the downwind side of the yawed rotor. This displacement is more clear on the negative- z side, but it is possible to estimate this effect on the upwind side: the peak moves to 86% and to 77% of the rotor radius for $\alpha=10^\circ$ and $\alpha=20^\circ$ respectively.

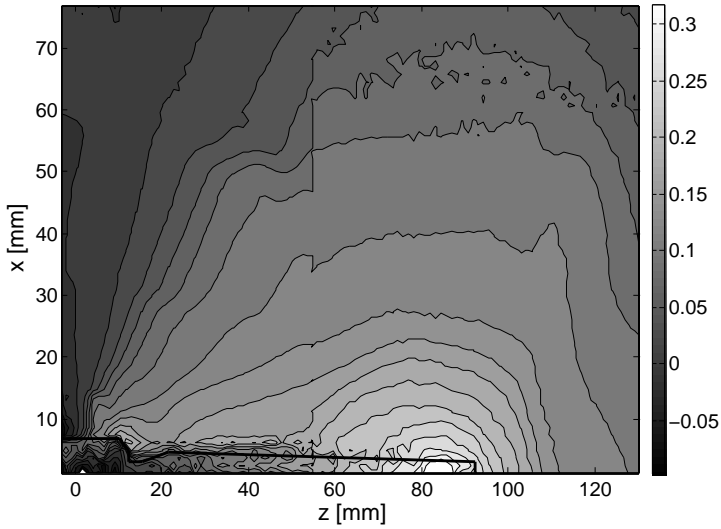
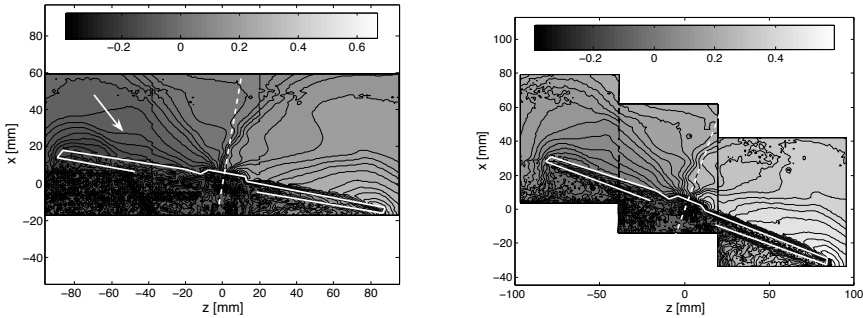


FIGURE 6. Radial velocity for yaw = 0° . The peak close to the blade tip marks the vortex position.



(a) Radial velocities for yaw = 10° , the white line points at the zero-contour line.

(b) The radial velocities for yaw = 20° are positive in the entire flow field.

FIGURE 7. Radial velocity variation with the yaw angle.

The radial velocities are an indication of the lateral displacement of the flow, i.e. how large it is the component left for the power production. A function

$$C_P = C_{P0} \cos^n(\alpha - \alpha_0) \quad (1)$$

can be fitted to the power coefficient vs. the yaw angle, where C_{P0} is the power at $\alpha=0$ and α_0 is the yaw angle which gives the maximum power coefficient. Different values of the exponent n of power loss can be found in literature. For this turbine model they are $n=3.09$ and $\alpha_0=-0.011^\circ$, which agree with the idea that the velocity component normal to the rotor disc decreases with the cosine and therefore the power with its cube. Other wind turbines may have a smaller side force, deflect the flow less strongly to the side and consequently produce more power.

3.3. Static pressure and axial interference factor

In order to fully utilize the potential of yaw as an Active Wake Control on a wind turbine it is necessary to have a good knowledge of the velocity field and the pressures acting on the rotor. In a wind tunnel it is possible to measure the velocity in the wake, but it is difficult to reach the upstream side of the rotor with a probe. On the other hand, the pressure can be derived by the velocity field assuming that the flow upstream is irrotational.

A typical example of the streamwise and radial velocities U and W approaching the rotor can be seen in figure 8. The data are plotted as a function of the streamwise distance from the rotor for $z = +36$ and $\alpha=0^\circ$. The static pressure is calculated in each point of the two-dimensional flow as

$$p = p_{atm} + \frac{1}{2}\rho U_\infty^2 - \frac{1}{2}\rho(U^2 + W^2) \quad (2)$$

where p_{atm} is the static pressure at the Pitot position and U_∞ is the corresponding freestream velocity. Both the velocity components must be included in the equation, since the Bernoulli equation can be applied only along a streamline. The velocity and consequently the pressure, changes gradually up to $x = +7.4$, where the values drop since the out-of-plane velocity component (along the y -axis) is not measured by the PIV. Therefore the *actuator disc* is considered to be at the point where the flow is still 2-dimensional, typically 3-4 mm upstream of the rotor. The explanation for this out-of-plane velocity is in the behaviour of the fluid particles approaching the wind turbine. Two effects can contribute to this change of the flow direction: the pressure around the blade and the viscosity. The azimuthal velocity would indicate that the fluid particle is "following" the rotation of the blade if the viscosity rules, i.e. in case of a flow separation on the profile. This is likely to happen at the blade root, since the separation has been measured for $z < +27$ with hot-wires behind a one-bladed wind turbine with the same tip-speed ratio. On the other hand, the azimuthal velocity vector would head towards the approaching blade if the pressure field

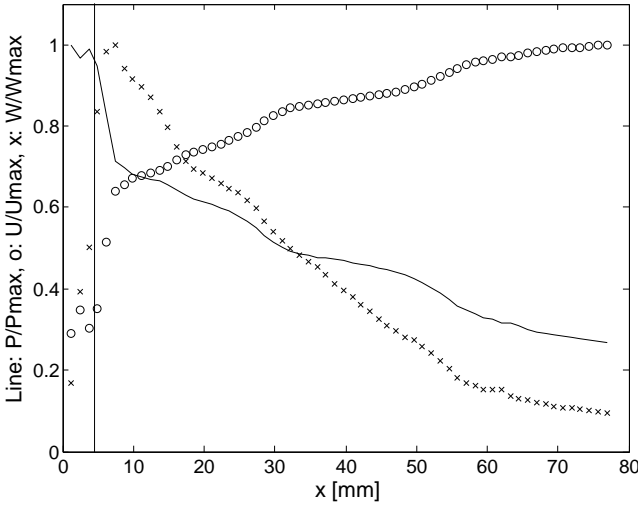


FIGURE 8. Streamwise (\diamond), radial (x) and pressure (solid line) variation as function of the distance to the rotor for $z=+36$ mm. The flow is from right to left. The blade is at $x=4.52$ mm (solid line) and the step rise in the pressure takes place at $x=7.4$ mm.

is strong: the fluid must turn towards the leading edge. The determination of the sign of the azimuthal velocity upstream of the rotor requires a different technique (LDV or 3D PIV). The pressure p^+ and the velocity U^+ immediately upstream of the actuator disc are known in all the field measured by the PIV system and the data can be compared with the classical momentum theory. These quantities are computed for all the yaw angles along the actuator disc, which rotates with the rotor and uses a radial r -axis as a reference.

The variation of the pressure as a function of the radial position for $\alpha=0^\circ$ can be seen in figure 9. The contribution to the drag on the upstream side of the actuator disc can be found by integrating the pressure $p^+(r)$:

$$D_{up} = 2\pi \int_0^R r \cdot p^+(r) dr = 0.412 \text{ N} \quad (3)$$

The total value as measured by the strain-gauge balance is $D = 0.752$ N, hence the upstream side of the actuator disc contributes to 55% of the total drag.

The axial interference factor is defined as $a(r)=(U_\infty - U^+)/U_\infty$ and its average is

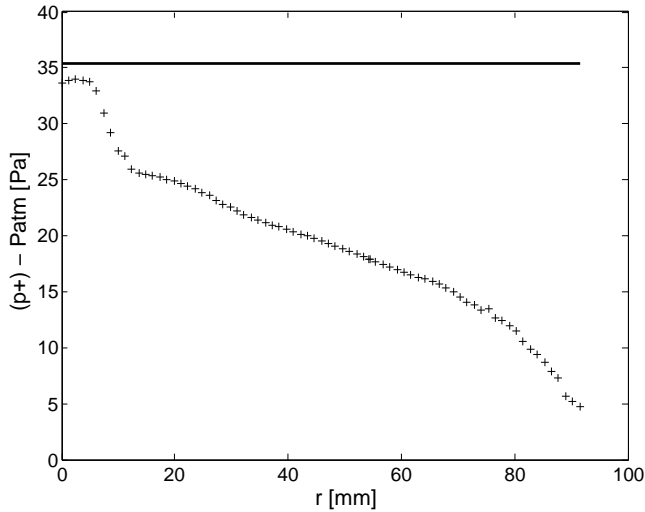


FIGURE 9. Static pressure in Pascal at the actuator disc for $\alpha=0^\circ$. The solid line is the total pressure level at $U_\infty=7.8$ m/s.

$$a = \frac{2\pi}{A_d} \int_0^R r \cdot a(r) dr = 0.305 \quad (4)$$

where A_d is the area swept by the blades. Using the well-known result of the momentum theory for the drag coefficient, the drag coefficient can be estimated as

$$C_D = 4a(1 - a) = 0.849 \quad (5)$$

which is very close to the drag coefficient $C_D=0.835$ as measured by the strain-gauge balance. Both include the contribution of the hub. It must be noted that the actuator disc chosen for the evaluation is upstream of the actual rotor, therefore the axial interference factor is probably underestimated. The static pressure and the axial interference factor for all the yaw angles are shown in figure 10 and figure 11. The pressure field upstream of the actuator disc suggests a restoring yaw moment, but nothing can be said about the contribution of the downstream side of the rotor. The pressure decreases with the yaw angle on the downwind side and it mostly increases on the upwind side. On the other hand, the behaviour of the axial interference factor implies that the velocity is lower on the downwind side (and consequently the pressure should be higher), but only the velocity normal to the actuator disc has been used in figure 11.

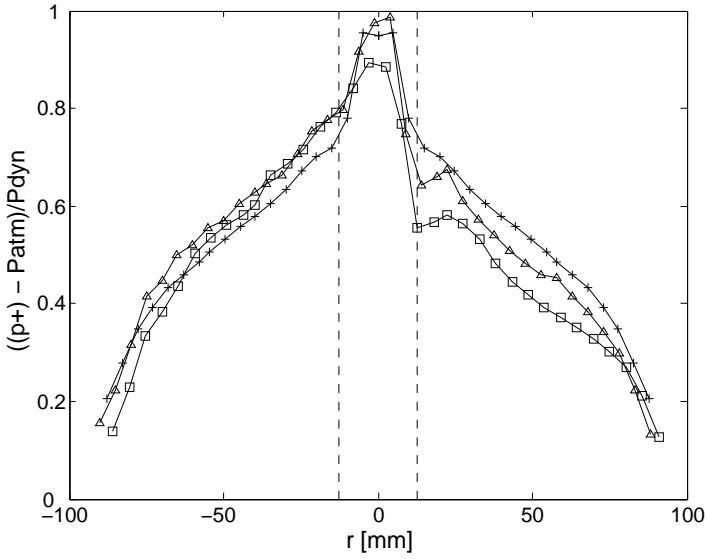


FIGURE 10. Static pressure at the actuator disc for $\alpha=0^\circ$ (+), 10° (\triangle) and 20° (\square) normalised with the total pressure.

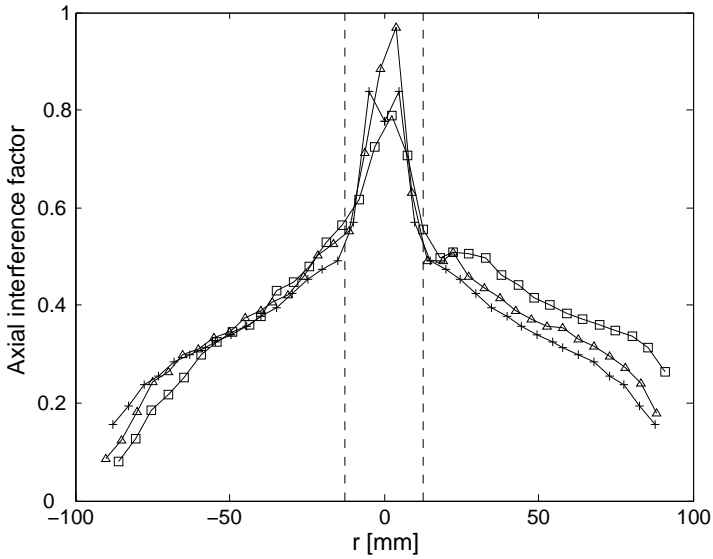


FIGURE 11. Axial interference factor at the actuator disc for yaw = 0° (+), 10° (\triangle) and 20° (\square).

4. Conclusions

The flow field approaching a wind turbine is important both for the study of the performances on the airfoil and for the simulation of a wind farm by means of actuator discs. The latter can offer a relatively simple and efficient way to simulate the interaction between a wind turbine and an oncoming wake. The theory states that the flow upstream of a wind turbine (or propeller) is two-dimensional. This is proved by the results presented in this paper, where an out-of-plane velocity is measured only 3-4 mm upstream of the rotor. The behaviour of the average velocities in the xz -plane shows that the presence of the turbine is affecting a large region upstream and that the side force created by the yawed turbine deflects not only the wake but also the oncoming flow. According to the pressure field, the upstream side of the rotor contributes to the total yaw with a restoring moment. The calculation of the axial interference factor suggests an opposite behaviour, but only the velocity normal to the rotor was used for this purpose. The drag coefficient was independently determined by a strain-gauge balance and by the velocity field at the actuator disc position, showing an excellent agreement.

References

- ALFREDSSON, P. H., DAHLBERG, J. A. & BARK, F. H. 1980 Some properties of the wake behind horizontal axis wind turbines. In *Proc. Third Int. Symp. on Wind Energy Systems*, Copenhagen, BHRA Fluid Engineering, paper J5, pp. 469–484.
- CARLÉN, I. & DAHLBERG, J. A. 2005 Simulation of loads and performance for wind turbines operating in the near wake. FOI scientific report, ISRN FOI-S-1707-SE.
- CORTEN, G. P., SCHAACK, P. & EECEN, P. 2003 Heat and flux. In *Proc. European Wind Energy Conference and Exhibition*, Madrid, (published on CD).
- DAHLBERG, J. A. & MEDICI, D. 2003 Potential improvement of wind turbine array efficiency by active wake control (AWC). In *Proc. European Wind Energy Conference and Exhibition*, Madrid, (published on CD).
- GLAUERT, H. 1926 *The elements of airfoil and airscrew theory*. Cambridge University Press.
- GRANT, I. & PARKIN, P. 2000 A DPIV study of the trailing vortex elements from the blades of a horizontal axis wind turbine in yaw. *Exp. Fluids* **28**, 368–376.
- VAN KUIK, G. A. M. 2003 An inconsistency in the actuator disc momentum theory. *Wind Energy* **7**, 9–19.
- MEDICI, D. & ALFREDSSON, P. H. 2005 Measurements on a wind turbine wake: 3D effects and bluff-body vortex shedding. Published online.
- MONTGOMERIE, B. & DAHLBERG, J. A. 2003 Vortex system studies on small wind turbines. FOI scientific report, ISRN FOI-R-0936-SE.
- PARKIN, P., HOLM, R. & MEDICI, D. 2001 The application of piv to the wake of a wind turbine in yaw. In *Proc. 4th International Symposium on Particle Image Velocimetry, PIV'01*, Göttingen (Ed. J. Kompenhans) DLR-Mitteilung 2001-03 (published on CD).

- RIEGELS, F. W. 1961 *Airfoil sections, results from wind tunnel investigations, theoretical foundations*. Butterworth & Co. LTD.
- SCHRECK, S. 2002 The NREL full-scale wind tunnel experiment. *Wind Energy* **5**, 77–84.
- SHARPE, D. J. 2004 A general momentum theory applied to an energy-extracting actuator disc. *Wind Energy* **7**, 177–188.
- SØRENSEN, J. N., SHEN, W. Z. & MUNDUATE, X. 1998 Analysis of wake states by a full-field actuator disc model. *Wind Energy* **1**, 73–88.
- VERMEER, L. J., SØRENSEN, J. N. & CRESPO, A. 2003 Wind turbine wake aerodynamics. *Prog. Aerospace Sci.* **39**, 467–510.

Paper 5

Measurements on a wind turbine wake: 3D effects and bluff-body vortex shedding

By **D. Medici and P. H. Alfredsson**

KTH Mechanics, SE-100 44 Stockholm, Sweden

Accepted for publication in Wind Energy Journal.

The velocity field in the wake of a two-bladed wind turbine model (diameter 180 mm) has been studied under different conditions using a two-component hot-wire. All three velocity components were measured both for the turbine rotor normal to the oncoming flow as well as with the turbine inclined to the free stream direction (the yaw angle was varied from 0 to 20 degrees). The measurements showed, as expected, a wake rotation in the opposite direction to that of the turbine. A yawed turbine is found to clearly deflect the wake flow to the side showing the potential of controlling the wake by yawing the turbine. An unexpected feature of the flow was that spectra from the time signals showed the appearance of a low frequency fluctuation both in the wake and in the flow outside the wake. This fluctuation was found both with and without free stream turbulence and also with a yawed turbine. The frequency expressed as a Strouhal number was shown to be independent of the freestream velocity or turbulence level, but the low frequency was only observed when the tip speed ratio (or equivalently the drag coefficient) was high. The shedding frequency changed also with the yaw angle. This is in agreement with the idea that the turbine shed structures as a bluff body. The phenomenon, noticeable in all the velocity components, was further investigated using two point cross-correlations of the velocity signals.

1. Introduction

The wake development behind wind turbines is of considerable practical interest, it both gives information on power losses in turbine parks as well as increased turbulence levels which may be affecting flow induced rotor loads. For wind engineering purposes the main interest is in the region up to $10D$, where D is the turbine diameter, downstream the turbine. The main characteristics of the wake are the mean velocity deficit and the tip vortices shed by the blades forming two (or three for a three bladed turbine) spiral vortices downstream the turbine. For a recent comprehensive review on wind turbine wakes the reader is referred to Vermeer *et al.* (2003).

Only few wind tunnel experiments on the wake flow behind rotating wind turbine models have been made as is clear from the the review of Vermeer

et al. (2003). In such experiments it is not possible to keep the same Reynolds number as for the full scale turbine and this will have an influence on the boundary layer development on the blades. This will result in different turbine characteristics and especially the maximum power coefficient will be lower for the model turbine (see e.g. Alfredsson *et al.* (1982)). However many features of the wake flow are the same in model and full scale, such as the tip vortices and wake rotation. If also the drag coefficient is similar one may assume that the Reynolds number of the wake flow is sufficiently large in order to give a similar wake development for the two cases. Previous measurements behind turbine models have mainly been limited to measurements of the streamwise velocity component in order to determine the wake development and the velocity deficit. Therefore it is of interest to also make measurements of the full velocity field (all three velocity components) behind the turbine. For instance Hansen & Butterfield (1993) point out that knowledge of all three velocity components in the flow field is essential in order to predict wind park rotor loads. It should also be noted that a full scale turbine works in the atmospheric boundary layer, i.e. in a turbulent environment and this will have an influence on the wake dispersion.

The flow (wake) behind simple axis-symmetric bodies has been studied for long times, however the most interest has been focused on the far wake development (see e.g. Johansson *et al.* (2003)). It is well known that two-dimensional bodies (i.e. cylinders or plates) give rise to large scale vortex shedding, however a similar type of large scale shedding may also appear behind three-dimensional blunt bodies. For instance the study of Bevilaqua & Lykoudis (1978) focussed on the near wake behind a porous disc and a sphere and they found distinct differences which they attributed to different vortex structures for the two cases. Some early studies (Calvert (1967*a*), Calvert (1967*b*)) showed that the large scale vortex shedding was more pronounced for an inclined disc than for a disc oriented normal to the flow. A typical Strouhal number (based on the diameter of the disc) when the disc is placed normal to the flow was 0.13 and this value increases (i.e. the shedding frequency increases) when the disc is inclined.

The connection between the wake behind a wind turbine rotor and that of a solid body is not altogether clear. The solidity, i.e. the ratio of the blade area to the swept area, is of the order of 5-15% (the lower value for a large scale turbine, the higher for a typical wind turbine model), but for increasing tip speed ratio the drag increases and therefore the blockage experienced by the flow goes towards that of a porous disc. The momentum deficit in the wake is directly related to the drag on the turbine and in this respect the turbine acts as an axisymmetric body or disc. The torque on the turbine gives a similar torque back on the flow, which will give the wake a slight rotation.

An interesting possibility to avoid or minimize the interaction between the wake and a downstream turbine is to actively yaw the upstream turbine (see Dahlberg & Medici (2003)). Since in that case the wind will also give a force on the turbine which is normal to the wind direction, an equal force but in opposite

direction will act on the wind, thereby deflecting the wake somewhat. Here we present results obtained with hot-wire anemometry showing the velocity distribution for all velocity components downstream a model turbine both for flow normal to the turbine disc as well as for yawed conditions. For the latter case the wake deflection is clearly illustrated.

As mentioned, the rotating turbine gives rise to a flow blockage similar to that of a stationary disc. Therefore it may also be anticipated that the regular large scale vortex shedding found behind solid discs should appear also for turbines. In this paper we describe wind tunnel experiments where such vortex shedding has been observed and we can show that this behaviour is close to what has been observed for solid discs. Finally it is hypothesized that this vortex shedding is the cause for the observed meandering of wakes measured behind full scale turbines.

2. Experimental set-up and methods

The experiment was performed in the MTL (Minimum Turbulence Level) wind tunnel at KTH Mechanics. The test section has a width and height of 1.2 and 0.8 m respectively, and its length is 7 m.

The turbine model is two-bladed, with a diameter of 0.180 m and is mounted on the wind tunnel floor on the centreline, 1.45 m from the test section inlet. The height of the hub above the floor is 0.24 m. The blockage due to the turbine is less than 3%. Details on the blades and their construction can be found in Montgomerie & Dahlberg (2003) and in the appendix of the present paper, together with a more detailed description of the wind tunnel.

In order to measure the drag on the turbine, the tower was mounted on a strain-gauge balance which is calibrated by applying a known force at the centre of the hub. In figure 1 the drag and the power coefficients of the wind turbine model as function of the tip speed ratio (λ =tip speed/wind speed) are shown. The data were measured both at 5 m/s and at 8 m/s, as well as with the turbulence grid mounted. The tip speed ratio was varied by keeping the wind speed constant, and changing the electrical loading of the generator from short circuiting to free-running (open circuit) conditions. It can be noted how the drag coefficient tends to a value of 0.17, when linearly extrapolated to $\lambda=0$. This value seems reasonable if the blade can be approximated with a flat plate with an aspect ratio of 8 (crudely resembling the blades used here). Such a plate has a drag coefficient of 1.17 (see e.g. Hoerner (1965)) and since the solidity of the turbine model is 13%, a value of 0.152 is obtained when applying the same percentage to the drag coefficient of a plate. This value is close to the extrapolated value of 0.17 at $\lambda=0$, so the behaviour of the wind turbine could be connected to that of a plate facing the flow when no rotational effects are present.

The velocity field was measured with two-component hot-wires (X-wires) which were calibrated against a Prandtl tube. The X-wires were built in the laboratory and had a measuring volume of 1 mm³. One X-wire was fixed on

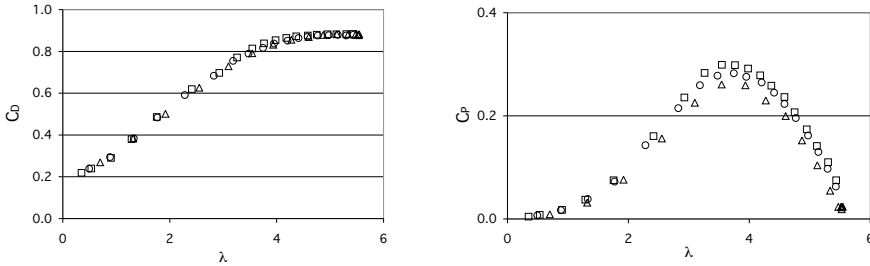


FIGURE 1. Drag and power coefficients as function of the tip speed ratio λ . \circ : $U_\infty = 8.3$ m/s, no turbulence, \square : $U_\infty = 8.5$ m/s, 4.5% grid turbulence, \triangle : $U_\infty = 5.5$ m/s, no turbulence.

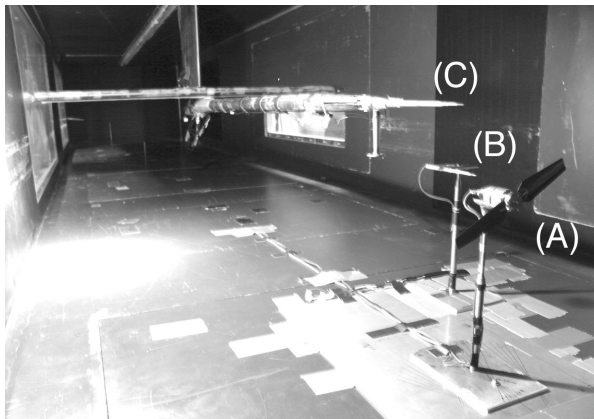


FIGURE 2. Experimental set-up. The view is from upstream looking downstream into the test section. The turbine model is marked with (A), the stationary X-wire used for the correlation (B) and the traversing system with the X-wire on the tip of the sting (C) are visible.

the tip of a 2 m long sting, connected to the wind tunnel traversing system. It has 5 degrees of freedom: streamwise (x), vertical (y), spanwise (z), as well as rotation of the probe around the x -axis and the y -axis. The latter degree of freedom, together with the computer-controlled movement, allowed an automatic calibration of the X-wires. Time-correlation measurements between two signals were also performed: a second X-wire was placed $1D$ downstream and on the right hand side of the turbine when looking from upstream, where the tip vortex had its centre. The X-wires acquired data at 5 kHz, for a typical

sampling time of 30 s. A photograph of the experimental set-up is shown in figure 2.

The coordinate system is centered in the middle of the rotor plane. Looking from upstream, the x -axis is directed in the undisturbed wind direction, the y -axis points upwards and the z -axis is positive towards the right hand side of the wind turbine model (see figure 3). The turbine is yawed around the centre of the rotor, but the coordinate system is kept fixed relative to the test section. The yaw angle is defined positive when the right hand side of the turbine is turned upstream (rotation around the negative y -axis).

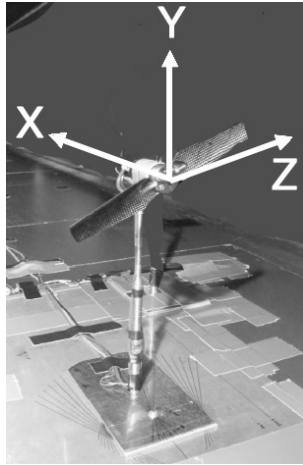


FIGURE 3. Wind tunnel coordinate system. A positive yaw angle is when the RHS of the rotor (positive z) is turned upstream, i.e. rotation around the negative y -axis.

3. Wake measurements

3.1. Wake under zero yaw conditions

In the present experiments all three velocity components were measured at several downstream positions, ranging from $x/D=0.5$ to 9. The running conditions of the turbine are given in table 1. The measuring grid in the cross-stream plane for the traversed probe was chosen to follow radial directions at 0° (corresponding to $y=0$ and varying the z -position on the positive side), and then anti-clockwise every 30° until 180° ($y=0$, negative z -positions). In each point the X-wire was turned around its x -axis so that either the streamwise and azimuthal velocity components or the streamwise and radial velocity components were measured. In this way the coupling between the azimuthal and the radial components was avoided. Along each radial direction measurements were taken at 18 positions, starting at the centreline ($y=0$, $z=0$ or $r=0$) and with the last position at $r=330$ mm. In the central part of the wake the step size is 15 mm,

	λ	C_D
No turbulence grid	3.66	0.794
4.5% FST	3.73	0.835

TABLE 1. Drag coefficient of the turbine with and without free stream turbulence (FST).

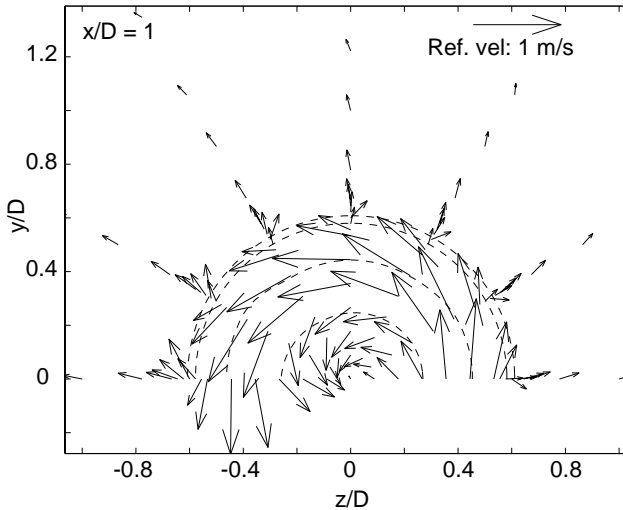


FIGURE 4. Average cross stream velocity vectors, no turbulence, no yaw, $x/D=1$, $U_\infty=8.5$ m/s. The dashed contours are lines of constant streamwise velocity (2, 4, 6, 8 m/s).

in the region of the tip vortices 7 points are taken with a step size of 4 mm, and in the outer region the step size increases to 20 mm. In the following only a few x -positions, which illustrate the flow development, are shown. The results are shown in mainly two different ways, I: vector plots of the cross stream velocity in the yz -plane, overlapped with contour-lines showing the streamwise velocity (see figure 4) and II: contour plots of each of the three components (see figure 5).

Figure 4 shows the average velocity field at $x/D=1$ as seen from the upstream side. The turbine is rotating clockwise, and the wake rotation is hence in the opposite direction. The freestream velocity is determined as the average result from the points $r/D \geq 1.4$ and is at this position determined to be 8.5 m/s. In the figure a reference velocity vector with a length corresponding to 1 m/s is also shown. The dashed contour lines represent lines of constant streamwise velocity. It is seen that the measured velocity field at this position has a fairly axis-symmetric appearance.

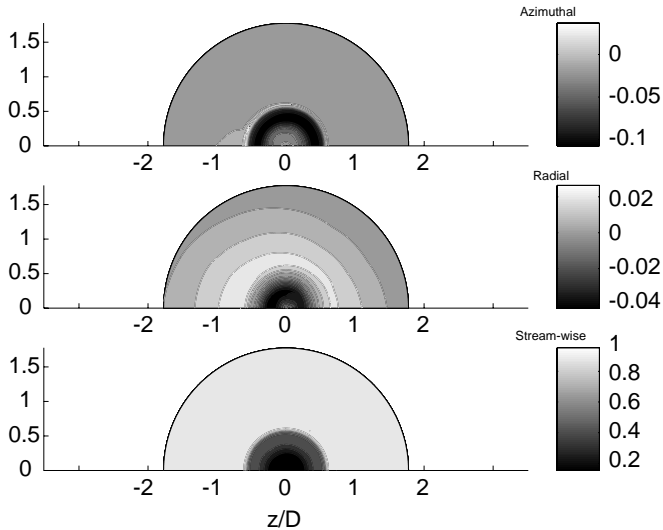


FIGURE 5. Same data as in figure 4, but the components are separated. The three figures show from top the azimuthal, radial and streamwise velocity components, respectively. All velocity components are normalized with the freestream velocity.

The most apparent observation in figure 4 is the large values of the azimuthal velocity component. The largest azimuthal velocity is found around $r/D=0.5$ and is of the order of 1 m/s where the streamwise velocity is around 4 m/s. This would give a swirl flow angle of about 15° inside the wake.

To further illustrate the flow field in the wake we plot the three different velocity components separately, namely the streamwise, radial and azimuthal components in terms of shaded contours. To construct this type of plot the values between the grid points are linearly interpolated at a constant radius for each component. The azimuthal component is considered positive if clockwise, i.e. in the same direction as that of the turbine rotation and all the velocity components are normalized with the free stream value.

Figure 5 shows the corresponding contour plots. The streamwise velocity shows a high degree of axial symmetry for all x/D . This is not the case for the radial and azimuthal components, although these velocities are only a few percent of the free stream value. The radial velocity shows that the flow field is expanding both in the outer part of the wake as well as outside the wake, but in the core region the radial velocity is directed towards the centre. The change in sign appears for this case at approximately $r/D=0.38$. Inspection of other cross-stream planes shows that already at $x/D=1.5$ the radial velocity is negative everywhere, indicating that the entrainment of fluid into the wake

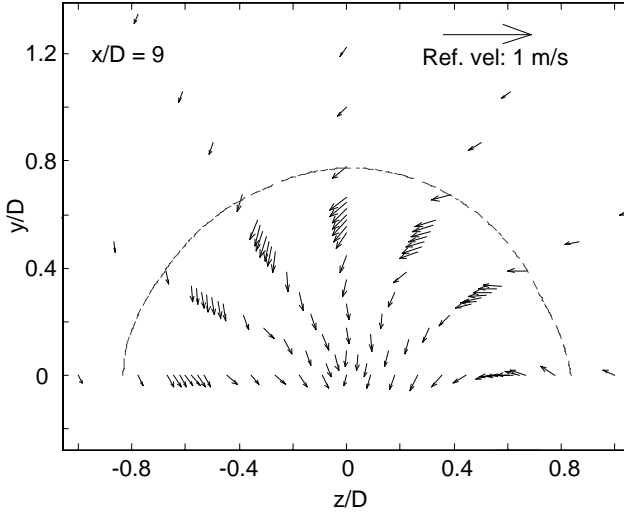


FIGURE 6. Average cross stream velocity vectors, no turbulence, no yaw, $x/D=9$, $U_\infty=8.5$ m/s. The dashed contour is for constant streamwise velocity (8 m/s). The wake is clearly pulled down by the presence of the ground.

also affects the flow outside the wake itself. The reason for the lack of axial symmetry mentioned above may be related to the presence of the ground, which bounds and pulls down the wake as seen more clearly further downstream (figure 6).

3.2. Wake under yawed conditions

In order to fully utilize the potential of using yaw as an active control on the wind turbine (see Dahlberg & Medici (2003)) it is necessary to have a good knowledge of the velocity field downstream the yawed turbine, especially with respect to the horizontal velocity component normal to the wind direction and the resulting wake displacement. Wind turbines often operate under yawed conditions as a result of the changes in the wind direction and therefore the loading may increase significantly, but the effect of yaw control on the structural loads is not investigated in this paper. Some velocity measurements, mainly of the streamwise velocity, downstream of a yawed turbine has earlier been carried out using PIV (see Parkin *et al.* (2001)). In the present study we have determined the three-dimensional velocity field downstream a yawed turbine, using hot-wires, to better understand the phenomena involved. Measurements were made for yaw angles (γ) 0° , 10° and 20° , although only the results for 0° and 20° are shown here.

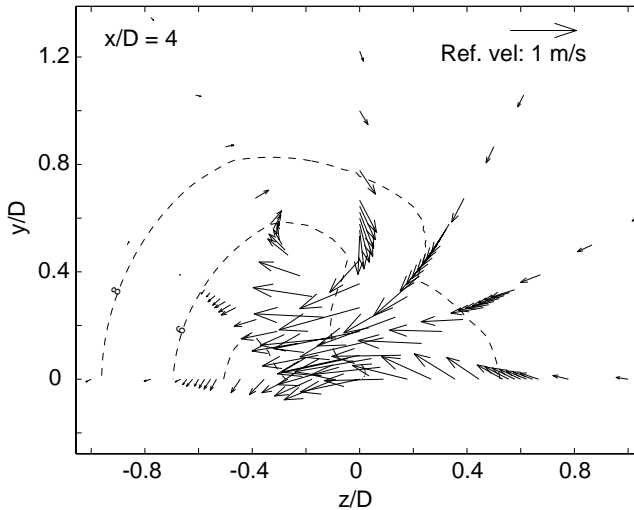


FIGURE 7. Average cross stream velocity vectors for $\gamma = 20^\circ$, $x/D = 4$. Positive yaw is for the right hand side of the turbine moved upstream.

Figure 7 shows the vector plots with $\gamma=20^\circ$ at $x/D=4$. The wake is no longer axis-symmetric and the displacement and deformation of the streamwise contour lines toward the left hand side is clearly visible, as a response to the side force on the turbine in the positive z -direction.

The contour plots in figures 8 and 9 show the change of the displacement of the wake under yawed conditions ($\gamma = 20^\circ$) at $x/D=4$ and 9. This is most evident from the streamwise velocity component where the wake minimum is shifted approximately $0.5D$ towards negative z at $x/D=4$ and even further to the left downstream. Also the radial component is towards negative z , although its magnitude is reduced by a factor of two between the two positions.

3.3. Free stream turbulence

In the present study we have also investigated the influence on the wake of free stream turbulence created by a turbulence-generating grid. The value of the turbulence intensity was 4.5% of the freestream velocity at the turbine position and has decayed to 2.5% at $x/D=9$. The turbulence level reproduced in this experiment is comparable to what a turbine would experience from a boundary layer which has developed over the sea.

It is well known that the wake will recover faster when influenced by free stream turbulence, however the behaviour of the wake immediately downstream the rotor plane is not well studied. The same measurements as for the case with no turbulence were made and in figure 10 the streamwise velocity for the

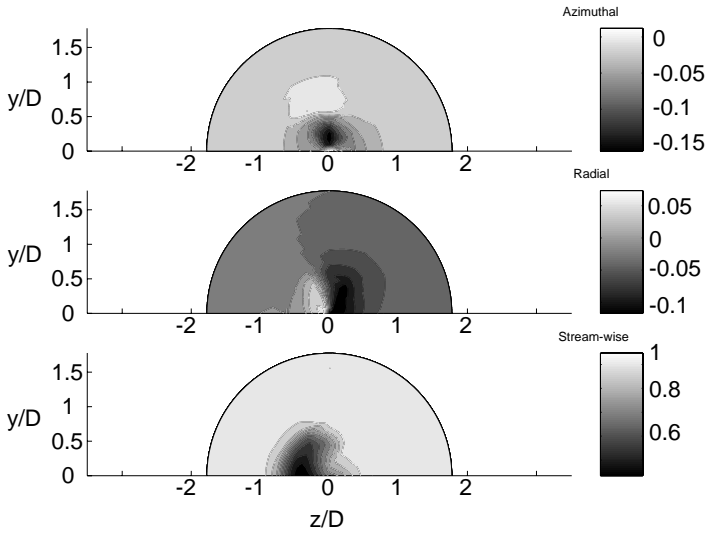


FIGURE 8. Same data as in Figure 7, $\gamma = 20^\circ$ and $x/D = 4$.

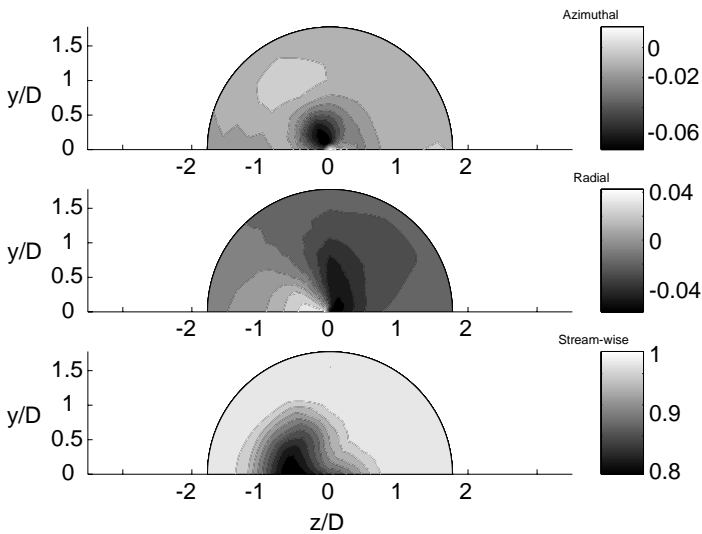


FIGURE 9. Same conditions as Figure 8. $x/D = 9$.

two cases are compared. It is clearly seen that the initial wake is quite similar in the two cases up to $x/D=2$. Also for the two other velocity components the differences between the two cases are negligible close to the turbine. It can also be noted that the drag coefficient is similar for the two cases (see

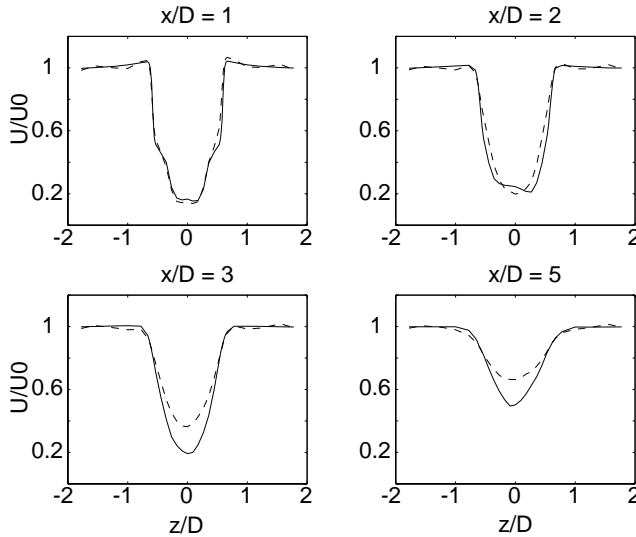


FIGURE 10. Difference between the streamwise velocity without free stream turbulence (solid line) and with turbulence (dashed line). $x/D=1, 2, 3, 5$.

table 1). The small difference may be explained by the fact that the loading circuit only allows finite control steps. The similar drag coefficient indicates that the momentum deficit in the wake should be approximately the same. When a wake develops downstream, the transport of momentum from the free stream into the wake is responsible for the wake recovery. The effect of the free stream turbulence, i.e. of the enhanced radial transport of momentum due to the velocity fluctuations, is clearly seen at $x/D=3$.

4. Meandering

4.1. Bluff-body vortex shedding

The flow that approaches the turbine rotor feels the turbine as an object giving a drag force, much the same way as a bluff body or disc would. A characteristic of bluff body flows is the so-called vortex shedding, maybe most known as the Von Karman vortex street for two-dimensional cylinders. However vortex shedding may also appear behind three-dimensional bluff bodies such as circular discs.

When the time signal of the streamwise velocity was observed in the region of the tip-vortices an unexpected behaviour was detected. The signal shown in figure 11 (top) is an example. The signal shows velocity peaks which can be identified as peaks coming from the tip vortices themselves with a time interval of about 10 ms, corresponding to one vortex shed by each blade per revolution giving twice the rotation frequency (approximately 55 Hz) of the

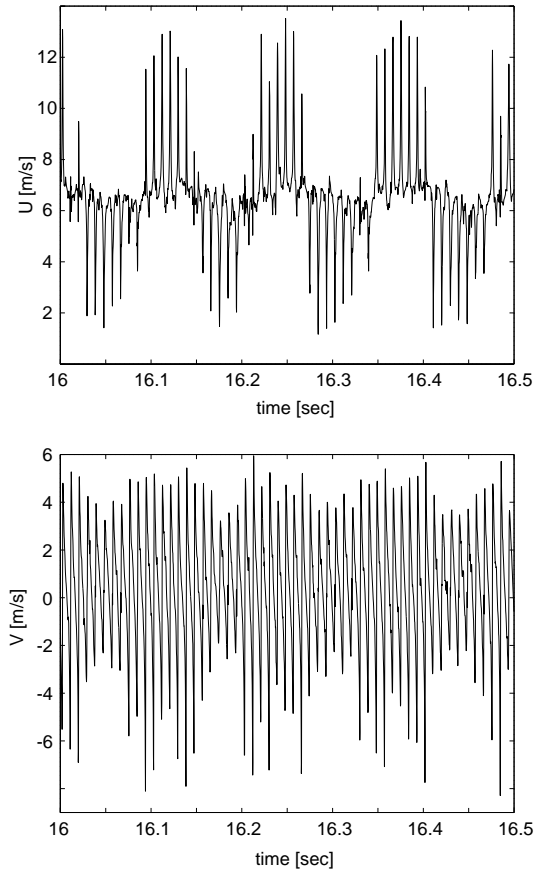


FIGURE 11. Time signal of the streamwise velocity (top) and the radial velocity (bottom) close to the centre of the tip vortices ($x/D=1$, $y/D=0$, and $z/D=0.6$), clearly showing the 7.9 Hz fluctuation.

turbine. However this signal seems to be overlaid by a much lower frequency than that of the tip vortices themselves. Also the radial component of the velocity (figure 11 (bottom)) shows a modulation with the same low frequency. If a frequency analysis of the time signals is made, a clear peak in the energy spectrum at 7.9 Hz is seen. This frequency is not only detected in the wake but also in the free stream and for all three velocity components. Our hypothesis is that this behaviour is connected with vortex shedding from the turbine disc, much in the same way as one would expect for a solid disc. This may also be connected to the observed "meandering" of wakes downstream of full scale turbines. In the following we will show that the data may be interpreted in this way.

In a coordinate system following the centre of the tip vortex, the vortices may be viewed as a central core rotating as a solid body and an outer rotating flow with a decreasing rotational velocity with increasing r . With respect to the reference frame of the laboratory, the centre of the tip vortex may be viewed as convected with a velocity close to the mean velocity of the flow at that position. If the radial position of the measuring point is at the outer part of the tip-vortex with respect to its centre, the measurements of the streamwise velocity will show a high velocity peak at every vortex passage. On the other hand, if the measurement point is in the inner part with respect to the vortex centre, the velocity signal will show a periodic velocity dip.

A time signal with the appearance shown in figure 11 (top) can on the other hand be obtained if the probe is positioned close to the centre of the tip vortices, and the wake and hence the tip vortices are moving radially at a low frequency in such a way that the two sides of the vortices are alternating at the probe position. It can also be noted that the amplitude of the radial velocity signal varies in relation to the downstream velocity: when the streamwise velocity has an overshoot, the amplitude of the radial component is large, whereas when the inner side of the vortex is passing the measuring point, a lower amplitude of the radial velocity can be observed. The reason for this may be due to the fact that the probe is not located exactly at the average position of the tip vortex centre.

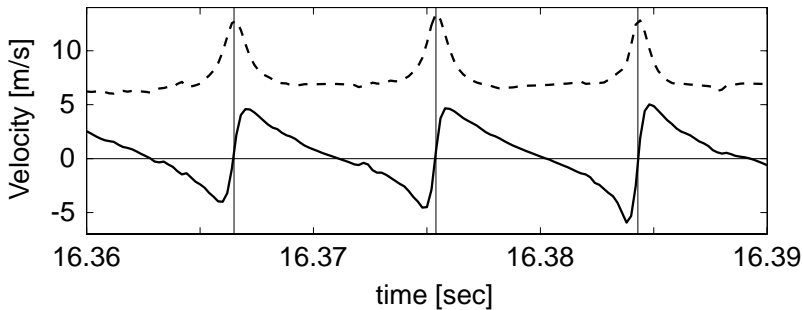


FIGURE 12. Close-up on the streamwise component (dashed) and radial component (solid line) of the velocity ($x/D=1$, $y/D=0$, and $z/D=0.6$). Three vertical lines passing through the peaks of the streamwise velocity are plotted as reference, together with the zero velocity axis.

Short time segments taken from figure 11 are shown in figure 12. It is clearly seen that the maximum in u is where $v=0$, which is what would be expected during a vortex passage. The v -signal is also shown to be anti-symmetric with respect to its zero passage and finally we can observe that the largest (absolute) value of v is about the same as the velocity increase between the base level of

u and that of the measured peak. All these results are in accordance with the idea that the signal is due to the tip vortex passage.

The close up of the time signal in figure 12 shows how the probe is at first measuring the approach of the vortex, i.e. the radial velocity becomes negative, then during the vortex passage (i.e. between the negative and the positive peaks of the velocity) the peak in the streamwise velocity is observed. These velocity patterns indicate that the probe is located slightly outside the vortex centre.

The low frequency shedding is detected in all the velocity components, indicating that the shedding is three-dimensional. The shedding frequency f can be normalised using the diameter of the turbine D and the local freestream velocity, as it is usually done for bluff bodies. The resulting non-dimensional frequency, the so called Strouhal number, is then defined as:

$$St = \frac{fD}{U_\infty} \quad (1)$$

For a bluff body like a disc, St is independent of the Reynolds number if the Reynolds number is sufficiently high.

The frequency of the bluff body shedding was obtained through spectral analysis (FFT) of the time signals of the streamwise velocity measured at $x/D=1$ and in the region where the tip vortices are found. The Strouhal number as function of the tip speed ratio can be found in figure 9. The data shown are for $U_\infty=8.5$ m/s and 8.3 m/s with and without free stream turbulence, as well as measurements at $U_\infty=5.5$ m/s without free stream turbulence. First of all it can be noted that no data points were obtained for cases with λ smaller than 3. i.e. no low frequency shedding was observed for $\lambda < 3$. A plausible explanation is that for lower λ than 3 the flow does not see the blockage as a disc, but rather sees the individual passage of the blades which thereby does not give rise to the large scale vortex shedding. As can be seen, the Strouhal number decreases with increasing tip speed ratio and for $\lambda>4.5$ it levels out around 0.12. This value is similar to what has been reported for solid discs. It is interesting to note that the drag coefficient also is nearly constant for $\lambda>4.5$ (see figure 1). The increase in St for smaller λ may be seen as a decrease of the effective diameter of the turbine with respect to the vortex shedding phenomenon. A similar result is seen for the turbine under yawed conditions; the St is larger than for the zero yaw case, suggesting a smaller effective diameter of the yawed turbine.

The results for the yawed turbine could also be compared with the results of a yawed disc reported by Calvert (1967*a*). The same data as in figure 9 ($\lambda\approx 3.7$) are plotted in figure 14 and the change of St is seen to be similar as compared to the data from the disc, although the absolute values are shifted somewhat.

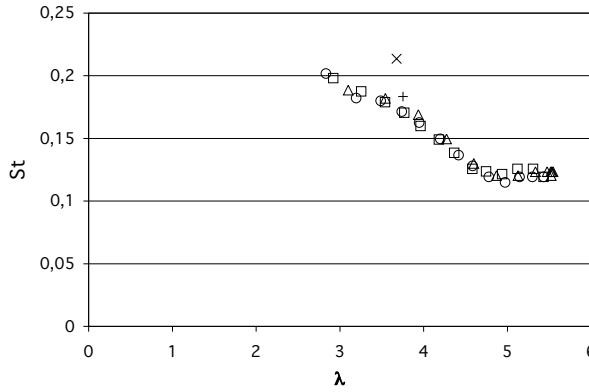


FIGURE 13. Strouhal number as function of the tip speed ratio λ with yaw angle $\gamma=0$. \circ : $U_\infty=8.3$ m/s, no turbulence, \square : $U_\infty=8.5$ m/s, 4.5% grid turbulence, \triangle : $U_\infty=5.5$ m/s, no turbulence. Also two data points with $\gamma=10^\circ$ (+) and $\gamma=20^\circ$ (\times) are included.

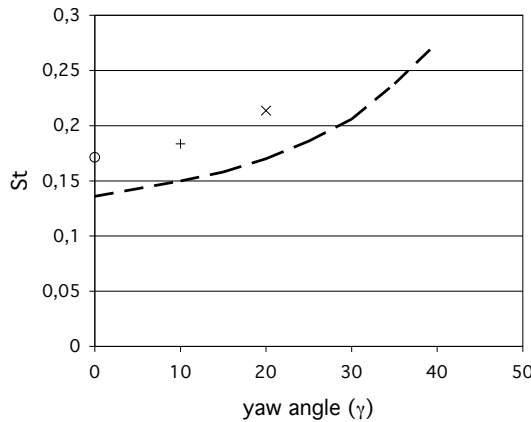


FIGURE 14. Strouhal number as function of the yaw angle, compared with the behaviour of a disc (from Calvert (1967a)). Same data as in figure 9, with the data point for $\gamma=0$ taken at $\lambda=3.74$.

4.2. Space-time structure of the wake

In order to obtain further understanding of the space-time structure of the vortex shedding behind the turbine we carried out measurements using two X-probes which were separated in space. One probe (named probe 2) was stationary and placed at $x/D=1$, $y/D=0$ and $z/D=0.6$. The other probe (probe 1) was mounted on the traversing system and could hence be moved with respect

to the stationary probe. For the measurements presented in the following this probe was located on the other side of the turbine (i.e. negative z) at $y/D=0$, and moved both in the spanwise direction (111 points starting at $z=-80$ to -300 mm with a step length of 2 mm) and at different x . In the following we use the spanwise velocity component which for $z > 0$ is equal to the radial component, but for $z < 0$ has the opposite sign compared to the radial component.

In order to illustrate the correlation between the two signals, figure 15 shows the velocity signals obtained from the X-wires when they are placed at the same downstream position but in opposite points with respect to the wake centreline. The velocity signals corresponding to the spanwise velocity show the expected behaviour, the velocity measured by probe 2 is a mirror image of the signal from probe 1. On the other hand the streamwise velocity signals show a behaviour which indicates that probe 2 is on the inner side of the vortex whereas probe 1 is on the outer side. Now the picture for the streamwise velocity may change due to the meandering of the wake as was seen in figure 11 (top), whereas the spanwise signal will qualitatively stay the same. Note that probe 2 in figure 15 is at the same position as for the measurements shown in figure 12, however the time sequence here is for the case when the vortices have shifted outwards with respect to the probe, giving a decrease in the streamwise velocity during the vortex passage.

The space-time structure of the wake can be further elucidated by calculating the correlation between the velocity signals at the two positions. The correlation $R_{u_1 u_2}(\tau)$ between the signals $u_1(t)$ and $u_2(t)$ (both with zero mean) is defined as

$$R_{u_1 u_2}(\Delta t) = \frac{1}{u_{1rms} u_{2rms}} \frac{1}{T} \int_{-T/2}^{T/2} u_1(t + \Delta t) u_2(t) dt \quad (2)$$

where u_{1rms} and u_{2rms} are the rms values of the two signals. T is the integration time and is in our experiments typically 30 seconds. The time delay Δt can then be used to show how a disturbance propagates in the flow field. As an example the correlation between the signals in figure 15 is shown in figure 16. The figure shows both the frequency of the tip vortices themselves as well as the frequency connected to the large scale shedding.

The time correlation was computed for each of the 111 measurement points in the spanwise direction, between $z/D = -0.44$ to $z/D = -1.67$. The results can be seen in figures 17–19. In these figures the time axis has been made non-dimensional with the freestream velocity and the rotor diameter. Both the correlation between the streamwise velocity components and that between the spanwise components are shown. In figure 17 both probes are placed at $x/D=1$. In the spanwise component the tip vortices are clearly observed for the whole displayed time interval which shows that the frequency and signals are steady. The vortices are also seen in the correlation of the streamwise velocity, however it is less clear so. The main difference between the plots is found in

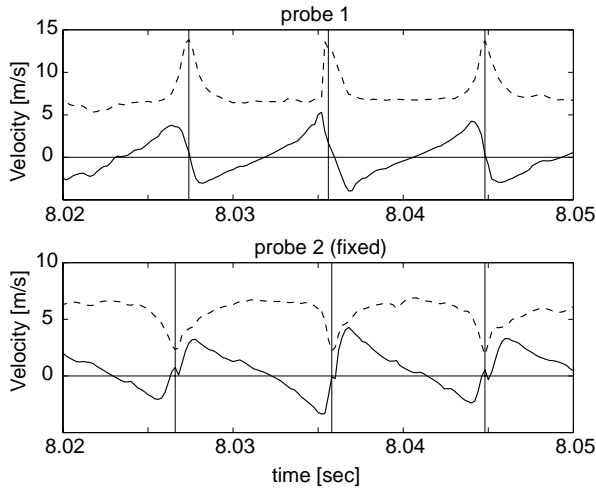


FIGURE 15. Velocity traces for two probes at $x/D=1$ and $y/D=0$, with $z/D = -0.578$ (probe 1, top) and $z/D = +0.6$ (probe 2, bottom). The dashed lines correspond to the streamwise velocity. The full lines correspond to the velocity in the z -direction, which for probe 2 also correspond to the radial direction. Consequently for probe 1 we have the mirror image of the radial velocity.

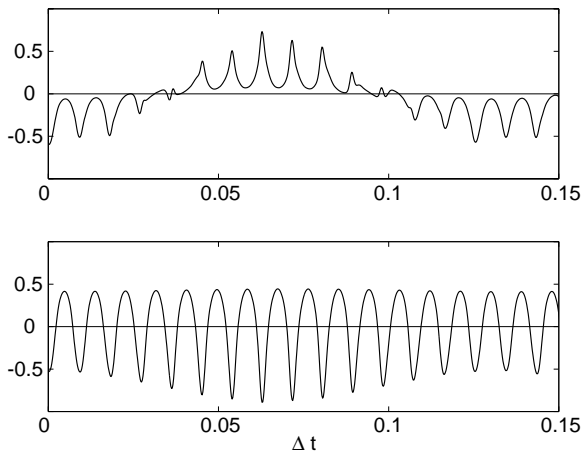


FIGURE 16. Correlation coefficients between the streamwise velocities (top) and the spanwise velocities (bottom) as function of the time displacement between the signals.

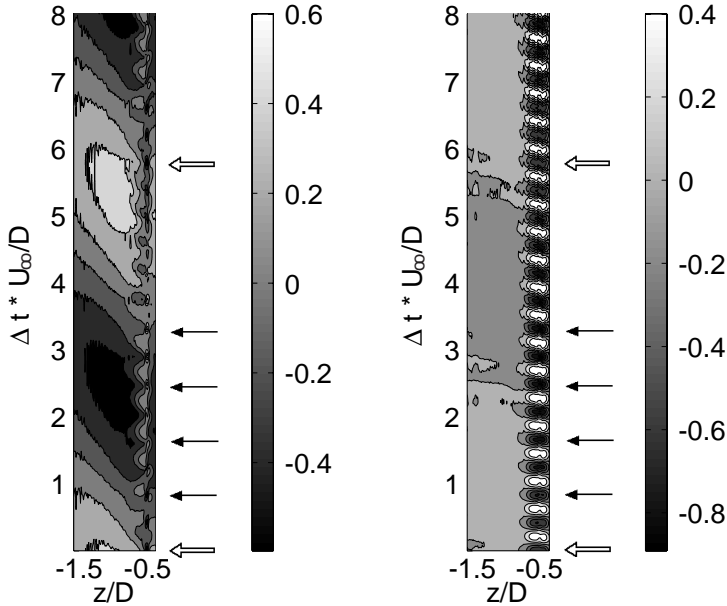


FIGURE 17. Correlation between velocities measured with both probes at $x/D=1$. The fixed probe is at $z=108$ mm, i.e. $z/D=0.6$. Left: correlation between the streamwise velocities. Right: correlation between the spanwise velocities. The large scale shedding frequency corresponds to a period of $\Delta t \cdot U_\infty/D = St^{-1} = 5.8$ and is marked by the hollow arrows. The rotational frequency is given by the black arrows.

the region outside the wake, where a periodicity of much larger time scale is found in the streamwise correlation. The correlation time length is the same as that of the large scale shedding from the turbine. It is interesting to note that it can be clearly detected far outside the wake region. Similar results are observed also at $x/D=2$ in figure 18, although the correlation is overall smaller and for the streamwise velocity it becomes more blurred in the region of the tip vortices, whereas at $x/D=3$ (see figure 19) the correlation for the streamwise component of the tip vortices has vanished. It is however still quite clear in the correlation for the spanwise component. At this position it can be noted that the large scale shedding dominates for the streamwise component and this picture is seen even further downstream (not shown here). This indicates that the large scale shedding is persistent and may influence the motion in the wake region.

As was mentioned previously, the correlation results in the tip vortex region shown here were used to calculate a propagation speed of the tip vortices by following for instance one maximum in the downstream direction. In this way

the propagation speed of the tip speed vortices was found to be about 75% of the freestream velocity.

5. Conclusions

The measurements have shown that the wake rotates opposite to the turbine direction and after a few diameters, the wake has lost its axial symmetry because of the effect of the ground. It is observed that yawing the turbine clearly deflects the wake to the side, although the effect of the rotation is still evident. The effect of the side force on the wake as a result of the yawed condition depends on the angle and the downstream position, but may be of the order of the rotor diameter. The wake is substantially changed by the presence of the free stream turbulence: the recovery of the velocity defects is faster due to an higher energy mixing and to a shorter persistence of the tip vortices.

An unexpected finding was the low frequency shedding from the turbine. The frequency of this shedding is an order of magnitude smaller than that of the blade frequency and the phenomenon seems to be similar to the vortex shedding occurring for solid discs. The shedding is observed both with and without free stream turbulence. Previously the meandering of turbine wakes, which has been observed in field measurements, has been interpreted as a result of the transverse velocity fluctuations of the wind (see e.g. Thomsen *et al.* (2001)), however the observed shedding may be a more likely candidate responsible for the meandering motion.

Although the tip speed ratio of the turbine model is lower than that of a full-scale turbine, their drag coefficients are comparable. The power coefficient of the turbine model when interacting with an oncoming wake is also similar to the Alsvik wind farm turbine (see Dahlberg & Medici (2003)). The meandering of the turbine model wake was detected from $C_D = 0.7$ and higher. The low frequency peak in the velocity spectra at Alsvik was reported by Hassan (1996) for wind speeds up to 9 m/s, i.e. for $C_D \geq 0.73$ (G. Schepers, ECN, private communication), thus showing a similar behaviour. However in that case the Strouhal number was around 0.3.

Acknowledgements

The work was sponsored by the Swedish National Energy Agency (STEM). The authors thank Jan-Åke Dahlberg (FOI) for providing the model and for many fruitful discussions. We also want to thank the referees and the editor for useful suggestions.

References

- ALFREDSSON, P. H., DAHLBERG, J. Å. & VERMEULEN, P. E. J. 1982 A comparison between predicted and measured data from wind turbine wakes. *Wind Engng.* **6**, 149–155.

- BEVILAQUA, P. M. & LYKODIS, P. S. 1978 Turbulence memory in self-preserving wakes. *J. Fluid Mech.* **89**, 589–606.
- CALVERT, J. R. 1967*a* Experiments on the flow past an inclined disk. *J. Fluid Mech.* **29**, 691–703.
- CALVERT, J. R. 1967*b* Experiments on the low-speed flow past cones. *J. Fluid Mech.* **27**, 273–289.
- DAHLBERG, J. Å. & MEDICI, D. 2003 Potential improvement of wind turbine array efficiency by active wake control (AWC). In *Proc. European Wind Energy Conference and Exhibition*, Madrid, (published on CD).
- HANSEN, A. C. & BUTTERFIELD, C. P. 1993 Aerodynamics of horizontal-axis wind turbines. *Annu. Rev. Fluid Mech.* **25**, 115–149.
- HASSAN, G. 1996 Dynamic loads in wind farms II. Final report Joule Project, JOU2-CT92-0094.
- HOERNER, S. F. 1965 *Fluid-dynamic drag*. Hoerner Fluid Dynamics.
- JOHANSSON, P. B. V., GEORGE, P. B. V. & GOURLAY, M. J. 2003 Equilibrium similarity, effects of initial conditions and local Reynolds number on the axisymmetric wake. *Phys. Fluids* **15**, 603–617.
- MONTGOMERIE, B. & DAHLBERG, J. Å. 2003 Vortex system studies on small wind turbines. FOI scientific report, ISRN FOI-R-0936-SE.
- PARKIN, P., HOLM, R. & MEDICI, D. 2001 The application of piv to the wake of a wind turbine in yaw. In *Proc. 4th International Symposium on Particle Image Velocimetry, PIV'01*, Göttingen (Ed. J. Kompenhans) DLR-Mitteilung 2001-03 (published on CD).
- RIEGELS, F. W. 1961 *Airfoil sections, results from wind tunnel investigations, theoretical foundations*. Butterworth & Co. LTD.
- THOMSEN, K., MADSEN, H. A. & LARSEN, G. C. 2001 A new method can predict detailed response for turbines in wind farms. In *Proc. IEA 16th Symp. Aerodyn. Wind Turbines*, Boulder, FOI-S-0877-SE, pp. 171–187.
- VERMEER, L. J., SØRENSEN, J. N. & CRESPO, A. 2003 Wind turbine wake aerodynamics. *Prog. Aerospace Sci.* **39**, 467–510.

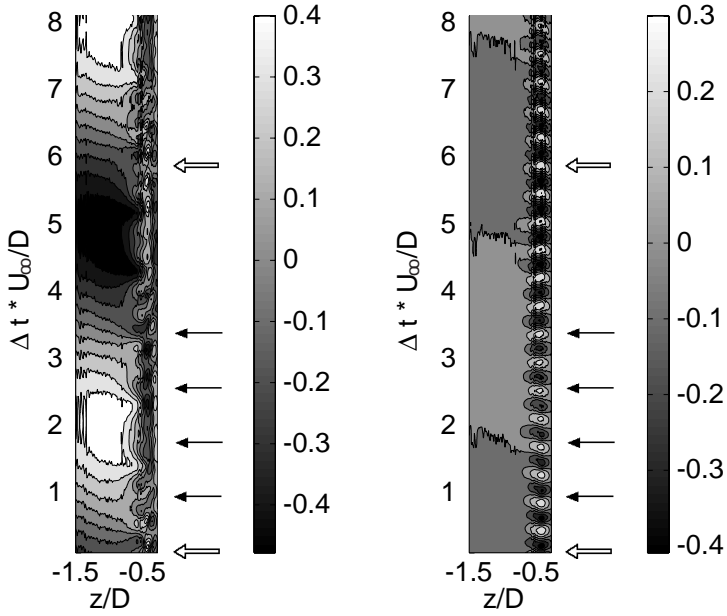


FIGURE 18. Same type of data as in figure 17, but with the movable probe at $x/D=2$.

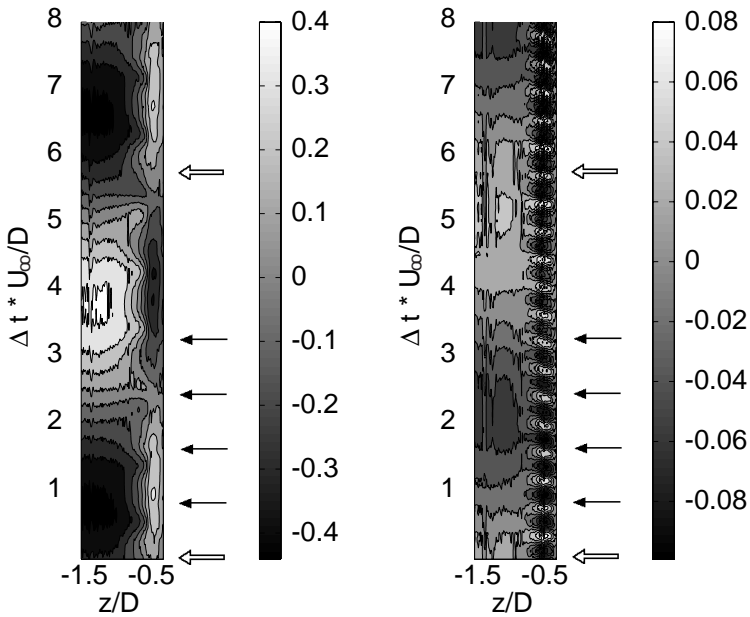


FIGURE 19. Same type of data as in figure 17, but with the movable probe at $x/D=3$.

6. Appendix: experimental set-up and blade geometry

The experiment was performed in the MTL (Minimum Turbulence Level) wind tunnel at KTH Mechanics. The test section has a width and height of 1.2 and 0.8 m respectively, and its length is 7 m. The ceiling is adjustable, which makes it possible to provide a constant velocity in the streamwise direction despite the boundary layer growth on the test section walls. The maximum speed of the tunnel is more than 60 m/s, however for the present study a typical freestream velocity was 8 m/s. The wind tunnel provides stable conditions and the air temperature is controlled by means of a heat exchanger. Most of the measurements were made at low ambient turbulence level (less than 0.1%), however some measurements were made with a turbulence grid mounted 20 cm downstream the inlet of the test section. The grid is a monoplane grid, consisting of 10 mm square bars, with a mesh width of 50 mm. With the grid the turbulence level at the position of the turbine is about 4.5%.

The non-twisted blade is based on the Göttingen 417A airfoil and detailed data about the profile can be found in Riegels (1961). The Göttingen 417A profile is a constant thickness (2.9%) blade with a maximum camber of 6% at 40% chord. The blades have been built at FOI (Swedish Defense Research Agency), Stockholm, and consist of a four-layered structure of reinforced epoxy with a constant thickness of about 0.5 mm. The maximum chord is 27 mm at 12% of the radius, and the tip chord is 16 mm. A sketch of the blade as seen from downstream is in figure A.20. The solidity of the rotor is 13% and the rotation, from this view, is counter-clockwise. The position of the turbine model is seen in figure A.21. The blockage is less than 3% of the wind tunnel section. The blade is connected to the hub at the line A–F, while the axis M1–M2 goes through the centre of the rotor. Note that the hub is circular, but a segment of the hub has been cut off in correspondence of the line A–F to give a smoother connection.

The Cartesian coordinates of each of the points are reported in figure A.20. The corners are actually smoothed. The distance M1–M2 is 79 mm, and by adding 1 mm for the connection blade–hub and 10 mm of hub to the centre of the rotor, the turbine model radius turns out to be 90 mm.

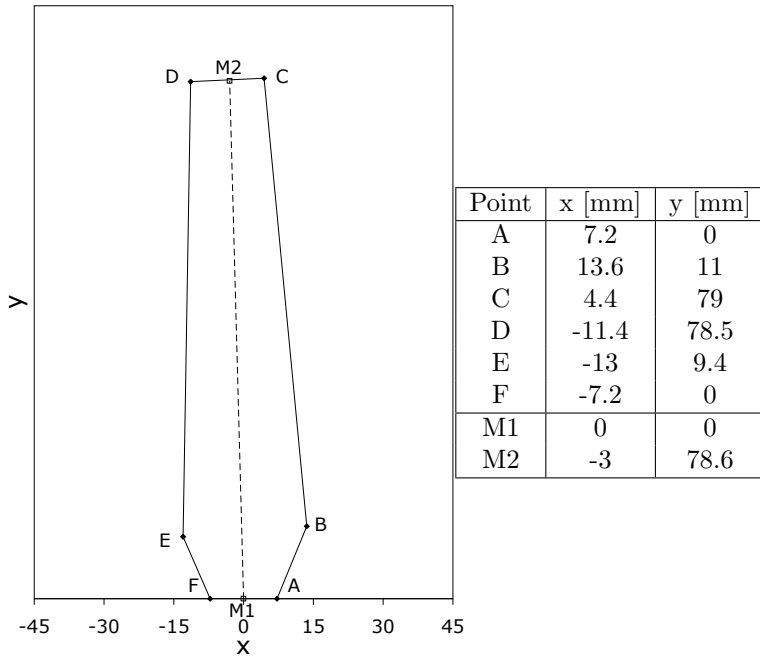


FIGURE A.20. Blade sketch as seen from downstream and the coordinates of the points. The leading edge is D-E-F.

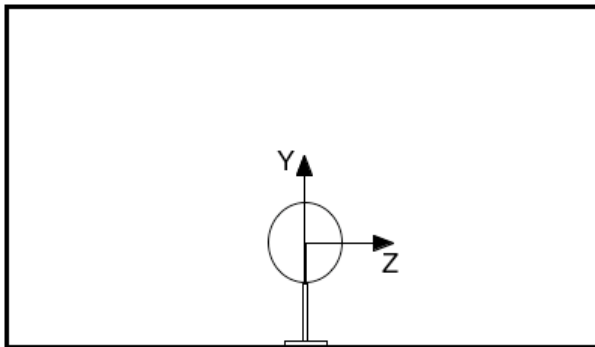


FIGURE A.21. Wind tunnel section and turbine model (actual scaling) as seen from upstream.

Paper 6

Wind turbine near wakes and comparisons to the wake behind a disc

By **D. Medici and P. H. Alfredsson**

KTH Mechanics, SE-100 44 Stockholm, Sweden

Presented at ASME Conference, January 2005, Reno, Nevada. AIAA-2005-0595

The wake development behind wind turbines affects power losses in turbine parks as well as the flow induced rotor loads due to wake turbulence. In the near wake region tip vortices are a distinct feature of the flow. Such vortices do not exist behind a circular disc but instead the flow is characterized by a large scale vortex shedding. In our wind tunnel experiments we have observed similar large scale vortex shedding in the wake of a two-bladed wind turbine model. The frequency of the shedding in terms of the Strouhal number decreases with increasing tip speed ratio and levels out at a value, which is close to that observed for a solid disc. For low tip speed ratios no large scale vortex shedding was observed. When the turbine was yawed the shedding frequency increased in a similar way as for an inclined disc. In order to further investigate this phenomenon we have studied the vortex shedding behind solid and porous discs. All our results indicate that a turbine at high tip speed ratio sheds large scale structures in a similar way as a disc. We also hypothesize that the vortex shedding is the cause for the observed meandering of wakes that has been observed behind full scale turbines.

1. Introduction

In order to achieve a significant contribution from wind energy to the overall electricity production it is necessary to place turbines in wind parks. In such parks the turbines will be close enough that aerodynamic interaction between turbines will occur, i.e. downstream turbines will work in the wake of one or several upstream turbines during at least some periods of time. This means that the wake development behind wind turbines is of considerable practical interest, it both gives information on power losses in turbine parks as well as information on increased turbulence levels and wind shear which may be affecting flow induced rotor loads. For wind engineering purposes the main interest is in the near wake region, say up to $10D$ (D is the turbine diameter) downstream the turbine.

Main characteristics of the near wake are the mean velocity deficit and the tip vortices shed by the blades forming two (or three for a three bladed turbine)

spiral vortices downstream the turbine. The tip vortices are a distinct feature of the flow behind a wind turbine and such vortices do not exist behind a solid body, such as a circular disc, but there may still be similarities between the wake flow development. Although the solidity of a turbine, i.e. the ratio of the blade area to the swept area, is of the order of 5-15% (the lower value for a large scale turbine, the higher for a typical wind turbine model), the drag of the turbine goes towards that of a near solid disc at high tip speed ratios. The momentum deficit in the wake is directly coupled to the drag on the turbine and in this respect the turbine acts on the flow as an axisymmetric body or disc.

1.1. Previous work on near wake flows

The flow (wake) behind axisymmetric bodies has been studied for long times, however the most interest has been focussed on the far wake development (see e.g. Johansson *et al.* (2003)). Much less work has been focussed on the near wake region. It is well known that two-dimensional bodies (i.e. cylinders or plates) give rise to large scale vortex shedding. This is also true for porous plates and the shedding frequency has been observed by Castro (1971) to increase with increasing porosity.

A similar type of large scale shedding may also appear behind three-dimensional blunt bodies. For instance in Bevilaqua & Lykoudis (1978) the near wakes behind a porous disc and a sphere are compared and the distinct characteristics are attributed to different vortex structures for the two cases. Some early studies (Calvert (1967*b*), Calvert (1967*a*)) showed that the large scale vortex shedding was more pronounced for an inclined disc than for a disc oriented normal to the flow. A typical Strouhal number (based on the diameter of the disc) with the disc placed normal to the flow was 0.13 and this value increased (i.e. the shedding frequency increased) when the disc was inclined.

In a more recent work by Lee & Bearmann (1992), two hot-wire probes have been used to study coherent structures in the wake behind a circular disc by spectral analysis and conditional sampling. It was shown that vortices on average are shed alternatively from opposite sides of the disc, which probably means that the shedding is not stationary but moves around the disc periphery, randomly clockwise or anti-clockwise. One possible interpretation is that the large scale shedding gives rise to helical structures which leaves the disc and propagates downstream. It has also been found (see Miao *et al.* (1997)) with both flow visualization and probe measurements that the vortex shedding was random in nature and a specific vortex structure could not be identified. A recent work by Johansson *et al.* (2002), using a hot-wire rake and proper orthogonal decomposition (POD) of the signals, showed a helical mode in the near wake, but also found a second near zero frequency (stationary) mode further downstream which was growing faster. An interesting study by Berger *et al.* (1990) showed how, by oscillating a disc in the nutation mode, the helical mode of vortex shedding was forced to become completely regular.

Relatively few wind tunnel experiments on the wake flow behind rotating wind turbine models have been made and for a recent comprehensive review on wind turbine wakes the reader is referred to Vermeer *et al.* (2003). The first studies reported were made in the end of 1970's (see e.g. Alfredsson *et al.* (1980)) and only a few more detailed studies have been presented since then. A recent study by Medici & Alfredsson (2005) showed measurements of all three velocity components behind a model turbine. In that study it was shown that the wake rotates in the opposite direction to the rotor rotation and the maximum azimuthal velocity is of the order of 10-15% of the freestream velocity at $x/D=1$. It was also shown that a turbine can shed large scale structures in a similar way as for solid discs. Since the rotating turbine gives rise to a flow blockage similar to that of a non rotating disc it may be anticipated that the large scale vortex shedding could appear. There is however an interesting difference, namely that for the turbine the symmetry around the streamwise axis is broken since the turbine is rotating. This also gives a rotation to the wake and this may affect the vortex shedding.

1.2. Present work

In the present work the vortex shedding in the wake of a two-bladed wind turbine model (diameter 180 mm) has been studied in the MTL (Minimum Turbulence Level) wind tunnel at KTH Mechanics, using hot-wire anemometry.

Spectra from the velocity signals show low frequency fluctuations both in the wake and in the surrounding flow. The frequency of the shedding in terms of the Strouhal number ($St = fD/U$, where f is the vortex shedding frequency and U the freestream velocity) decreases with increasing tip speed ratio and levels out at a value which is close to that for a solid disc. For low tip speed ratios no large scale vortex shedding was observed. For a yawed turbine the shedding frequency was found to increase in a similar way as for an inclined disc.

In order to further investigate this phenomenon we have studied the vortex shedding behind solid and porous discs. In the paper we make comparisons between the disc cases and that of the turbine. All our results indicate that a turbine sheds large scale structures in a similar way as a disc shaped body.

2. Experimental set-up

The experiments were performed in the MTL wind tunnel at KTH Mechanics. The test section has a width and height of 1.2 and 0.8 m respectively, and its length is 7 m. The ceiling is adjustable, which makes it possible to provide a constant velocity in the streamwise direction despite the boundary layer growth on the test section walls. The maximum speed of the tunnel is more than 60 m/s, however for the present study a typical freestream velocity was in the region 5–20 m/s. The wind tunnel provides stable conditions and the air temperature is controlled by means of a heat exchanger. Most of the measurements were made at low ambient turbulence level (less than 0.1%),

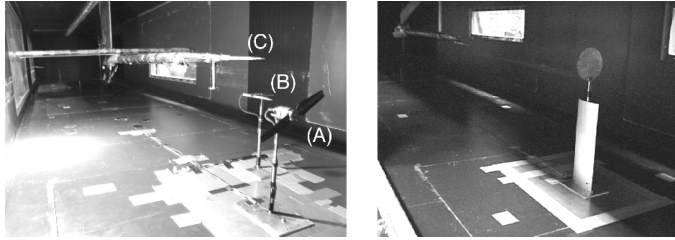


FIGURE 1. Experimental set-up. The view is from upstream looking downstream into the test section. Left figure: Set up for turbine measurements. The turbine model is marked with (A), the stationary X-wire used for the correlation (B) and the traversing system with the X-wire on the tip of the sting (C) are visible. Right figure: The disc is fixed on a support approximately 40 mm long and exposed to the free stream. The diameter of the support is 10 mm at the disc junction and 12 mm at the base. A longer section of the support is shielded by a wing profile to reduce the interference with the flow.

however some measurements with the turbine were made with a turbulence grid mounted 200 mm downstream the inlet. The grid is a mono-plane grid, consisting of 10 mm square bars, with a mesh width of 50 mm. With the grid the turbulence level at the position of the turbine is about 4.5%.

The coordinate system is centred in the middle of the rotor (or disc) plane. Looking from upstream, the x -axis is directed in the undisturbed wind direction, the y -axis points upwards and the z -axis is positive towards the right hand side of the wind turbine model. When yawing the turbine it is turned around the centre of the rotor (or disc), but the coordinate system is kept fixed relative to the test section.

The velocity field behind the turbine was measured with two-component hot-wires (X-wires) which were calibrated against a Pitot tube. The probes were built in the laboratory and had a measuring volume of 1 mm^3 . One X-wire was fixed on the tip of a 2 m long sting, connected to the wind tunnel traversing system. It has 5 degrees of freedom: x , y and z , as well as the rotation of the probe around the x -axis and the y -axis. The latter degree of freedom, together with the computer-controlled movement, allowed an automatic calibration of the X-wires. Time-correlation measurements between two signals were also performed: a second X-wire was placed $1D$ downstream and on the right hand side of the turbine when looking from upstream, where the tip vortex had its centre. The X hot-wire probes acquired data at 5 kHz, for a typical sampling time of 30 sec. The time signals behind the discs were however collected with

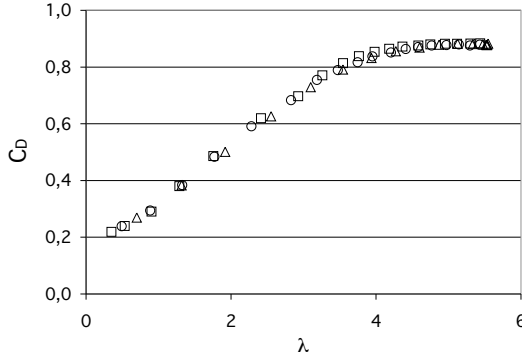


FIGURE 2. Drag coefficient as function of the tip speed ratio λ . \circ : $U_\infty = 8.3$ m/s, no turbulence, \square : $U_\infty = 8.5$ m/s, 4.5% grid turbulence, \triangle : $U_\infty = 5.5$ m/s, no turbulence.

a single wire probe. Photographs of the experimental set-up are shown in figure 1.

2.1. Turbine model

The turbine model is two-bladed, with a diameter of 180 mm and is mounted in the middle between the walls on the wind tunnel floor, 1.45 m from the test section inlet. The height of the hub above the floor is 240 mm. The non-twisted blade is based on the Göttingen 417A airfoil and has been built at FOI (Swedish Defense Research Agency), Stockholm. Details on the blades and their construction can be found in Montgomerie & Dahlberg (2003). The four-layered structure of reinforced epoxy composing the blade is about 0.5 mm thick. The maximum chord is 27 mm at 12% of the radius, and the tip chord is 16 mm.

In order to measure the drag on the turbine, the tower was mounted on a strain-gauge balance which is calibrated by applying a known force at the centre of the hub. In figure 2 the drag coefficient ($C_D = D / \frac{1}{2} \rho U_\infty^2 A$, where D is the drag of the turbine and A the swept area $= \frac{\pi}{4} D^2$) of the wind turbine model as function of the tip speed ratio (tip speed/wind speed $= \lambda$) is shown. The drag was measured both at 5 m/s and at 8 m/s, as well as with the turbulence grid mounted. The tip speed ratio was varied by keeping the wind speed constant, and changing the electrical loading of the generator from short circuiting to free-running (open circuit) conditions. As can be seen the data for the different cases show a nice collapse. It can be noted that the drag coefficient tends to a value of 0.17, when linearly extrapolated to $\lambda=0$. This value seems reasonable if the blade can be approximated with a flat plate with an aspect ratio of 4 (crudely resembling the blades used here). Such a plate has a drag coefficient of 1.17 (see e.g. Hoerner (1965)) and since the solidity of the turbine

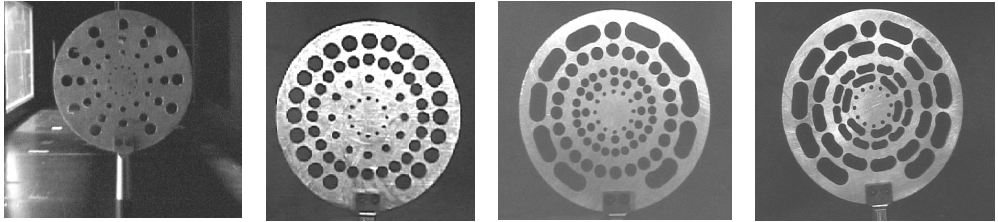


FIGURE 3. Four examples of the disc models used in the experiments viewed from upstream. The porosity of the models are 14, 30, 38 and 42% and the corresponding drag coefficients 1.06, 0.93, 0.90 and 0.85, respectively. The hole diameters are for all models increased with their radial position.

model is 13%, a value of 0.152 is obtained when applying the same percentage to the drag coefficient of a plate. This value is close to the extrapolated value of 0.17 at $\lambda=0$, so the behaviour of the wind turbine could be connected to that of a plate facing the flow when no rotational effects are present.

2.2. Disc models

A number of porous discs were tested during the present experiments where the basic structure for all discs was the same. The disc models were manufactured from a 5 mm thick aluminum plate and the diameter was 100 mm for all discs. The edge was phased at an angle of 45° such that the edge was sharp and the flat side of the disc was facing the flow. The discs were supported by a vertical sting that was mounted with screws to the lower end of the plate and fastened to the strain gauge balance. Different possibilities exist to form a porous disc, here the porosity was for most models achieved by drilling holes with increasing diameter for increasing radius. Some of the disc models are shown in figure 3. The drag coefficient of the discs varied from 1.16 for the solid disc and decreased monotonously to 0.85 for the disc with the largest porosity (42%). This value of the drag coefficient is approximately the same as the value obtained for the turbine at high tip speed ratios.

We should also note that the shedding becomes less distinct with increasing disc porosity. For instance by increasing the porosity to 44% we could not observe any stable vortex shedding. Some discs were also made with holes of constant diameter, and they showed similar results as the ones described above. However such discs could not be produced with a C_D less than 1. We also made some models with radially oriented slits. They failed to produce stable vortex shedding for porosities above 25%. In the following only data for discs similar to the ones shown in figure 3 will be presented.

3. Results

3.1. Overall wake development

A wind turbine wake can be detected far downstream and its decay scales on the turbine diameter. However many other factors affect the wake development such as the drag on the turbine (or for a given turbine the loading), the ambient atmospheric conditions (turbulence level, mean velocity gradient, wakes from upstream turbines, stratification), the turbine distance from the ground etc. In addition, the wind direction may change suddenly and misalign the wind turbine with respect to the oncoming flow. It has also been proposed to intentionally yaw the turbine in order to actively steer the wake direction (so called AWC, active wake control) in order to avoid interaction with downstream turbines.

To give an idea about the wake development behind a turbine we show in figure 4 contour plot of the streamwise velocity for the present model turbine at three different yaw angles, namely 0, 10 and 20 degrees. In this case the turbine is placed in the free stream with a low turbulence level ($<0.1\%$). The centre is $1.5D$ above the ground plane so ground effect can be assumed to be small. The data in these figures are from measurements made with an X-wire probe, making spanwise traverses at $x/D=0.5, 1, 1.5, 2, 3, 4, 5, 7$ and 9 . One should be slightly cautious about the measurements closest to the turbine since the instantaneous flow angles can be quite large, which may invalidate the hot-wire response. The figures are plotted to show the correct geometrical appearance of the wake and it is seen to approximately double its size in 9 diameters. For the case with free stream turbulence the wake spreading is of course larger (see e.g. Medici & Alfredsson (2005)).

Figure 4a shows the contour levels when the rotor plane is normal to the wind direction. We observe a fairly symmetric wake around the centerline and at $x/D=9$ the velocity at the centerline has recovered to about 75% of the undisturbed freestream velocity. What is not shown in this plot is that there is a region of higher than the freestream velocity near the turbine. At $x/D=1$ the maximum velocity is around $z/D=0.7$ and is about 5% higher than the freestream velocity.

Figure 4b,c shows the wake development when the turbine is yawed with respect to the oncoming flow. This gives a side force acting on the rotor and a force in the opposite direction will affect the flow and the wake will hence move sidewise. In figure 4 the turbine is yawed in the anti-clockwise direction (as seen in the figure) and therefore the wake moves clockwise (i.e. towards negative z/D).

Another feature of the near wake is a rotation of the wake in the opposite direction to the rotation of the turbine. Medici & Alfredsson (2005) reported a maximum azimuthal velocity of the order of 15% of the freestream velocity. Finally tip-vortices shed by the turbine blades are a distinct feature in the near wake region. The signatures of the tip vortices are very clear when measuring

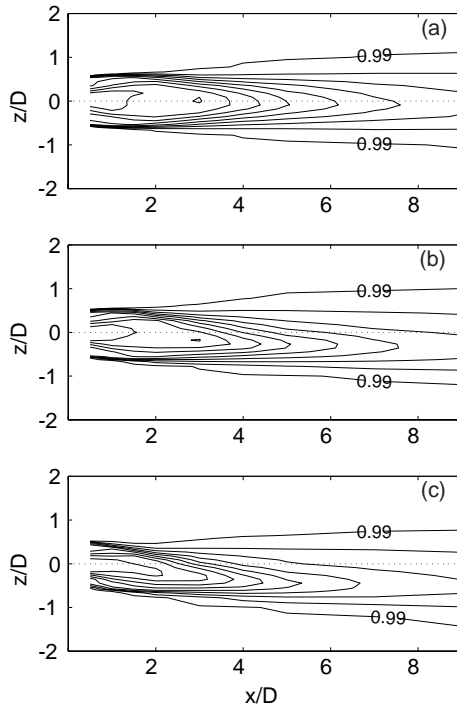


FIGURE 4. Contours of the mean streamwise velocity normalised with the freestream velocity behind the wind turbine model. (a) $\gamma = 0^\circ$, (b) $\gamma = 10^\circ$, (c) $\gamma = 20^\circ$. Contour lines are 0.2, 0.3, ..., 0.9, 0.99.

the streamwise velocity, giving a peak velocity difference (positive or negative) of the order of 75% of the freestream velocity during a vortex passage. The regular tip vortex signatures can usually be measured beyond 3 diameters downstream the turbine, whereas further downstream they merge, disintegrate and finally disappear. The vortex path lies in the region where the mean local streamwise velocity is approximately 75% of the freestream velocity.

Finally one should note that the contour lines in figure 4 are based on averages which would incorporate the tip vortices as well as any large scale vortex shedding and meandering. The rest of this paper deals with various aspects of the large scale vortex shedding.

3.2. Method of phase locking

In order to investigate the spatio-temporal structure of the large scale vortex shedding a two probe set-up was used. Figure 5 shows a typical streamwise velocity signal measured at $x/D=1$ in the region of the tip vortices. The reference probe was positioned near the middle of the shed vortices, i.e. at $x/D=1$

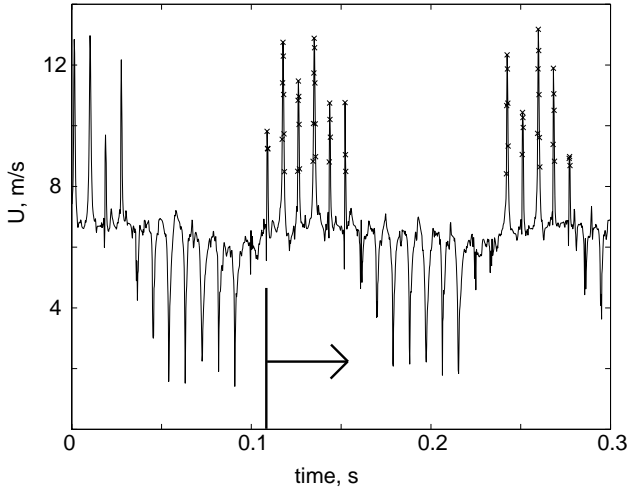


FIGURE 5. Signal from the reference probe. The points belonging to the velocity overshoots are marked and the first peak (marked by the arrow) is considered as the reference time for the measuring probe.

and $z/D=0.6$, a position which gave a clear and repeatable time signal. Two structures can be clearly seen: the tip vortex passage at each peak (negative or positive) and the low frequency meandering of the wake. The latter is seen through the movement of the vortices such that the reference probe alternatively measures the inner and outer side of the vortex.

The measuring probe was traversed in the wake at the opposite side ($z/D < 0$) as compared to the side where the reference probe was located. Data from both probes were simultaneously collected through the AD-converter. The following strategy was developed to obtain a time reference for the large scale motion. For each set of measurements, i.e. for each pair of data files obtained by the reference probe and the measuring probe, the “time zero” was chosen as the time when the reference probe detected the passage of the first in a full group of velocity overshoots (marked with a line and an arrow in figure 5). The same time reference was then used for the measuring probe. In this way the measuring probe signal was always accurately phase locked to the tip vortex passage. Since the phase of the large scale shedding also could be found in this manner (however with a time accuracy of \pm one-half of the time between successive vortex passages) the measuring probe could be phase locked to the large scale shedding as well.

3.3. Time signals in the near wake

Figure 6 shows velocity signals of the streamwise velocity at $x/D=1$ at some different spanwise positions. These signals have been phase-locked according

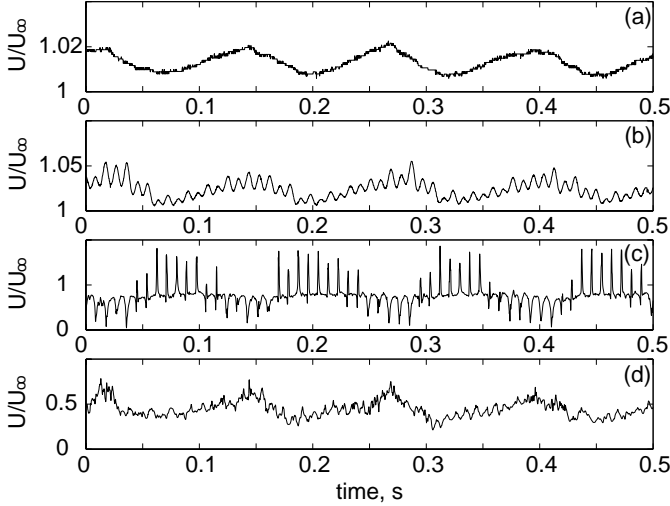


FIGURE 6. Streamwise velocity signals behind the turbine at $x/D = 1$. The signals are phased locked to the signal from the reference probe. $z/D =$ (a): -1.01 , (b): -0.78 , (c): -0.57 , (d): -0.44 .

to the method described above. The two positions at $z/D = -1.01$ and -0.78 are in the region where the flow was accelerated around the turbine and the mean velocity was 1.01 and 1.03 of U_∞ , respectively. When the signal in figure 6c shows peaks with a velocity less than the mean the wake has been shifted outwards with respect to the probe position, whereas the opposite is true for regions with positive peaks. The streamwise velocity signal in the outer region shows the corresponding behaviour, when the wake moves inwards the velocity measured by the probe decreases and *vice versa*. The behaviour inside the wake at $z/D = -0.44$ seems to be more complicated since here both the strong velocity gradient in the wake as well as the contribution from the tip vortices affect the signal (see figure 6d).

For the wind turbine the regular vortex shedding from the blades is most clearly seen at $z/D \approx 0.5$ and up to about $x/D = 3$ in the streamwise velocity. The large scale shedding is on the other hand observed across most of the wake as well as outside the wake. It is also clearly observed all the way downstream to the furthestmost measurement station at $x/D = 9$. Also the measurements behind the disc show the large scale vortex shedding in a similar manner, but here we find it more convenient to measure it around $z/D = 0.25$. We illustrate this in figure 7, which in the upper plots shows the time signals behind the turbine and the disc, respectively. These two signals look like two typical turbulent signals. Note that the length of time signal for the turbine is 1.7 sec whereas it is 0.7 sec for the disc. In order to be able to distinguish the low

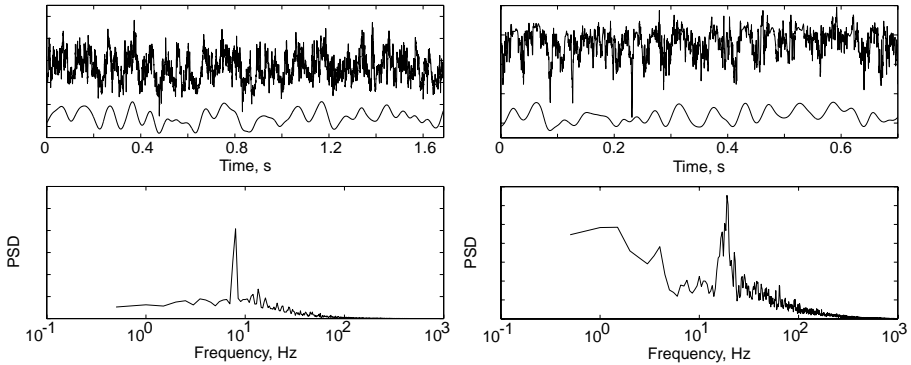


FIGURE 7. Time signals of the streamwise velocity behind the turbine model (left, $U_\infty = 8.3$ m/s) and disc model (right, $U_\infty = 15.3$ m/s) measured at $x/D = 5$ and $z/D = 0.25$. Comparison between original signal and low pass filtered signal (top figures), arbitrary scale. The bottom figures show the power spectral density (PSD) of the original, non-filtered signals. The peaks correspond to the large scale shedding.

frequency fluctuation part of the signal, the signals were low-pass filtered using a Butterworth 4th-order filter implemented in a Matlab routine. The cut-off frequency for the turbine model was set to 12.5 Hz, and the cut-off frequency of the disc to 25 Hz. As can be seen the low-pass filtered signals show a fairly regular, low frequency variation.

The two lower plots show the power spectra of the full signals and as can be seen both spectra are dominated by a large peak corresponding to the vortex shedding frequency. It is clear from the power spectral density that the energy contained in the large scale structure is, with respect to other disturbances, larger for the turbine than for the disc.

Table 1 shows the characteristic values for the two cases. It should be noted that the Reynolds number based on the diameter of the rotor and the disc is about the same.

As mentioned above the large scale vortex shedding is also clearly distinguishable when going downstream. Figure 8 shows the spectra at four different downstream positions behind both the turbine and the disc. The maximum amplitude is for both cases obtained at $x/D=4$. It is also clearly seen that the peak for the turbine case is more distinct than for the disc case.

	Turbine	Solid disc
U_∞ [m/s]	8.3	15.3
D [m]	0.18	0.10
Shedding frequency [Hz]	7.9	18.9
Strouhal number	0.171	0.123

TABLE 1. Experimental data corresponding to figure 7.

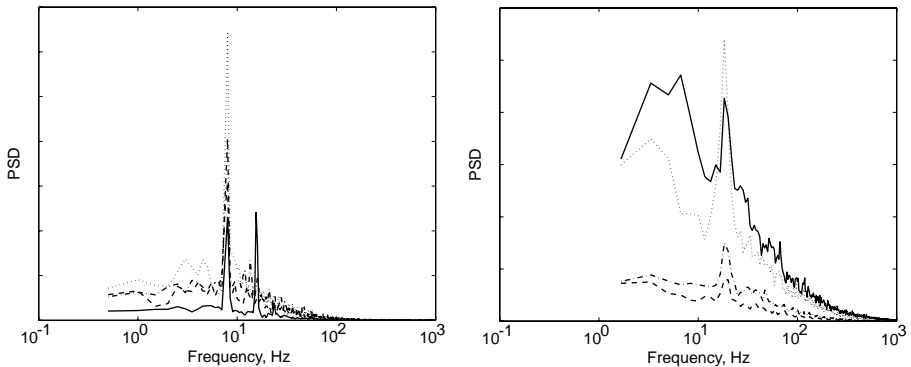


FIGURE 8. Power spectral density (PSD) of the streamwise velocity measured behind the turbine at $U_\infty = 8.3$ m/s (left) and solid disc at $U_\infty = 15.3$ m/s (right) at $z/D = 0.25$. (solid): $x/D = 2$, (dotted): $x/D = 4$, (dash-dotted): $x/D = 5$ (turbine) and 6 (disc), (dashed): $x/D = 7$ (turbine) and 8 (disc). Note that for both cases the highest shedding amplitude is obtained at $x/D = 4$.

3.4. Strouhal number variation for turbine and discs

In the following we will focus on the variation of the shedding frequency both behind the turbine and the discs. The strategy to measure the shedding frequency for the turbine and the discs was slightly different. For the turbine the probe was positioned at $x/D=0.5$ and in the region 0.44 to 0.58 z/D depending on the tip speed ratio.

For the discs the spectral peaks for the large scale shedding are not as clearly observable as for the turbine, however it was found that the best position was inside the wake and $z/D=0.25$ was used in all cases. Measurements were made in the region $x/D=1-10$ and the values shown are average values from 3 to 5 positions (variations were typically within a few per cent). It should be noted that for the discs with largest porosity the shedding was harder to detect and these data are based on measurements for $x/D=4-8$.

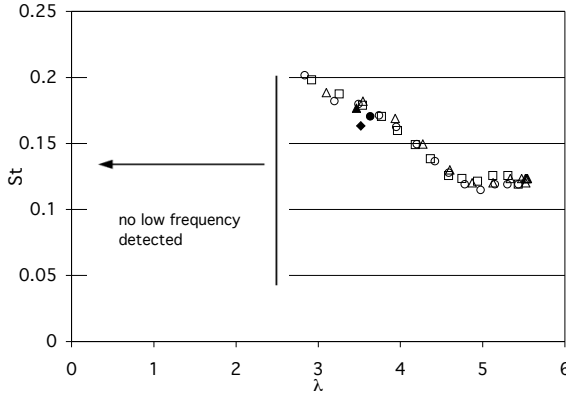


FIGURE 9. Strouhal number (St) as function of the tip speed ratio (λ). \circ : $U_\infty = 8.3$ m/s, no turbulence, \square : $U_\infty = 8.5$ m/s, 4.5% grid turbulence, \triangle : $U_\infty = 5.5$ m/s, no turbulence. Data from Dahlberg & Medici (2003) are also shown, \blacktriangle : $U_\infty = 5.2$ m/s, \bullet : 8.3 m/s, \blacklozenge : 11.6 m/s.

Figure 9 shows how the Strouhal number changes with the tip speed ratio for two different freestream velocities, 5.5 and 8.3 m/s. The data for this scaling of the frequency and rotational speed collapses nicely. It is interesting to note that no large scale vortex shedding could be distinguished for $\lambda < 2.8$. We hypothesize that for too low tip speed ratios the flow ceases to see the rotor plane as an axisymmetric body and that for such cases no large scale vortex shedding is triggered.

Above $\lambda = 2.8$ the Strouhal number decreases monotonically with increasing λ , however St seems to level out for $\lambda > 4.5$. It is interesting to compare this result with the data in Figure 2 which shows that C_D also becomes constant above $\lambda > 4.5$. This indicates that C_D may be a more appropriate parameter in order to determine the shedding frequency.

Some data which were taken with free stream turbulence are also included in figure 9. Also in this case it is possible to detect the large scale shedding and those data seem to follow the same trend as those obtained with low turbulence level.

We have also included three data points from Dahlberg & Medici (2003) taken at 5, 8 and 11 m/s which were obtained at an earlier experimental campaign using the same turbine model. The 5 and 8 m/s points follow the trend of the present data nicely, however the 11 m/s is slightly off the trend of the other data. As we will see in the following this may be explained from the fact that C_D for this turbine is slightly larger for $U_\infty = 11$ m/s than at 8 m/s.

An alternative plot is figure 10, where the Strouhal number is instead expressed as function of the drag coefficient C_D . Now also the 11 m/s data

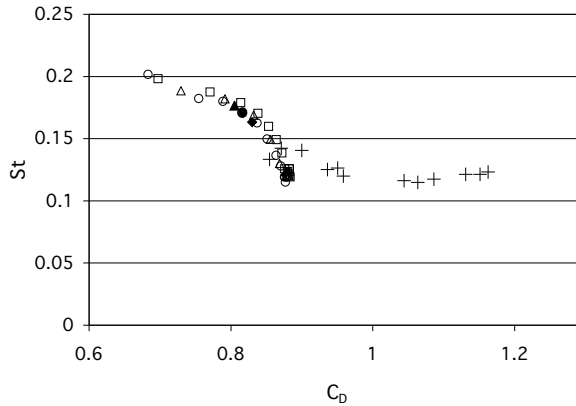


FIGURE 10. Strouhal number (St) as function of the drag coefficient (C_D), symbols as in figure 9. The Strouhal number from the disc measurements is given by (+). The porosity varies from 0% to 42%.

point adapted from Dahlberg & Medici (2003) shows the same tendency as the rest of the turbine data, namely that the Strouhal number decreases with increasing drag coefficient.

The Strouhal numbers obtained for the different disc models with different porosities (0–42%) are also plotted in this graph. As can be seen the variation for the different disc models is not very large, the St is in the range 0.12–0.14 and connects nicely to the turbine data at high tip speed ratios.

It is known from earlier studies such as the one by Calvert (1967*a*) that the Strouhal number changes when a disc is inclined with respect to the oncoming flow. For the solid disc model we observe the same behaviour as can be seen in figure 11. The Strouhal number and hence the frequency is increasing with the inclination and show no dependence with the freestream velocity (the freestream velocities were 11.9 m/s, 15.3 m/s and 18.8 m/s). Physically this may be viewed such that the transverse dimension of the body is decreasing with increasing yaw angle and hence the shedding frequency would increase. As can be seen in figure 11 the same variation with yaw angle is observed also for the shedding frequency behind the wind turbine model.

3.5. Spatial wake structure

So far we have only presented results regarding the vortex shedding frequency, but for wind turbine engineering it is of course also interesting to see how large wake deflections are associated with the shedding. To give some information about this we use velocity data at three different downstream positions ($x/D=1, 3$ and 9) at which the traversed probe has collected data within the

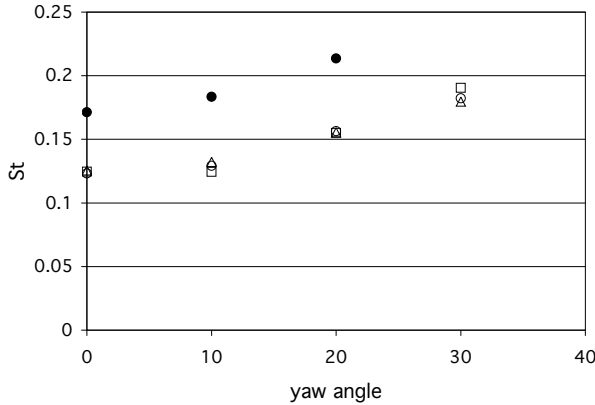


FIGURE 11. Strouhal number (St) as function of the yaw angle (γ). Filled symbols are for the wind turbine model, while the symbols used for the disc are: \triangle : $U_\infty = 11.9$ m/s, \circ : 15.3 m/s, \square : 18.8 m/s.

spanwise range $-1.66 < z/D < -0.44$. These data are phase locked with the reference probe as described earlier. In this way time-space maps of the velocity disturbance can be obtained and the results are shown in figure 12. In the uppermost figure which is taken at $x/D=1$ the tip vortices are well correlated over the full time span and the effect of the shedding on the movement can be clearly seen. One may estimate a shedding amplitude (top-to-top) to be almost $0.2D$. In the center figure at $x/D=3$ the tip vortices are less distinct but are still distinguishable and the shedding motion can be seen to have grown in amplitude. Finally the bottom picture shows data from $x/D=9$ and individual tip vortices cannot longer be distinguished. However the reminiscent of the vortices help us to mark the shedding motion which now seem to have grown to at least $0.5D$ (note that the vertical scale is compressed compared to the other two x -positions).

The appearance of the tip vortices in figure 12 at $x/D=9$ may at first look surprising but by looking at a typical time signal one clearly observes that at each position only one out of approximately ten vortices appear at the hot-wire position (see figure 13). There may be several reasons for this, first it is known that tip vortices have a tendency to merge with its neighbours, creating fewer but larger vortices which may also cause breakdown. The amplitude of the large scale shedding motion may also be so large that only one vortex per shedding actually passes the probe. In order to fully understand this complex scenario, measurements with e.g. PIV should be done.

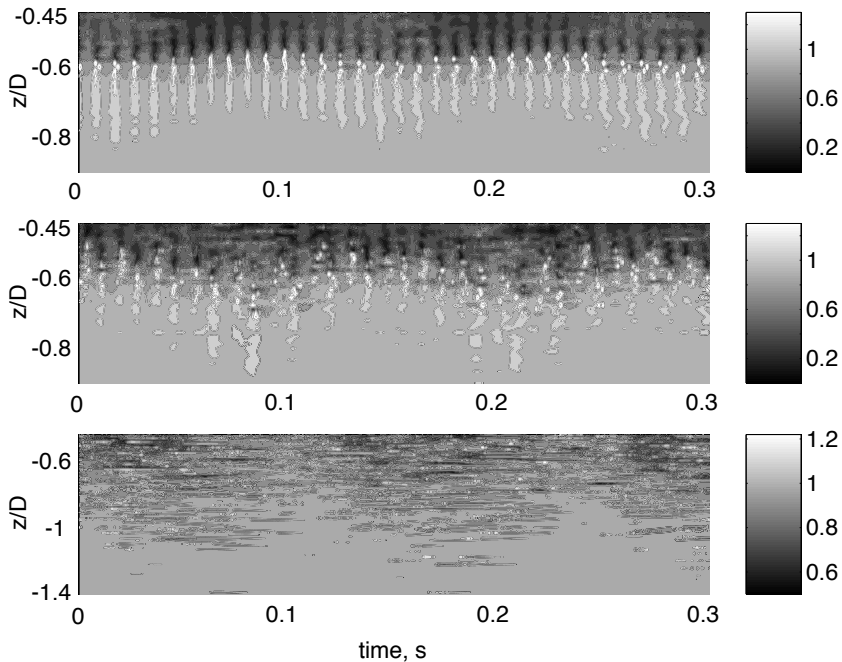


FIGURE 12. Contours of U/U_∞ as function of the time. The velocities in the z -direction are phase locked with the tip vortex passage detected by the fixed probe at $z/D = 0.6$ and $x/D = 1$. From top to bottom: $x/D = 1, 3$ and 9 , respectively. Note the difference in vertical scale.

4. Discussion

The present work has focussed on the large scale vortex shedding that has been detected behind wind turbine models. A similar type of vortex shedding has been observed behind discs and other axis-symmetric bodies. An interesting feature is that the tip speed ratio of the turbine has to be above a certain value in order to obtain the shedding motion. Our hypothesis is that there exist a critical rotational speed for which the rotor plane starts to act as a disc, whereas for small rotational speeds the rotor is just seen as a rotating pair of blades by the oncoming flow. We have shown that also porous discs (of various porosity) give rise to large scale vortex shedding and that the frequency seems to be fairly independent of the porosity up to the largest value tested here (42%). One should note however, that the shedding becomes less clear with increasing porosity.

Somewhat surprisingly the large scale vortex shedding is more clearly observed behind the turbine than behind the disc. A possible explanation is that

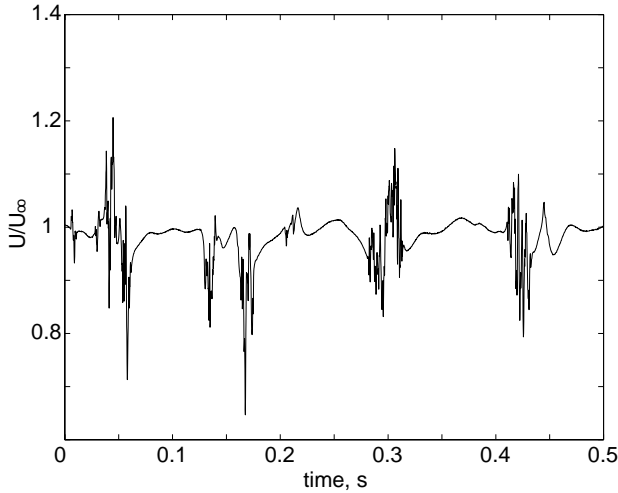


FIGURE 13. Time signal of the streamwise velocity component at $x/D = 9$ and $z/D = -1.01$.

for the disc there is no preferred direction of the shedding, it could be both clockwise and anti-clockwise with equal probability. However, since the turbine is rotating the symmetry is broken and one may speculate that this leads to a preferred direction of the motion of the large scale vortex shedding and therefore a more distinct frequency peak for the turbine as compared to the disc. Another mechanism is suggested by Berger *et al.* (1990), where it is found that a forcing near the natural frequency of the shedding makes it regular. Although the rotational frequency of the turbine rotor is much higher than the shedding frequency one may hypothesize that the rotor still may trigger the shedding through a subharmonic of the blade passage frequency. Further experiments using PIV and/or multiple hot-wire probes would give further information on this.

Previously the meandering of turbine wakes, which has been observed in field measurements, has been interpreted as a result of large scale transverse velocity fluctuations of the wind (see e.g. Thomsen *et al.* (2001)). We propose however that the observed shedding may be another candidate responsible for the meandering motion.

5. Acknowledgments

The work was sponsored by the Swedish National Energy Agency (STEM). The authors thank Jan-Åke Dahlberg (FOI) for providing the turbine model and for many fruitful discussions.

References

- ALFREDSSON, P. H., DAHLBERG, J. Å. & BARK, F. H. 1980 Some properties of the wake behind horizontal axis wind turbines. In *Proc. Third Int. Symp. on Wind Energy Systems*, Copenhagen, BHRA Fluid Engineering, paper J5, pp. 469–484.
- BERGER, E., SCHOLTZ, D. & SCHUMM, M. 1990 Coherent vortex structures in the wake of a sphere and a circular disk at rest and under forced vibrations. *J. Fluids Struct.* **4**, 231–257.
- BEVILAQUA, P. M. & LYKOURIS, P. S. 1978 Turbulence memory in self-preserving wakes. *J. Fluid Mech.* **89**, 589–606.
- CALVERT, J. R. 1967*a* Experiments on the flow past an inclined disk. *J. Fluid Mech.* **29**, 691–703.
- CALVERT, J. R. 1967*b* Experiments on the low-speed flow past cones. *J. Fluid Mech.* **27**, 273–289.
- CASTRO, I. P. 1971 Wake characteristics of two-dimensional perforated plates normal to an air-stream. *J. Fluid Mech.* **46**, 599–609.
- DAHLBERG, J. Å. & MEDICI, D. 2003 Potential improvement of wind turbine array efficiency by active wake control (AWC). In *Proc. European Wind Energy Conference and Exhibition*, Madrid, (published on CD).
- HOERNER, S. F. 1965 *Fluid-dynamic drag*. Hoerner Fluid Dynamics.
- JOHANSSON, P. B. V., GEORGE, P. B. V. & GOURLAY, M. J. 2003 Equilibrium similarity, effects of initial conditions and local Reynolds number on the axisymmetric wake. *Phys. Fluids* **15**, 603–617.
- JOHANSSON, P. B. V., GEORGE, P. B. V. & WOODWARD, S. C. 2002 Proper orthogonal decomposition of an axisymmetric turbulent wake behind a disk. *Phys. Fluids* **14**, 2508–2514.
- LEE, S. J. & BEARMANN, P. W. 1992 An experimental investigation of the wake structure behind a disk. *J. Fluids Struct.* **6**, 437–450.
- MEDICI, D. & ALFREDSSON, P. H. 2005 Measurements on a wind turbine wake: 3d effects and bluff-body vortex shedding. *Wind Energy*, published online.
- MIAU, J. J., LEU, T. S., LIU, T. W. & CHOU, J. H. 1997 On the vortex shedding behind a circular disk. *Exp. Fluids* **23**, 225–233.
- MONTGOMERIE, B. & DAHLBERG, J. Å. 2003 Vortex system studies on small wind turbines. FOI scientific report, ISRN FOI-R-0936-SE.
- THOMSEN, K., MADSEN, H. A. & LARSEN, G. C. 2001 A new method can predict detailed response for turbines in wind farms. In *Proc. IEA 16th Symp. Aerodyn. Wind Turbines*, Boulder, FOI-S-0877-SE, pp. 171–187.
- VERMEER, L. J., SØRENSEN, J. N. & CRESPO, A. 2003 Wind turbine wake aerodynamics. *Prog. Aerospace Sci.* **39**, 467–510.

Paper 7

A note on the frequency of wind turbine wake meandering

By D. Medici

KTH Mechanics, SE-100 44 Stockholm, Sweden

The frequency of wind turbine wake meandering has been studied using wind turbine model with one, two and three blades. The one bladed turbine did not give rise to any meandering motion, whereas both the two and three-bladed turbines did for high enough tip-speed ratio. It was shown that not only the drag of the turbine influences the frequency but also the blade passage frequency itself.

1. Introduction

In wind engineering it has since long been recognized the importance of knowing the behaviour of the wake behind wind turbines especially when arranging turbines in wind turbine parks. Two major issues are to be regarded, namely losses in power output of downstream turbines due to their position in the low velocity region of the wake, as well as an increase in forces due to the turbine working in a region of increased mean velocity shear and high turbulence. Recently it has been found that another effect also may influence the wake behaviour, namely the so called meandering of turbine wakes, i.e. a low frequency sideway oscillation of the wake, similar to vortex shedding behind a bluff body.

Earlier studies (Medici & Alfredsson (2005*a*), Medici & Alfredsson (2005*b*)) showed that it was appropriate to analyze the oscillations by defining a non-dimensional frequency in the form of a Strouhal number much in the same way as is done when studying vortex shedding behind bluff bodies. The Strouhal number was based on the low-frequency peak f determined from an FFT of the streamwise or radial velocity signal downstream of the turbine in the outer part of the wake and is defined as:

$$St = \frac{f \cdot D}{U_\infty} \quad (1)$$

where D is the turbine diameter and U_∞ the freestream velocity. It was previously shown that for high tip-speed ratios ($\lambda = \Omega R/U_\infty$, where Ω is the rotational speed of the turbine and $R = D/2$) the Strouhal number is close to what would be expected from a solid circular disc (around 0.12), whereas for lower λ the Strouhal number is larger. It has been proposed that the drag

coefficient of the turbine is related to the meandering frequency, however these results were obtained for a two bladed turbine which were tested at different tip-speed ratios.

In the present paper earlier studies of the meandering motion are complemented by showing the influence of the number of turbine blades, the blade pitch angle and the tip speed ratio on the frequency of the meandering motion. It is shown that it is not only the drag coefficient that influence the Strouhal number but also the blade passing frequency. In section 2 we describe the experimental set-up and section 3 gives the characteristics of the different turbines in terms of drag and power coefficients. Finally section 4 describes and discusses the results on the meandering frequency.

2. Experimental set-up and methods

Measurements were performed in the wake of turbine models equipped with 1, 2 or 3 blades. ($N=1, 2, 3$). The blades were all moulded in the same form and then mounted on the hub. The one and two bladed models were using the same hub; in the one blade experiment a counterweight was mounted on the opposite side of the hub, whereas the three-bladed was mounted on its own hub. The hub diameter was 25 mm for both hubs and the diameter of the turbine is 180 mm. The same blades were used by Medici & Alfredsson (2005a) and more details on the blade geometry can be found there. It was possible to adjust the pitch angle of the blades and here we will describe experiments with the blades mounted at two different pitch angles, namely 8° and 11° .

The turbine hub is mounted on a tower and the centre of the turbine is 240 mm above the ground plane of the wind tunnel. The test section is 1200 mm wide and 800 mm high so the blockage due to the swept area of the turbine is about 3%. The generator inside the hub is connected to a loading circuit so the generated power can easily be measured. Also the drag of the turbine was measured with a strain gauge balance mounted in the supporting tower.

The blade passing frequency (*bpf*) is registered by a laser beam intersecting the rotor plane from an upstream window and is picked up by a photodiode on the downstream side of the turbine. The circuit gives a voltage step when the blade interrupts the laser beam and the signal is sampled through the computer and the *bpf* was obtained through an FFT of this signal.

The freestream velocity was measured with a Prandtl tube in front of the turbine. The freestream velocity was close to 8.0 m/s if not otherwise specified. The meandering frequency was obtained from hot wire anemometry where an X-probe was used to measure both the streamwise and radial velocity components. The probe was mounted on a traversing equipment and was positioned at $x/D=1$ and around $z/D=0.5$ where the meandering motion was clearly observed. However the meandering frequency is seen across the full width of the wake except in the central region of the wake.

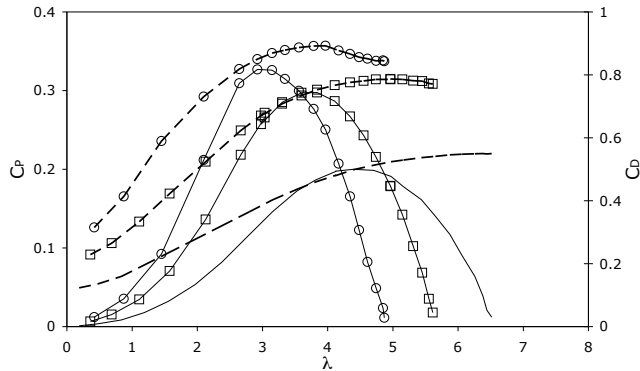


FIGURE 1. Power (C_P) and drag (C_D) coefficients as function of the tip-speed ratio (λ). The blade pitch angle is 11° and $U_\infty = 7.9$ m/s. Lines: $N = 1$, \square : $N = 2$, \circ : $N = 3$.

3. Wind turbine characteristics

Figure 1 shows the drag C_D and power coefficients C_P for the turbines with $N = 1, 2, 3$. In these measurements the pitch angle was 11° which was found to be close to the optimum angle in terms of the maximum power coefficient. It can be observed that the maximum C_P increases with the number of blades with the ratio 1.00:1.48:1.67. It is also clearly shown that the maximum C_P occurs for a smaller tip speed ratio when the number of blades increases. The drag coefficient is increasing with the number of blades. The drag coefficient C_D increases initially monotonously with λ but for both $N = 2$ and 3 there is a slight decrease at high λ .

In figure 2 the drag and power coefficients for the two bladed model is compared at two different blade pitch angles. The difference is not too large, but as can be seen C_P is slightly larger for the 11° case which at the same time has a smaller C_D .

In figure 3 we instead plot the drag coefficient as function of the blade passage frequency (bpf). This gives a similar appearance of the the three cases showing that at least for low rotational speeds, the drag on the turbine could be seen as the sum of the drag of the individual blades. When the bpf goes towards zero we have previously shown that C_D goes towards the drag coefficient of a flat plate (see **paper 3**). For the two bladed model this value is approximately 0.17. The one bladed model seems to approach a slightly higher value than half of this (however we also have to take into account the drag of the hub itself). Also the three-bladed model seems to fit into this picture. Hence it seems that to compare the drag performance of turbines with different number of blades it may be preferably to do so using the blade passage frequency rather than the tip speed ratio.

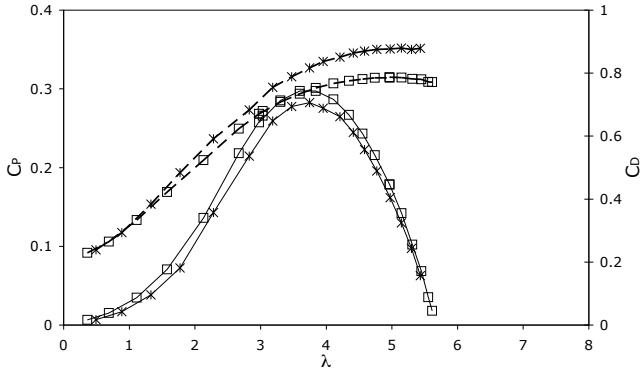


FIGURE 2. Power (C_P) and drag (C_D) coefficients as function of the tip-speed ratio (λ) for a two bladed turbine with two different pitch angles. *: 8° , \square : 11° .

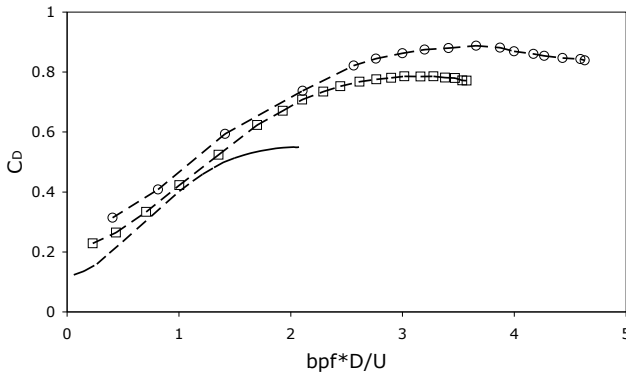


FIGURE 3. Drag (C_D) coefficient as function of the blade passage frequency. Same data as in figure 1.

4. Results and discussion

In the present work as well as previously we use FFT routines to obtain the frequency of the large scale vortex shedding from either the streamwise or the radial velocity signal. Here we use the radial velocity measured at $x/D=1$ and around $z/D=0.5$ which gives a clearly defined spectral peak. At this stage it should be pointed out that no vortex shedding was observed for the one-bladed model, hence it seems that it is not sufficiently "bluff" to give rise to vortex shedding. To exemplify the procedure, figure 4 shows the radial velocity measured at $x/D=1$ for two different λ for the three-bladed model. Also included in the left pictures are the low-pass filtered velocity signals (using

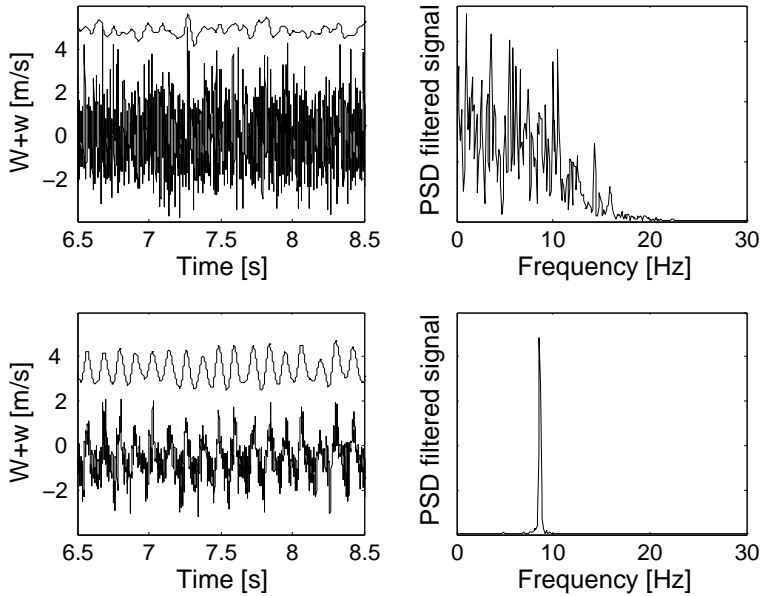


FIGURE 4. Radial velocity signal and its low-pass filtered form, $x/D = 1$ and $z = -48$ mm. Arbitrary vertical offset for the filtered signal. Top: $N = 3$, $\lambda=0.85$. Bottom: $N = 3$, $\lambda=2.68$

a Butterworth low-pass filter with a cut off frequency equal to 13 Hz). For the low λ we see a very irregular signal and no apparent peak is observed in the spectrum of the low-pass filtered signal. This is in accordance with earlier result, which has shown that for low enough λ no meandering occurs. However for the high λ the meandering motion is clearly observable as a dominant peak in the spectrum, and the frequency of the meandering motion can be accurately determined.

The relation between the Strouhal number and tip-speed ratio for the different cases can be seen in figure 5. The symbols used in the plots are listed in table 1. The two-bladed turbine gives similar curves for both pitch angles (8° and 11°) although for the larger pitch angle also the Strouhal number becomes larger. For both cases no meandering is observed below $\lambda \approx 2.7$. For the three-bladed turbine it seems that the curve is shifted to the left as compared to the two-bladed at the same pitch angle. It is also seen that it does not monotonously decrease with λ as is the case for the two-bladed turbine.

It has earlier been hypothesized that the Strouhal number is directly related to the drag coefficient of the turbine. In figure 6 we plot the same data as in figure 5 as function of C_D instead. The two different pitch angles are shown

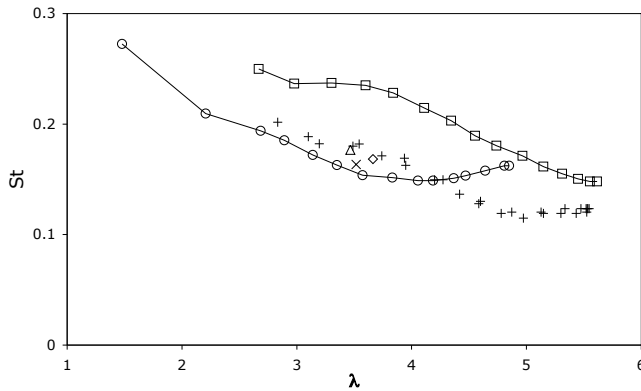


FIGURE 5. Strouhal number as function of the tip-speed ratio. The single symbols (+, Δ , \diamond , \times) are for $N = 2$ and pitch= 8° . $-\square-$ are for $N = 2$ and pitch= 11° , whereas $-\circ-$ are for $N = 3$ and pitch= 11°

Experiment description	λ	symbol
N=2, pitch= 8°	0.49 \rightarrow 5.43	+
N=2, pitch= 8° , $U_\infty=5.53\text{m/s}$	0.69 \rightarrow 5.53	
N=2, pitch= 8° , $U_\infty=5.25\text{m/s}$	3.46	Δ
N=2, pitch= 8° , max C_P	3.66	\diamond
N=2, pitch= 8° , $U_\infty=11.63\text{m/s}$	3.51	\times
N=2, pitch= 11°	0.36 \rightarrow 5.61	$-\square-$
N=3, pitch= 11°	0.42 \rightarrow 4.85	$-\circ-$

TABLE 1. Experiments and symbols used in the plots.

in different figures for clarity. For the 8° case the Strouhal number shows a monotonous decrease with C_D and approaches the value 0.12 around $C_D = 0.88$, which is the Strouhal number observed for the solid disc. However for the 11° case the curves show a more complicated behaviour. For instance, referring to the three-bladed turbine, we observe that when C_D decreases above a certain λ also the Strouhal number increases again, although it does not retract on the same curve as before. This still indicates, however, that the drag is an essential parameter when determining the meandering frequency.

A different way to plot the data is instead to show the Strouhal frequency as function of the blade passage frequency (bpf). Such a plot is shown in

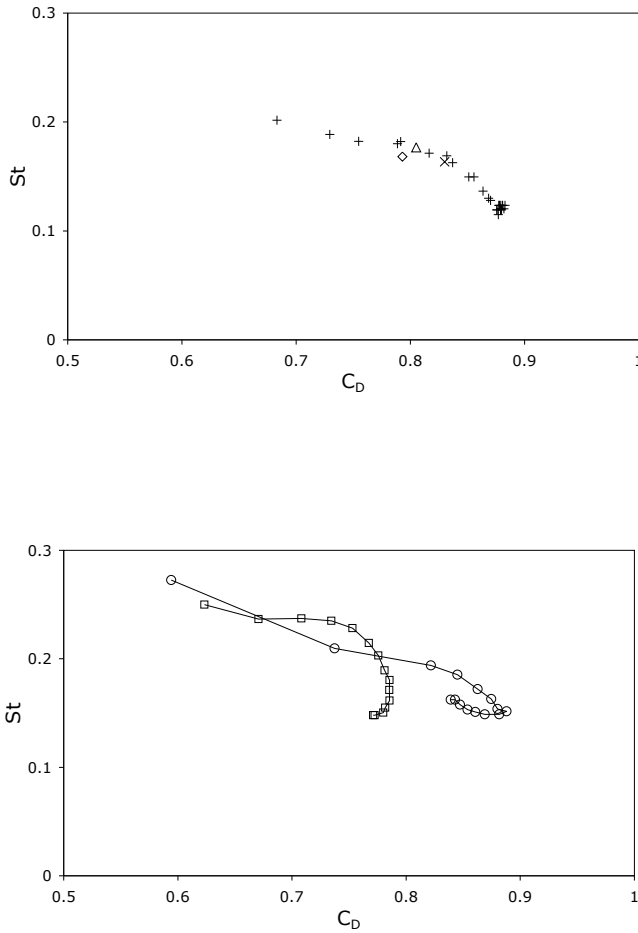


FIGURE 6. Strouhal number as function of the drag coefficient for turbines Top): pitch angle 8° , Bottom): pitch angle 11° . \square : $N = 2$, \circ : $N = 3$.

figure 7. Of course the data for the two-bladed model with pitch angle 8° collapses as before, but an interesting observation is now that the two and three-bladed models with pitch angle 11° comes close together, although the Strouhal number for these cases are still higher than for the two-bladed turbine.

5. Conclusions

In the present work we have studied the dependence of the meandering frequency of a wind turbine wake varying both the number of blades, the blade

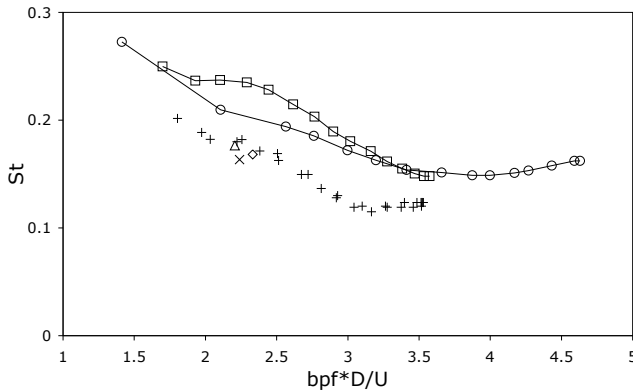


FIGURE 7. Strouhal number versus the normalised blade passage frequency.

pitch angle and the turbine rotation frequency. These three parameters all influence the drag on the turbine, but we have shown that it is not only the drag on the turbine that influences the meandering frequency. It is also shown that the blade passage frequency may be a more appropriate variable than the tip speed ratio when comparing turbines with different number of blades.

References

- MEDICI, D. & ALFREDSSON, P. H. 2005*a* Measurements on a wind turbine wake: 3D effects and bluff-body vortex shedding. *Wind Energy*, published online.
- MEDICI, D. & ALFREDSSON, P. H. 2005*b* Wind turbine near wakes and comparisons to the wake behind a disc. AIAA paper 2005-0595, 24th ASME Wind Energy Symp., and 43rd AIAA, Aerospace Sciences Meeting and Exhibit, Reno.